CRANFIELD UNIVERSITY

Vincenzo Di Giandomenico

Surface structured bonded composite-metal joint

School of Applied Science
Advanced Materials

MRes
Academic Year: 2013 -2014

Supervisor: Andrew R. Mills, David Ayre
April 2014

CRANFIELD UNIVERSITY

School of Applied Science
Advanced Materials

MRes

Academic Year 2013 -2014

Vincenzo Di Giandomenico

Surface structured bonded composite-metal joint

Supervisor: Andrew R. Mills, David Ayre
April 2014

ABSTRACT

The design of structural joints is one of the critical challenges for the development of composite lightweight aircraft and motorsport structures. Despite the universal reliance upon mechanical fastening and adhesive bonding, the disadvantages of both when applied to high stiffness composites are considerable. For bolting and riveting these include added weight as laminates are thickened to account for stress concentrations. For bonding these include chemical uncertainties of the bonding process, inability to inspect for adhesive application quality and vulnerability to catastrophic failure. These concerns stimulated the drive for the development of new hybrid metal/composite joints which combine onlythe advantages of adhesive bonding and of mechanical interlocking by means of the pin-locking concept.

This research project investigated the performance of several hybrid joint configurations obtained with the permutations of two different plate designs (double-scarf and double-stepped) and two surface feature shapes (spike and “shark teeth” pins).

Tensile mechanical performance testing using the Digital Image Correlation (DIC) technique was carried on to examine the influence of the metal fitting geometry on the joint performance and strain distribution.

The pins were manufactured using the processes of micro-machining (MM) and electron beam melting (EBM).

The experimental results show a progressive pin failure advancing from the end of the overlap. Both surface features provide an increase in mechanical performance of the joint. Pin geometry such as the diameter, base width, length and shape critically affect the strength of the joint. The highest values of tensile strength are obtained with shark teeth pins which cause a severe reduction in stress concentration at the joint overlap edges and provide a more even strain distribution across the joining area increasing the joint strength. The plate design affects the strain distribution at high loads and can be modified so as to reduce the peel stress. The manufacturing process (EBM or MM) does not

affect joint strength significantly (for spike pins) and the process choice can be made on economic grounds.

The results provide a strong basis for more detailed stepped lap joint optimisation using tailored surface features designs to assist with the provision of robust, safe, very high strength and weight optimised joints.

Keywords:

Metal fittings, surface features, embedded, hybrid metal/composite joint, digital image correlation, electron beam melting, micro-machining, pins

ACKNOWLEDGEMENTS

I would like to express my gratitude to my supervisors Mr. Andrew Mills and Dr. David Ayre for giving me the opportunity to work on exciting project, develop my skills and for constantly helping me with anything I required.

Many thanks to Jim Hurley for being so helpful during the project.

Thanks to my family for understanding and supporting me during my life: they are the reasons of all my achievements.

Thanks to my friends. Whether you are I would like to express my gratitude for your advices and support.

Grazie a tutti!!

TABLE OF CONTENTS

LIST OF FIGURES

LIST OF TABLES

LIST OF ABBREVIATIONS

ALM	Additive Layer Manufacture
BALD	Bleed Air Leak Detect
CBN	Cubic Boron Nitride
CVD	Chemical Vapour Deposition
CFRP	Carbon Fibre Reinforced Polymer
CMT	Cold Metal Transfer
DIC	Digital Image Correlation
DMLS	Direct Metal Laser Sintering
EBM	Electron Beam Melting
EPSRC	Engineering and Physical Sciences Research Council
FE	Finite Elements
FRP	Fibre-reinforced plastic
HTCL	Hybrid Titanium Composite Laminate
MM	Micro-machining
PTFE	Polytetrafluoroethylene
PVD	Physical Vapour Deposition
SLM	Selective Laser Melting
SLS	Selective Laser Sintering
TWI	The Welding Institute

1 INTRODUCTION

1.1 Overview

The great potential of composite lightweight aircraft and motorsport structures is obtained ensuring that the joints do not reduce structural efficiency.

The design of structural interconnections is one of the critical challenges throughout development of composite structures. Composite technology reduces the necessity for structural coupling by means of manufacturing techniques and integral design.Joining parts to subassemblies remains mandatory due to inspection, production methods, material limitation, transportation requirements and repair.

The aerospace industry has to cope with the highest safety requirements in operation as well as economic efficiency. The design of safe aircraft structures is based on safe-life and damage tolerance concepts:in accordance with them the structure is thought to have a minimum life during which it will not experience a catastrophic failure.

Aerospace companies are looking for a new joining technique to move away from metal fasteners in composites such as the titanium interconnections between the wings and fuselage (figure 1-1): the metal fasteners increase the weight of the aircraft and disturb the laminar flow across surfaces causing aerodynamic issues.

Moreover the use of adhesive joints is limited: chemical uncertainties of the bonding process, impossibility to inspection and catastrophic failure are some of several aspects that do not respect the safety requirements.

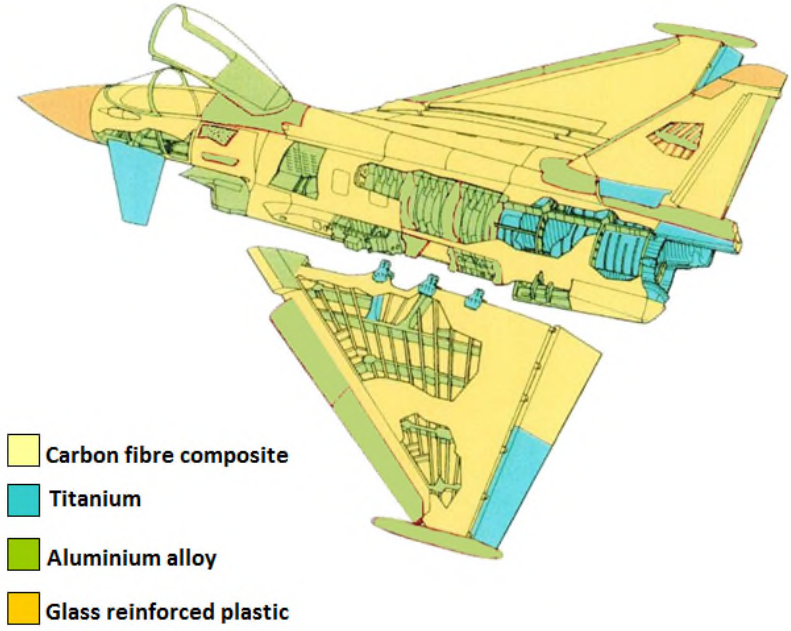

Figure 1-1 Aircraft structural design

In the last years composite materials have found increasing application in the automotive sector: reducing the weight of the car improves the engine efficiency with the consequent reduction of CO_2 emissions and fuel consumption.

BMW invested more than 600 million of euros to develop the project of i3 electric vehicle, a car that uses carbon fibres not only for the body panels but also is built on a carbon fibre frame. Using carbon fibre rather than traditional steel for structures allowed BMW to save enough weight to cancel out the weight of the battery packs that power the engine in the i3, while still maintaining safety standards (figure 1-2).

Figure 1-2 BMW I3 Upper Body

Moreover the motorsport industry has invested a large budget in design optimization to reduce the weight of the car: The use of composite materials and, where needed, metal fittings seems to be the answer. Although current F1 race teams are capable of producing a car with a mass less than 640 kg (FIA minimum).However, the disbond of titanium fittings and composite structures represents one of the biggest problems, specifically for the suspension arms of F1 cars (figure 1-3).

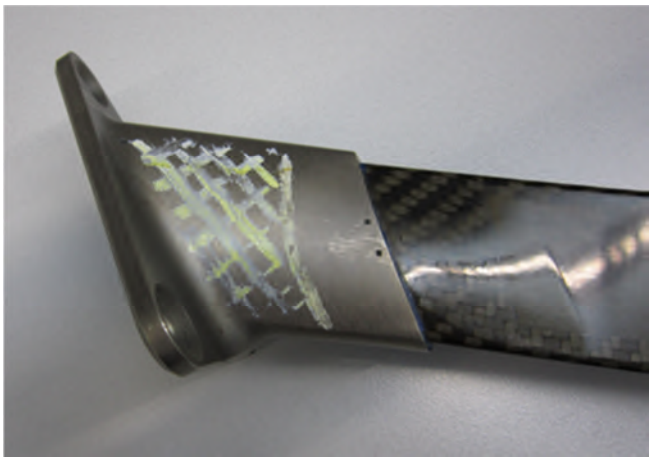

Figure 1-3 F1 car suspension arm

This research project "***Surface structured bonded composite-metal joint***" aims to optimise the design of a high performance titanium/carbon fibre hybrid joint that is a practical alternative to mechanical fastening and adhesive bonding. Moreover the understanding of mechanical properties and failure mechanism of carbon fibre composite and titanium is essential in order to improve any design of an embedded metal fitting. In addition a capability analysis of different manufacturing processes is provided to understand the relationship between design and manufacturing process.

This thesis is divided into three main sections: the first one corresponding at chapter 2 shows the background of joining concepts through an extensive literature review.

The second section includes the chapter 3 which details the work carried out in joint design, manufacturing process and describes the testing procedure.

The last section includes chapters 4where the mechanical testing results are presented and discussed while chapter 5concludes the research project summarising and highlighting the improved joint options discovered.

2 LITERATURE REVIEW

2.1 Conservative Joining concept design

2.1.1 Fastened joint

In a composite structure any joint may act as a damage initiator point if it is not designed appropriately and may lead to failure of the component at that location.

Bolted joints are the predominant fastening mechanisms used in connecting of structural parts made from advanced composites[1]. They offer the benefits of disassembly without destroying the structure and are not sensitive to service temperature, humidity or surface preparation.

The design process of bolted joints is based on experimental data and the analytical models are largely empirical in nature. According to this, ASTM International, NASA and FAA developed relevant testing methods to evaluate mechanical properties of the fastened joint such as bearing failure (figure 2-1).

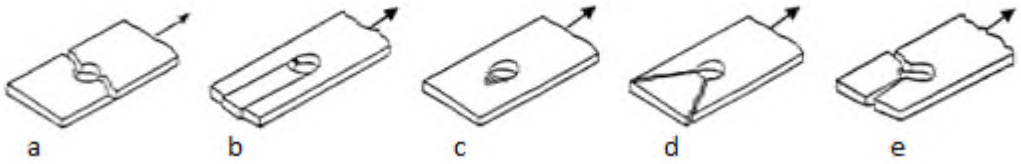

Figure 2-1 Bearing test failure modes for ASTM D 5961/D 5961M-05: (a) lateral, (b) shear out, (c) bearing, (d) tearout, (e) cleavage. From [1]

A review study highlighted that there was no consensus on which type of failure modes and which studies have to be used to predict the strength of the mechanical fastened joints [2]. The unlimited combination of composite materials and fibre pattern determine a complex 3D strain and stress distribution in these kinds of joints, causing a failure that is not predicted by the traditional methods.

Several parameters such as geometric parameters and materials selection affect the bolted joint design: if one of these parameters doesn't respect a specific design recommendation the fastened joint becomes a failure starting point, which may propagate in the through-the-thickness direction, producing the composite structure failure.

Generally bolts are oversized and tightened to achieve the optimum strength while in service, due to fatigue loading, the bolt-hole and surrounding material is worn down. The stress concentration developed around the holes reduces the structure strength causing local damage and, finally, a catastrophic failure of the whole structure.

Camanho and Lambert [3] established that to design an optimised mechanically fastened joint in a composite material it is necessary to develop a methodology that can predict the elastic limit, the crack initiation and the failure load of the joint in addition to the prediction of the failure mode of the double shear mechanically fastened composite joint in bearing, shear and tension.

Due to the complexity of the stress concentration several methods were developed to evaluate the failure load of the joint[4-6]. Whitney and Nuiser [7] and Nuiser and Labor [8] proposed a method for tensile and compressive cases defining a characteristic length in tension (or compression) as the distance from the edge of the hole to the point where the stress concentration is equal to the corresponding unnotched laminate.

Because the methods exposed before are available for pure compressive or tensile stress, Chang et al.[9]elaborated a method to evaluate the combined stress cases. That method combines the characteristic lengths with Yamada failure [10] through characteristic curves. The characteristic curve is a curve that connects the characteristic length in tension and compression.

The fastener materials selection is the other parameter that involves the joint design. It depends on several factors that have to be investigated such as difference between thermal expansion parameters of fastener and composite, delamination caused by fastener under load, weight of the fastener and water

intrusion between fasteners and composite that may cause galvanic corrosion. Generally the fasteners are made of titanium, steel or stainless steel.

2.1.2 Bonded joint

The alternatives to mechanical fasteners, the application of adhesively bonded joints in structural components, has increased in the recent years due the potential advantages of strength-to-weight ratio, design flexibility, lower structural weight, higher damage tolerance and lower fabrication cost [11].

For these reasons the bonded joint has found applications in several high technology areas such as automotive, aerospace and electronics industries.

Adhesive bonding can be chemical or physical bonding process result of a reaction between the adherent surface atoms and the adhesive. The chemical bonds represent the load transfer mechanism between the adherents.

Bonding of postcured composites parts is generally physical/mechanical bonding rather than chemical [12].

The adhesive selection is a difficult process and includes many factors such as stresses and expected environments, adhesive application method and cure, type and nature of substrates.

The adhesives used in structural applications include: epoxies, cyanoacrylates, acrylics, polyurethanes, silicones and high temperature adhesives. Epoxy adhesives are frequently used to bond composites based on an epoxy matrix due to the compatibility between resin and adhesive.

Since the surface integrity directly influences the durability of the adhesive bond, surface treatments prior to the application of adhesives are recommended to achieve maximum mechanical strength [13]. For thermoset composites typical surface treatments include abrasion/solvent cleaning techniques while thermoplastic composites require surface chemistry and surface topographical changes to ensure strong bond strength [13, 14].

Adhesive performance is sensitive to environmental factors such as humidity and temperature. Several studies demonstrate that the absorbed moisture may weaken not only the interface between the adhesive and the adherent but also the physical and chemical properties of the adhesive [15-19]. The exposure to elevated temperatures causes a reduction of bond strength due to chemical and physical changes within the adhesives.

The standard ASTM D5573 defines six typical failure modes for FRP composite adhesive joints: adhesive failure, thin-layer cohesive failure, cohesive and light-fibre-tear failure, stock-break failure, mixed failure or fibre-tear failure (figure 2-2):

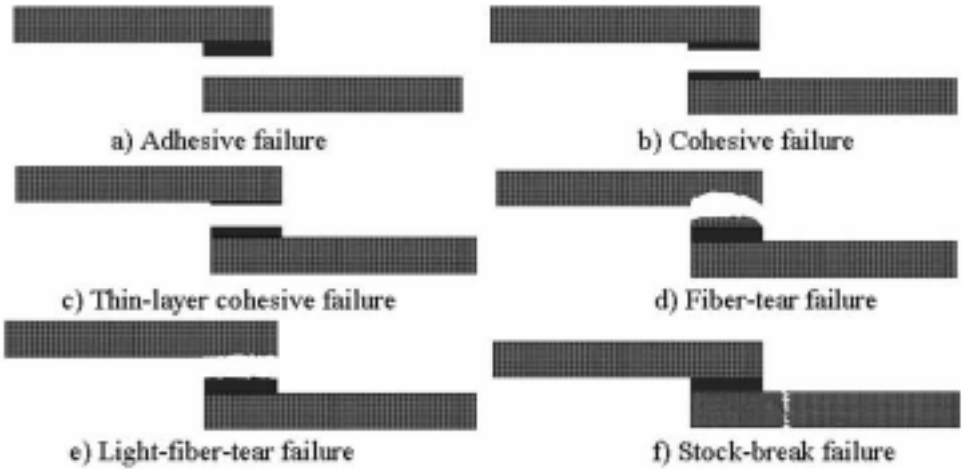

Figure 2-2 Failure modes in bonded joints [11]

The bonding parameters such as surface condition, fillet, bond thickness, surface ply angle and stacking sequence were investigated to explain their influences on the failure behaviours and develop a method to predict the composite bonded joint failure [20-25].

2.1.3 Available joint design

Mechanical properties of adhesive joints are influenced by joint design. The load capability curve (figure 2-3) illustrates the transition from adherend failure to failure of the adhesive for a variety of joint configurations.

Analysing all the joint configurations from the single-lap joint to the scarf joint the shear-stress concentrations and the peel-stress become the limiting factors on joint strength.

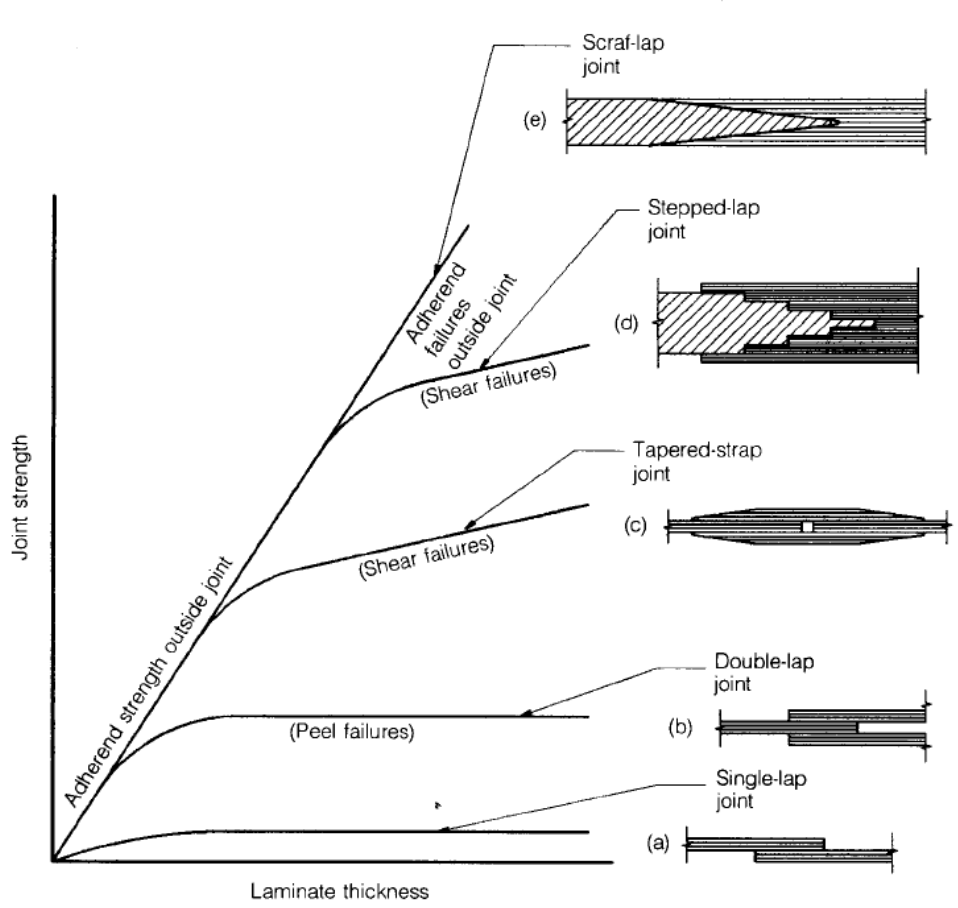

Figure 2-3 Joint configuration VS Strength [26]

The single–lap joint behaviour under tensile loading is illustrated in figure 2-3(a). The loading eccentricity requires greater overlap lengths to alleviate adherent bending stress [27]. Joint failure is expected into the laminate because

laminates are weaker in interlaminar shear and tension than the shear carrying ability of adhesive [26].

For double-lap joint (figure 2-3(b)) the shear load transfer is accomplished through a tight effective zone at the ends of the overlap. The shear stress distribution in the middle of the adhesive carries the same small load regardless of the length of the total overlap (figure 2-4). The strength is affected adversely by the presence of a laminate stiffness unbalance in the joint. It is tolerant of manufacturing imperfections.

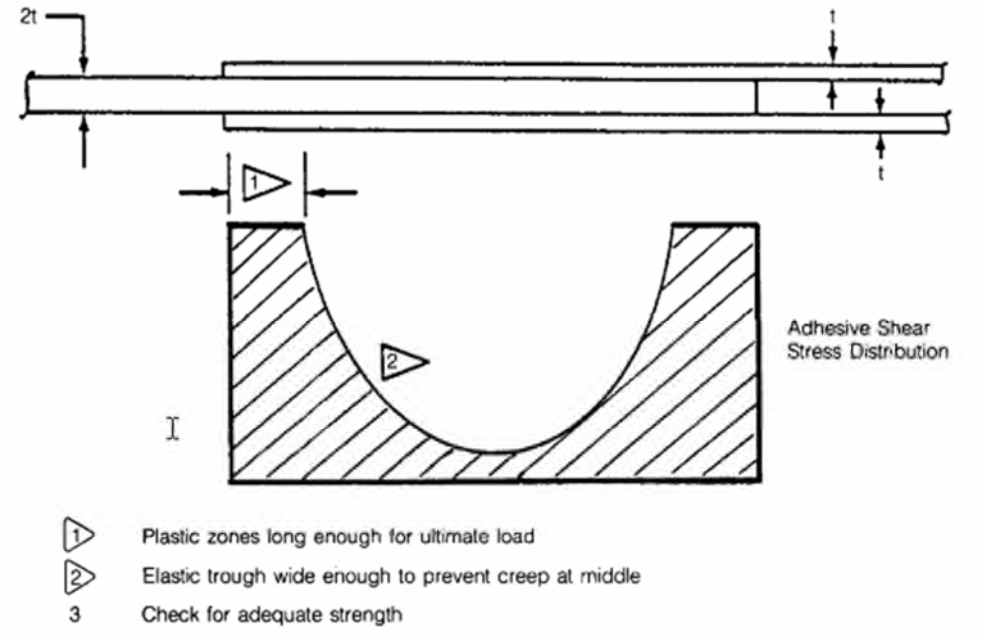

Figure 2-4Shear stress distribution of double-lap joint

The stepped-lap joint, sharing some characteristics of double-lap and scarf joint, offers greater efficiencies for thick laminates than is possible with single/double-lap joints (figure 2-3(d)). The joint strength can be increased by increasing the number of steps up to the number of plies in the laminate where no further strength increase can be developed.

The tail end of the thin step represents the critical section of this joint where fatigue failure is likely to occur.

As illustrated in figure 2-3(e) the shear stress in the scarf joint is virtually constant with the laminate thickness; it means that scarf design provides 100% joint efficiency. A small scarf angle (between 6-10°) can be selected to give a joint adhesive strength equal to the laminate failure load and ensures that laminate failure occurs outside the joint.

At the moment the efficiency of scarf joint is less than 100% due to the manufacturing constraints that require angles greater than optimal in order to avoid the tip breaking off.

2.2 Novel joining concept design

2.2.1 Local sheet interleaving

Several designs concepts have been developed in the past to obtain a satisfactory coupling efficiency of composite structures joined with mechanical fasteners. One of these techniques is based on the use of bonded metallic insert (figure 2-5), specially designed, that promote alternative paths for the load transfer [28-31].

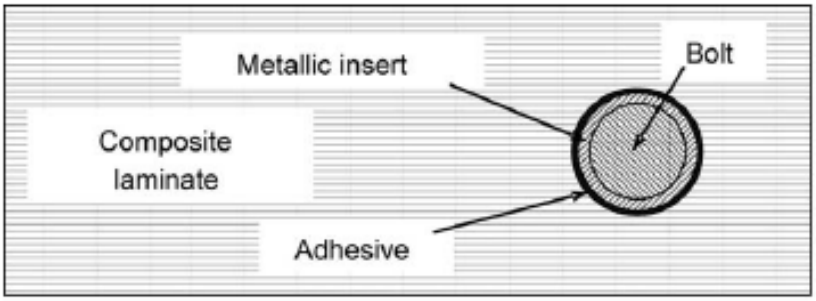

Figure 2-5 Bonded metallic insert [32]

The German Aerospace Centre, using ply substitution techniques with thin high-strength metal foils, applied local reinforcement to the joining area to improve the coupling efficiency of highly loaded composite joints [33-35]. This configuration consists of a transition region between a pure fibre composite region and a joining region formed with a combination of thin titanium foils and continuous fibre plies (figure 2-6).

The joining region is done by the gradual substitution of composite layers by titanium foils; the remaining composite layers are not interrupted and pass from the hybrid region to the pure composite region through the transition region.

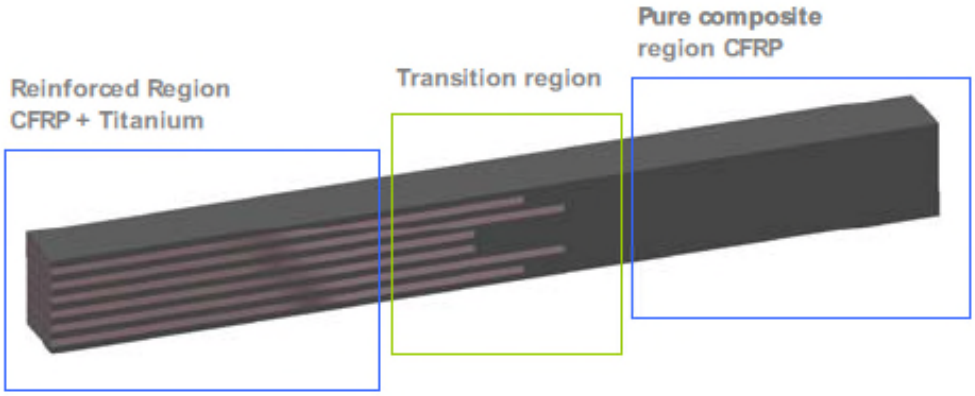

Figure 2-6Hybrid metal configuration

This local reinforcement technique finds application especially to the bolt-bearing area of composite laminate. It enhances the bearing strength and the coupling stiffness while reduces the sensitivity of the mechanical properties to the laminate configuration (figure 2-7).

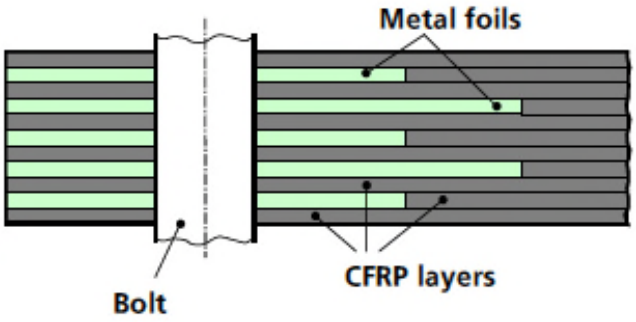

Figure 2-7Local reinforcement at bolted joint, modified from[36]

Experimental analysis established how the hybrid laminates with 20% titanium content increased the tensile strength of a bolted joint by 91% and the specific tensile strength by 32% if compared with a CFRP laminate [34].This hybrid joint is lighter and does not require a local increase of thickness that would generate secondary bending effects and increases bolt bending [33-35].

2.2.2 Through-thickness pin concepts

The through-thickness pin interlocking design tries to combine the advantages offered by mechanical fastener and adhesive bonding. It aims to provide the mechanical interlocking behaviour of ‘bolted’ joint by protrusions created in the metal adherent. Instead of fasteners, the small size of these surface features avoids severe damages on the laminate composites while the resin of the CFRP acts like an adhesive agent between the two parts.

In this way, mechanical interlocking and adhesive bonding are coupled together in the hybrid metal-composite joint without drilling holes and destroying reinforcing fibre-bundles.

Several FE models have been developed to evaluate the effect of design parameters of a pinned lap joint when subjected to tensile loading [37].

Several manufacturing technologies like Comeld™, Cold Metal Transfer (CMT), Laser Sintering (LS), Electron Beam Melting (EBM) and Micro-Machining (MM) are available at the moment to manufacture pins onto titanium metal plate. Realising components with high repeatability, reproducibility and acceptable quality is mandatory especially for the main industries: aerospace and motorsport.

It is essential to understand the effects of processing on microstructure and properties of metal plates to choose the right manufacturing technology.

2.3 Metal features manufacturing technology

2.3.1 Comeld™ joint

The development of Surfi-Sculpt™ by The Welding Institute established the basis for a hybrid joining method [38]: the metal surface is locally melted by an electron beam providing an array of protrusions and cavities (figure 2-8).

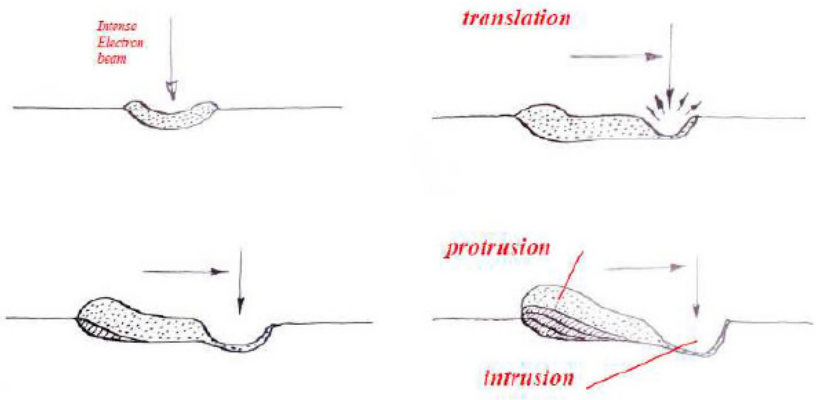

Figure 2-8 Sculpted surface by Electron beam

This technology to produce joints is actually known as Comeld™. According to Smith et al. [39] Comeld™ provides an increase in ultimate strength and energy absorption in tensile and bending loads. FE models have been developed to analyse the stress concentration around the end of protrusions to predict the

failure of this joint. These successful strategies can be applied to varying geometry and distribution of the protrusion to optimise the joint design [40].

2.3.2 Cold Metal Transfer

Cold Metal Transfer is an arc-welding technology to create pins on metal plates/surfaces. Developed by Frönius [41] it consists of a welding wire being melted onto the metallic surface. The wire gets torn/fractured/fused at a specific height when a high current is applied, leaving a ‘pin attached to the metal substrate. It is possible to manufacture pins with different shapes, heights and angle according to the welding control. The computerized process-repetition and the movement of the wire allow an array of pins to be created on the metal plate [42, 43] (figure 2-9,2-10).

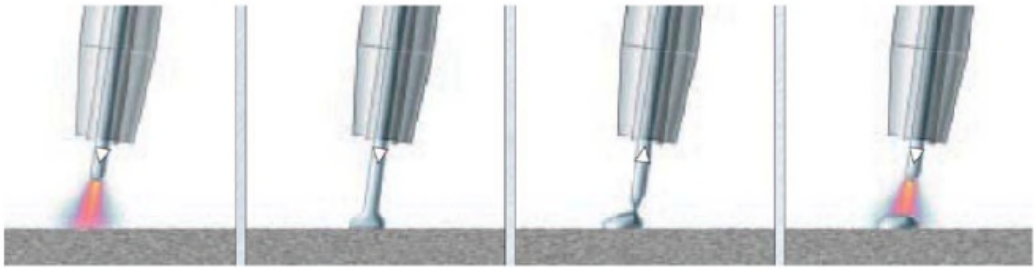

Figure 2-9Backward movement of the wire[42]

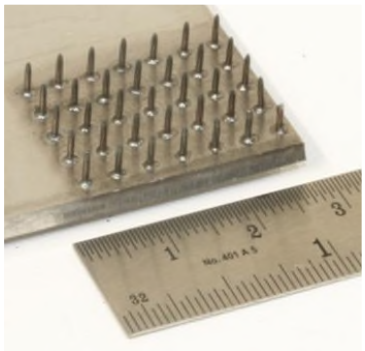

Figure 2-10Array of pins, Courtesy of Adam Joesbury

Due to the low thermal input, CMT causes less distortion to the parent material compared to Surfi-Sculpt technology [39]. However this does present problems when pins are welded with titanium alloy that reacts with oxygen, nitrogen and hydrogen. To achieve complete welds the process depends on surface cleanliness and correct use of inert gas shielding.

Ucsnik et al. [44] and Fleischmann et al. [45]compared the mechanical properties of a CMT stainless steel hybrid metal composite joint, highlighting how a different pins shape provides a different failure mode (figure 2-11) and increases the strength of the joint.

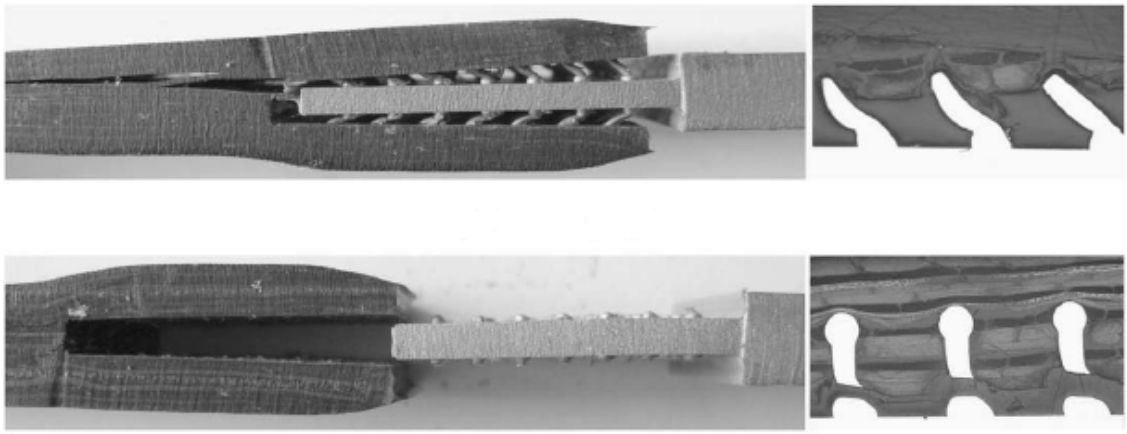

Figure 2-11 Hybrid joint failure [44]

2.3.3 Selective Laser sintering

Developed by University of Texas for plastic materials [46], this technique has been recently advanced for metal materials and it is designated as selective laser melting. This additive layer manufacturing consists of a laser beam which melts a very fine metal powder to obtain very complex geometries with precise details and better surface finishes that are impossible to create by machining (figure 2-12).

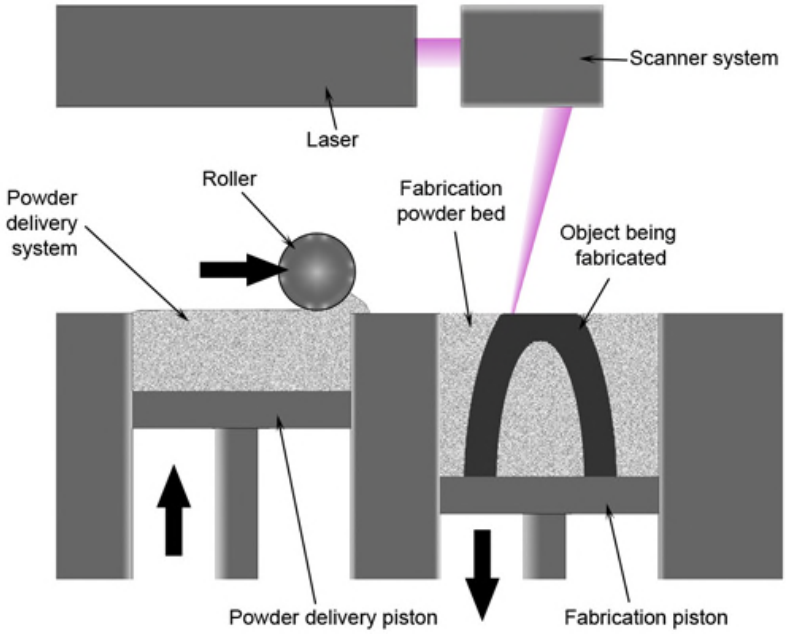

Figure 2-12 SLS process diagram [47]

During the processing of reactive metals, the content of the oxygen in the powder is controlled/critical and a shielding gas is needed.

From the concept of Rapid Prototyping [48, 49] the Direct Metal Laser Sintering (DMLS) technology provided metallic components for use within some of the most demanding environments and applications [50-52]. One of the most important aspects of DMLS technology is that design and production costs do not increase exponentially with the potential design complexity.

Testing results by Red Bull [53] on thin walled hydraulic channels made by DMLS technology confirmed the robust capabilities and the consistency of components made by this route outlining also the benefits of this technology in engineering design context.

2.3.4 Selective Laser Melting

Selective laser melting (SLM) (figure 2-13) is a three dimensional laser printing technique very similar to selective laser sintering with the only difference that SLM manufactures a product by melting powder into the desired shape, whereas SLS does not completely melt the materials [54].

Moreover the use of this high power laser to liquefy materials from a powder bed causes a surface roughness due to an increase in materials vaporization and spatter generation during process [55].

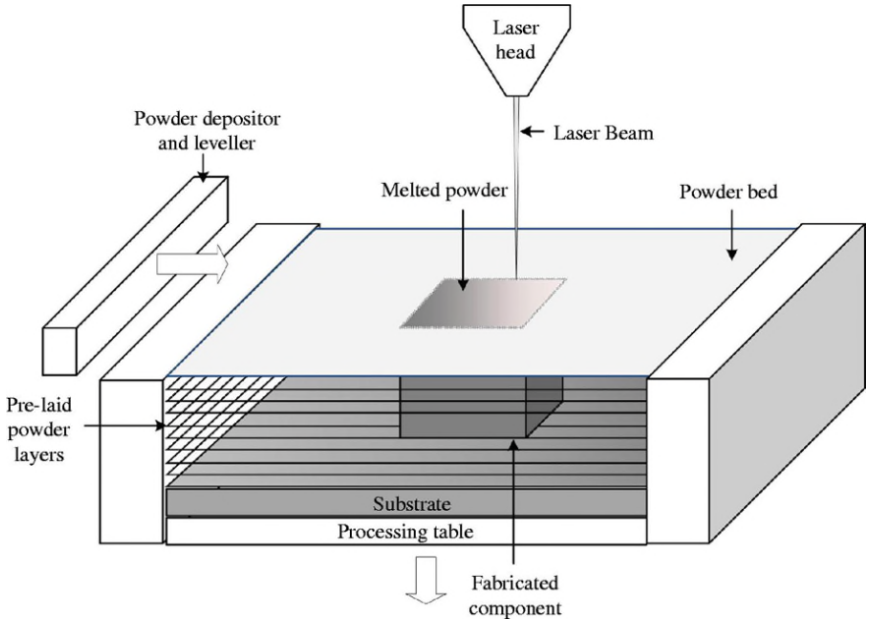

Figure 2-13 Selective laser melting diagram [47]

The SLM was used to manufacture the J-2X rocket engine (figure 2-14) for the Space Launch System. Due to the complex geometry of the J-2X, NASA utilized SLM to ensure accuracy of this component because without manually welding the parts are structurally stronger and more reliable.

Figure 2-14 J-2X rocket engine

2.3.5 Electron Beam Melting

EBM is a layer-by-layer additive manufacturing technique that exhibits great promise to manufacture components (figure 2-15). An electrons beam melts the metal powder in a vacuum environment and reproduces the geometry of the piece defined by computer model. The absences of oxides and impurities make the process suitable for reactive materials such as titanium. Before melting, preheating every individual layer of the build allows control of thermal effects and the parts do not require any subsequently stress relieving [47].

The Arcam A2 machine employs the EBM technology to rapidly fabricate flight-ready titanium components for commercial and military aircraft even impossible to create with traditional manufacturing processes. According to the development manager of Arcam, this machine with EBM saves a considerable amount of money and time throughout the prototyping and design process.

A Bleed Air Leak Detect (BALD) is made as an applicable case study of EBM technology. The result of that study concluded that EBM is a suitable technology to produce aerospace components such as BALD bracket.

Due to a coarser powder, thicker layers and larger melt pool the EBM technology built components from a CAD model with rougher surface finish and less design detail when compared with laser sintering which represent the limits for this technology.

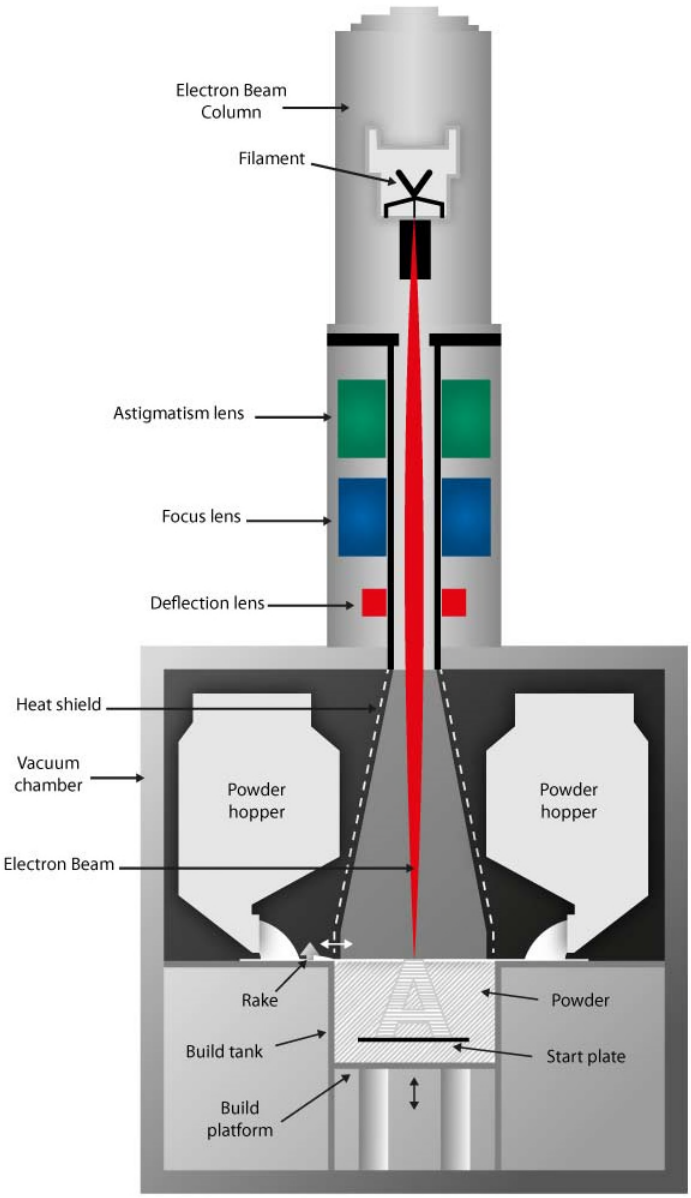

Figure 2-15 Electron Beam Melting process diagram

2.3.6 Micro-machining

Machining is the most important of basic manufacturing process; it consists of removing unwanted materials from a workpiece in the form of chips.

The properties of the work material are important in chip formation: high strength materials require larger forces than lower strength materials, causing a series of disadvantages on machining facilities such as deflection, increases friction, heat generation etc..

Machining centres have automatic tool-change capability and are capable of milling, boring, reaming, drilling, tapping and others processes (figure 2-16, 2-17).

Milling is a basic process that generates a surface from a workpiece by progressive chip removal. The desired surface is created feeding the workpiece into a rotating cutting tool or indifferently the workpiece is stationary and the cutter is fed to the work. Moreover, a multiple-tooth cutter is used to improve the production rate and the surface finish quality, making this manufacturing process well suited and widely used for mass-production work.

Operation	Block diagram	Most commonly used machines	Machines less frequently used	Machines seldom used
Facing	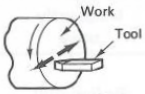	Lathe	Boring mill	
Broaching	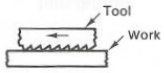	Broaching machine		Turret broach
Grinding	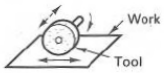	Surface grinder		Lathe (with special attachment)
Sawing	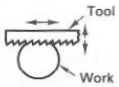	Cutoff saw	Contour saw	
Shaping	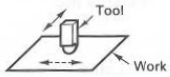	Horizontal shaper	Vertical shaper	
Planing	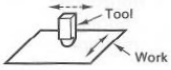	Planer		
Milling	slab milling 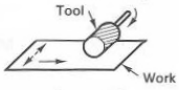 face milling 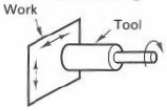	Milling machine Milling machine Machining center	Lathe with special milling tools Lathe with special milling tools	Drill press (light cuts)

Figure 2-16 Operation and machines for machining: part 1 [56]

Operation	Block diagram	Most commonly used machines	Machines less frequently used	Machines seldom used
Turning	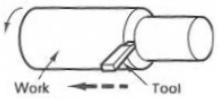	Lathe NC lathe machining center	Boring mill	Turret lathe
Grinding	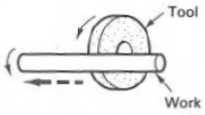	Cylindrical grinder		Lathe (with special attachment)
Sawing (of plates and sheets)	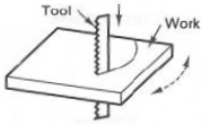	Contour or band saw	Laser Flame cutting Plasma arc	
Drilling	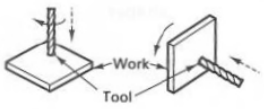	Drill press Machining center (nc) Vert. milling machine	Lathe Horizontal boring machine	Horizontal milling machine Boring mill
Boring	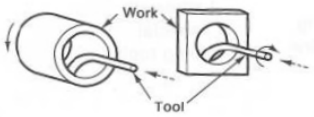	Lathe Boring mill Horizontal boring machine Machining center		Milling machine Drill press
Reaming	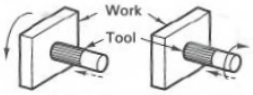	Lathe Drill press Boring mill Horizontal boring machine Machining center	Milling machine	
Grinding	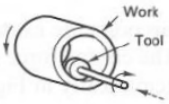	Cylindrical grinder		Lathe (with special attachment)
Sawing	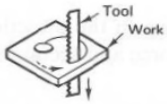	Contour or band saw		
Broaching	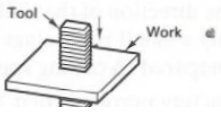	Broaching machine	Arbor press (keyway broaching)	

Figure 2-17 Operation and machines for machining: part 2[56]

The productivity of the machining operation is directly influenced by cutting tool material, cutting parameters, and tool geometry selection.

Cutting tools are subjected to severe conditions such as high local stress, severe friction and high temperatures. A wide range of cutting tool materials is

available with a variety of properties, capabilities and costs. These includes high carbon steels and low/medium alloy steels, high-speed steels, cast cobalt alloys, cemented carbides, cast or coated carbides, sintered polycrystalline diamond and single-crystal natural diamond. Coated and uncoated are the most extensively used and about 15 to 20% of all tool steel are coated by PVD or CVD. Diamond and cubic boron nitride (CBN) are used in applications where despite the higher cost, their use is justified [56].

2.3.7 State of the art of hybrid joint

The presented literature review highlights a lack of knowledge in these new joining concepts and especially in mechanical pin interlocking joint. This research project aims to fill this gap providing a joint design guideline. Coupling all the knowledge on different joining technologies, the study is based on design of embedded metal plate with surface features and evaluations of mechanical properties and manufacturing process.

3 MATERIALS AND TESTING METHODS FOR JOINTS MANUFACTURE

3.1 Titanium / CFRP hybrid joint Design

3.1.1 Selected Joint geometry

The new joint concept proposed tries to couple the mechanical properties of adhesive and pin interlocking joint.

Double stepped and double scarf plate configurations are selected to design the metal plate according with the previous studies on bonded joint (section 2.1.3).

According with the knowledge on pin interlocking (section 2.2.2) the pin shape influences the joint performance. Spike and shark teeth pins are designed to improve the joint strength.

The combinations of plates and pins provide four different joint configurations for investigations. The reasons to propose four different joint designs are due to the necessity to investigate the manufacturing process and provide a joint with high mechanical properties and a simple manufacturing process. To compare the mechanical properties both configurations have the same dimensions of plate, pinned surface and number of pins.

The cured sample presents a total length of 235 mm and a width of 25 mm.

More details about plate geometry and lay-up are provided in the following sections.

3.1.2 Lay-up selection

The modification of the lay-up near the overlap area of the joint represents a helpful design variable for structural connection in composite materials.

Few research studies are available in the literature on this subject and the findings about the influence of the ply orientation at the interface between adhesive and adherent.

Matthews and Tester [57] investigated the static properties of CFRP single lap joints: the joint strength increases with proportion of 0° plies and the same ply orientation at interface. Others researchers such as Meneghetti et al. [58], Renton and Vinson [59] and De Goeji at al. [60] found a reduction of high cycle fatigue strength moving from 0° to others ply orientation.

According to several studies, in order to improve the adhesive strength it is important to select a 0° layer at interface between metal plate and composite laminate [34, 61].

In order to evaluate the influence of lay-up on mechanical properties of hybrid joint two different stacking sequences are proposed. The joints are manufactured with 44 layers of M21-T800 prepreg from Hexcel industry.

The representation of fibre orientation is illustrated in figure 3-1.

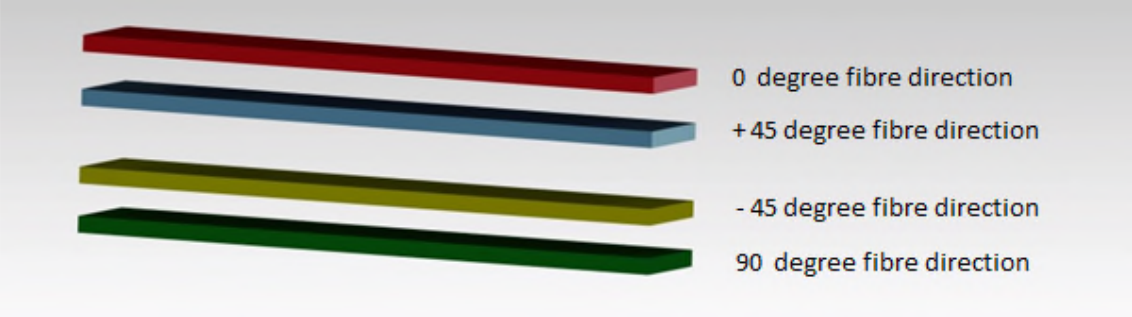

Figure 3-1 Fibre orientation

The first lay-up (figure 3-2) shows an equal distribution of fibre orientation in order to provide the same strength in all the directions. Accepting the recommendation regarding the interface layer, each step has a 0° prepreg layer at interface.

The amount of layers in each direction are summarised in table 3-1.

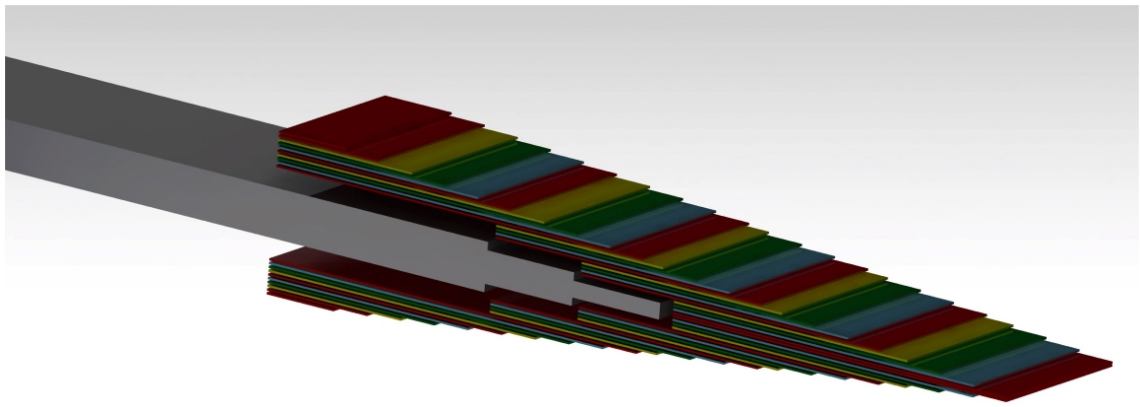

Figure 3-2 First lay-up

Fibre orientation	Number of layers	Total percentage
0	14	31.9%
± 45	20	45.4%
90	10	22.7%

Table 3-1First lay-up fibre orientation density

A second lay-up is designed according with research results detailed earlier [34, 57-59] and the recommendation of Gay [62] for fastened joint (figure 3-3). Gay suggests increasing the number of layers in the load direction (0° direction) instead of a reduction of the layers at orthogonal direction to reduce the stress concentration around the hole of the metal insert. Details about the second lay-up are summarised in table 3-2.

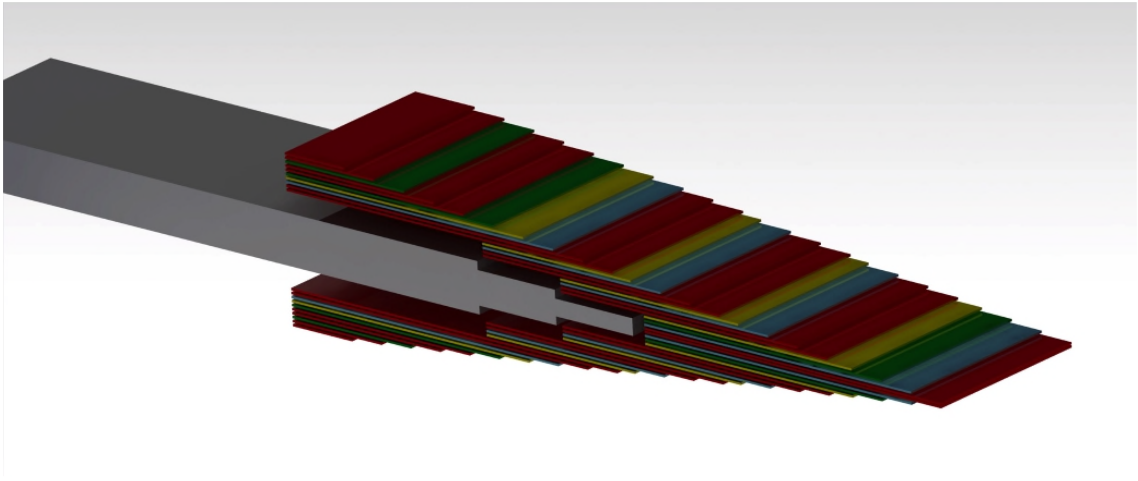

Figure 3-3 Second lay-up

Fibre orientation	Number of layers	Total percentage
0	22	50%
± 45	16	36.3%
90	6	13.7%

Table 3-2Second lay-up fibre orientation density

3.1.3 Double-Stepped lap joint with surface features

The double stepped joint is tested in three different configurations: a control configuration without surface features and other two with pins of different shape.

The plate geometry is fully described with the control double stepped configuration (figure 3-4).

The three steps plate is 25 mm width and 120 mm length with a variable thickness from 6 mm of the first step to the 4 mm of the second step until the 2 mm of the tip.

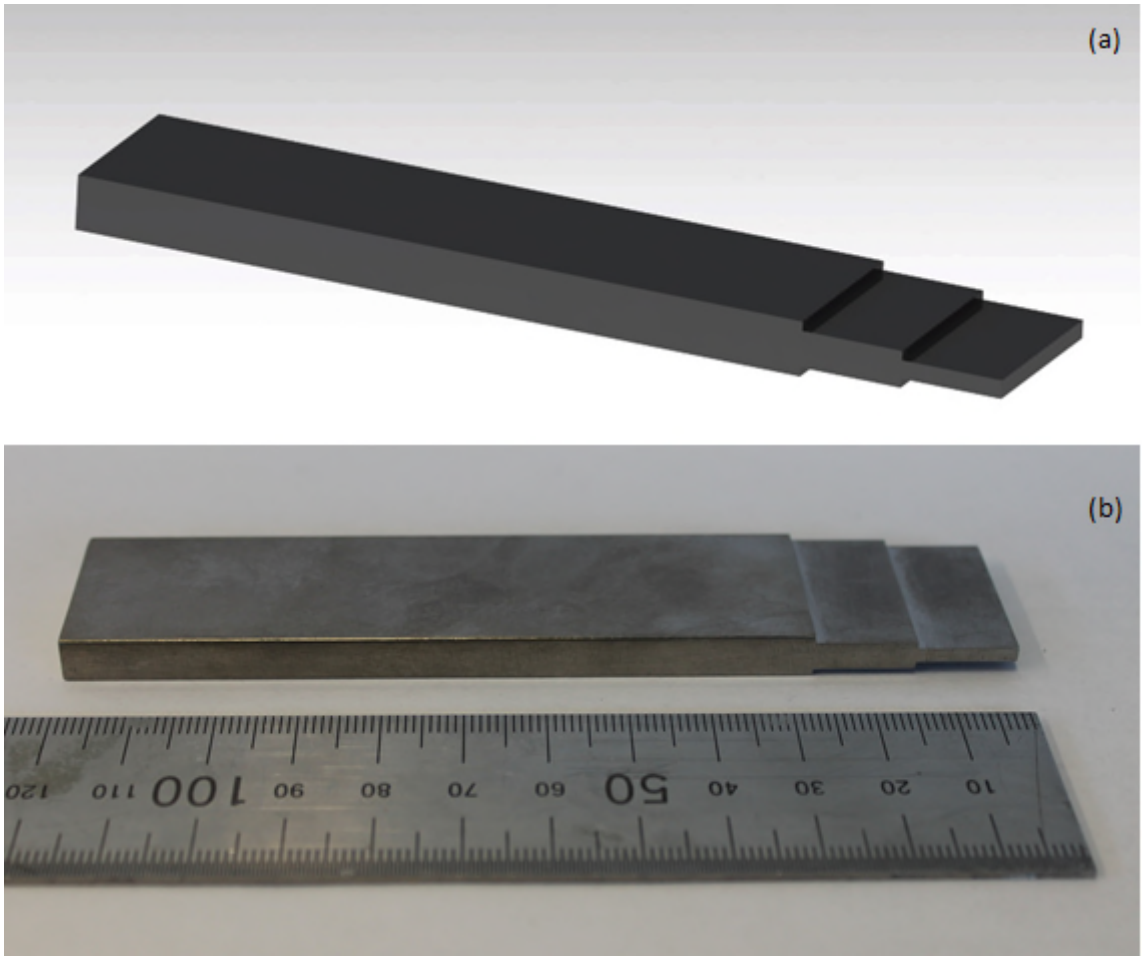

Figure 3-4 Control Double-stepped joint: (a) 3D CAD image, (b) micro-machined joint

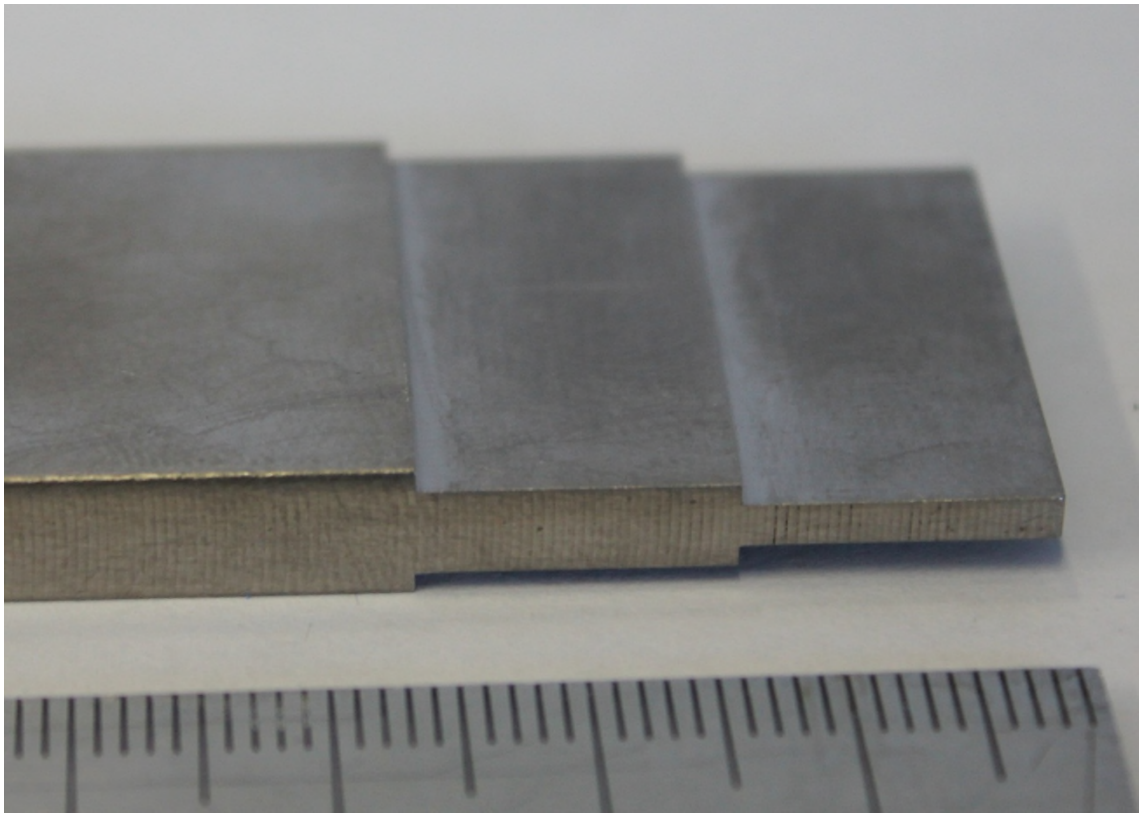

Figure 3-5 Details of control Double-stepped joint

Figure 3-6 shows the configuration of a double-stepped joint with spike pins. The plate geometry is the same as the control specimen.

According to previous studies [44], the same number of pins is produced on the joint to provide a parameter to compare the benefit of this configuration. All the pins have a diameter of 1.3 mm.

The metal reinforcements are arranged in three different arrays due to the stepped nature of the plate. A first array of 5 x 3 pins with a height of 2 mm is put into the first step of the plate, a second array of 5 x2 pins with a high of 3 mm in the second step and a last array of 5 x 2with 4 mm high pins in the tip step (figure 3-7). The difference in length of pins is due to the nature of the plate and the necessity to achieve the same total length for each step while the spacing between pins is calculated adapting Niu's recommendation for spacing of fasteners joint [26].

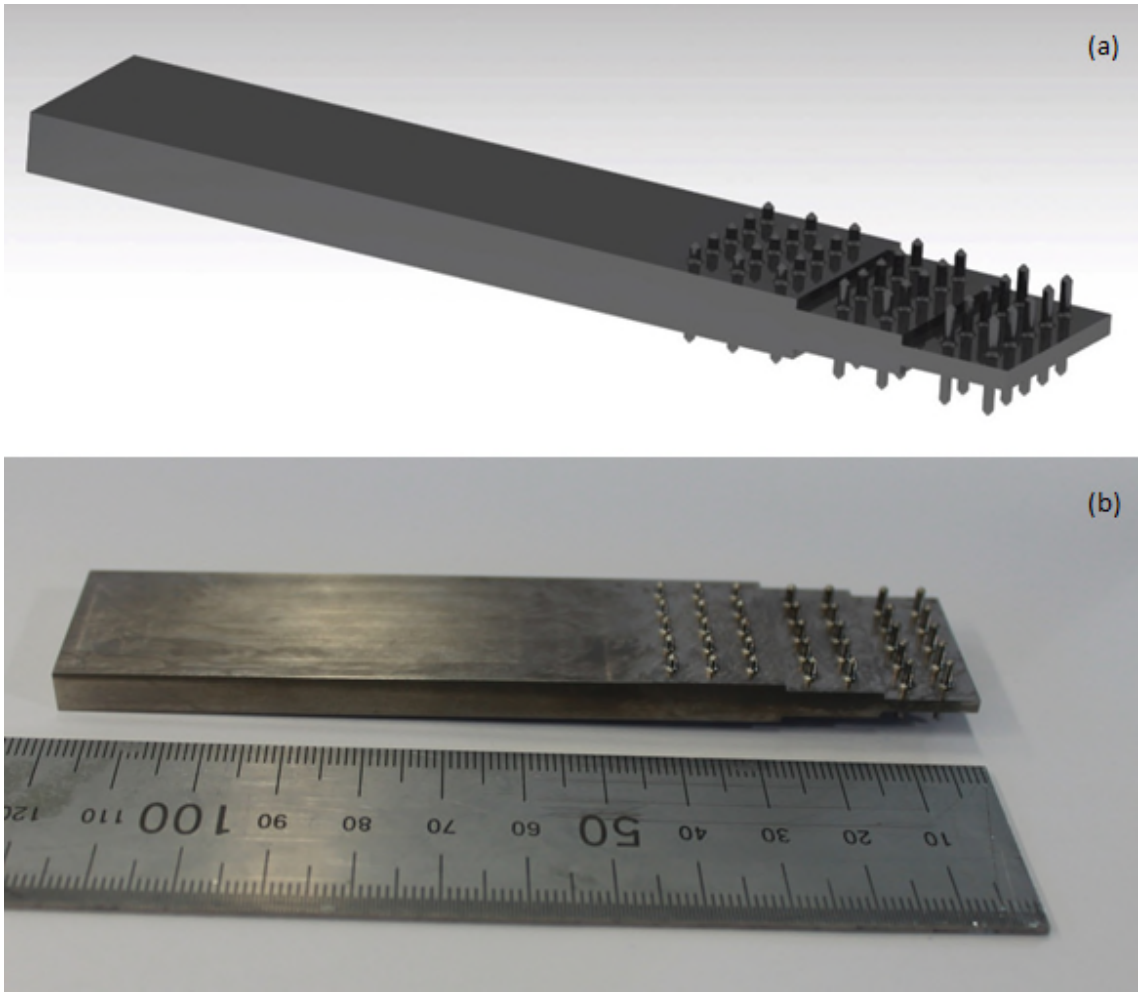

Figure 3-6Double-stepped joint with spike pins: (a) 3D CAD image, (b) micro-machined joint

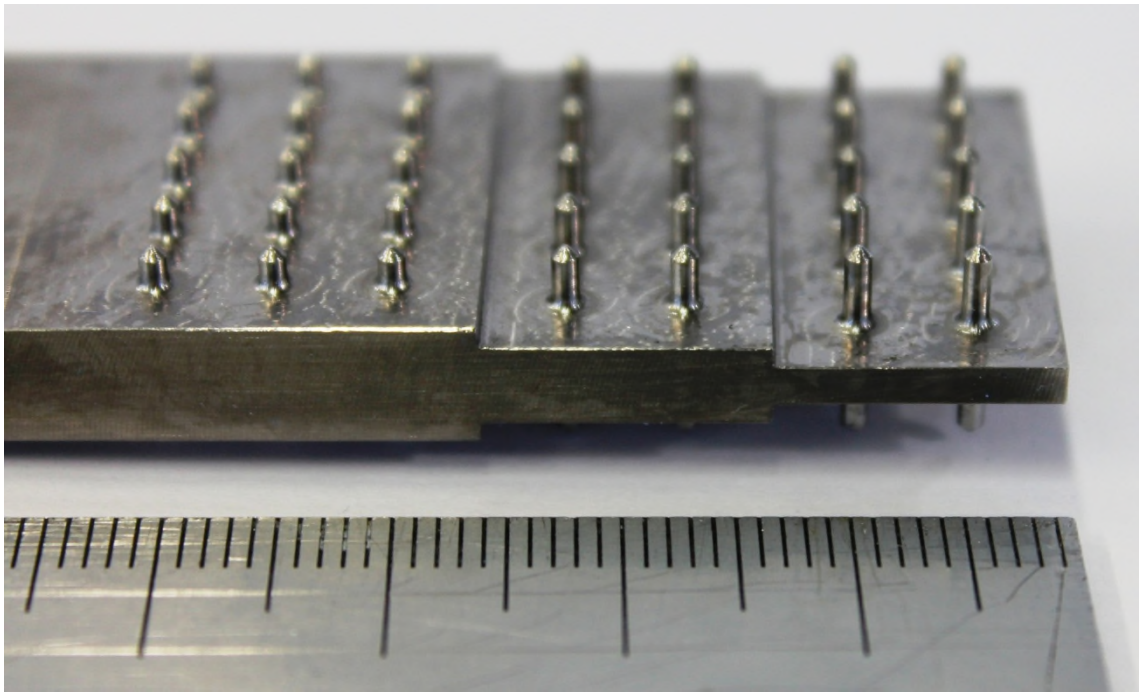

Figure 3-7 Detail of double-stepped joint with spike pins

The “shark teeth” configuration (figure 3-8) is designed according to the same spacing criteria of the spike configuration. A first array of 5 x 3 with 2 mm high “shark teeth” in the first step, a second one of 5 x 2 with 3 mm high “shark teeth” pins in the second step and a last array of 5 x 2 shark teeth pins with a high of 4 mm (figure 3-9). The variable height is the only difference in the shark teeth design: all pins have the same 3 mm base length and a thickness of 1.3 mm (comparable with the pin diameter of the spike pins).

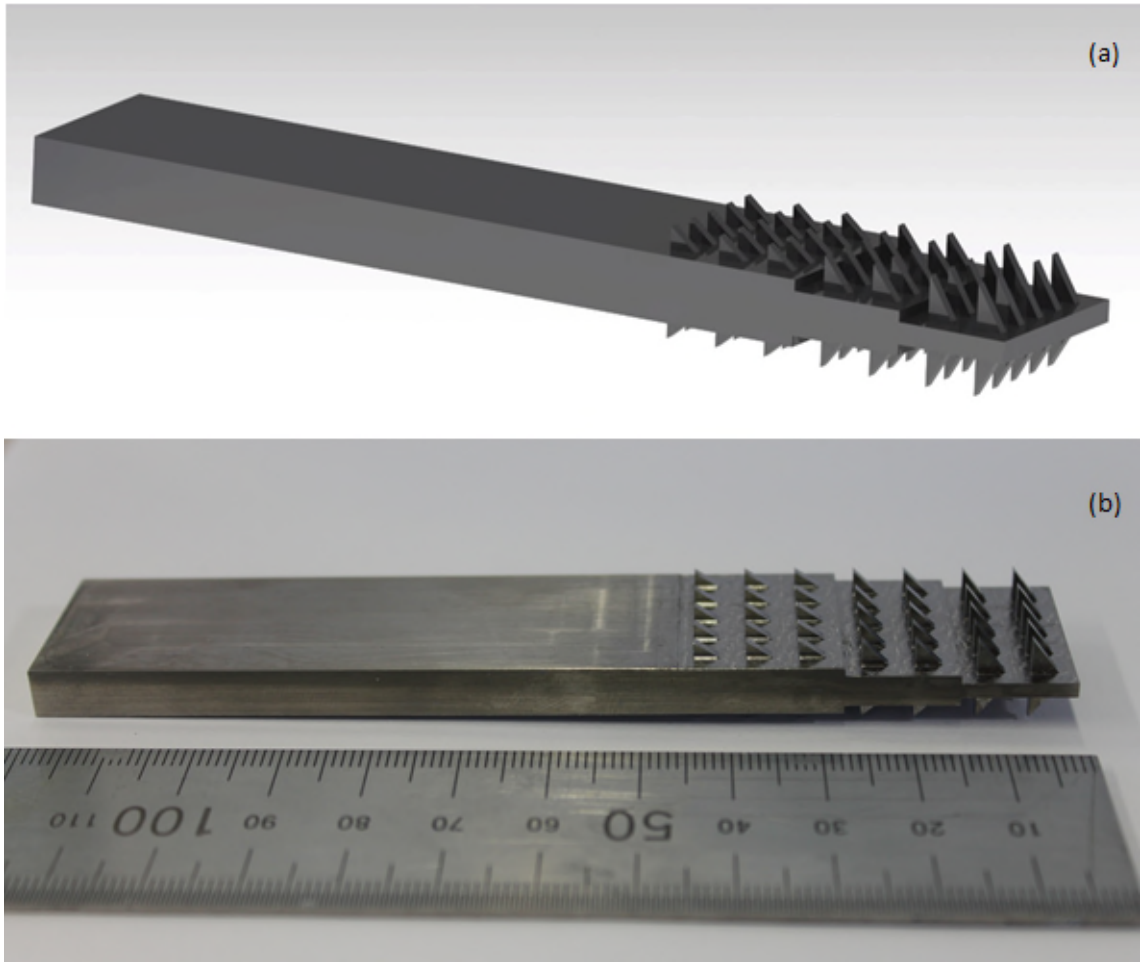

Figure 3-8Double-stepped joint with shark teeth shape pins: (a) 3D CAD image, (b) micro-machined joint

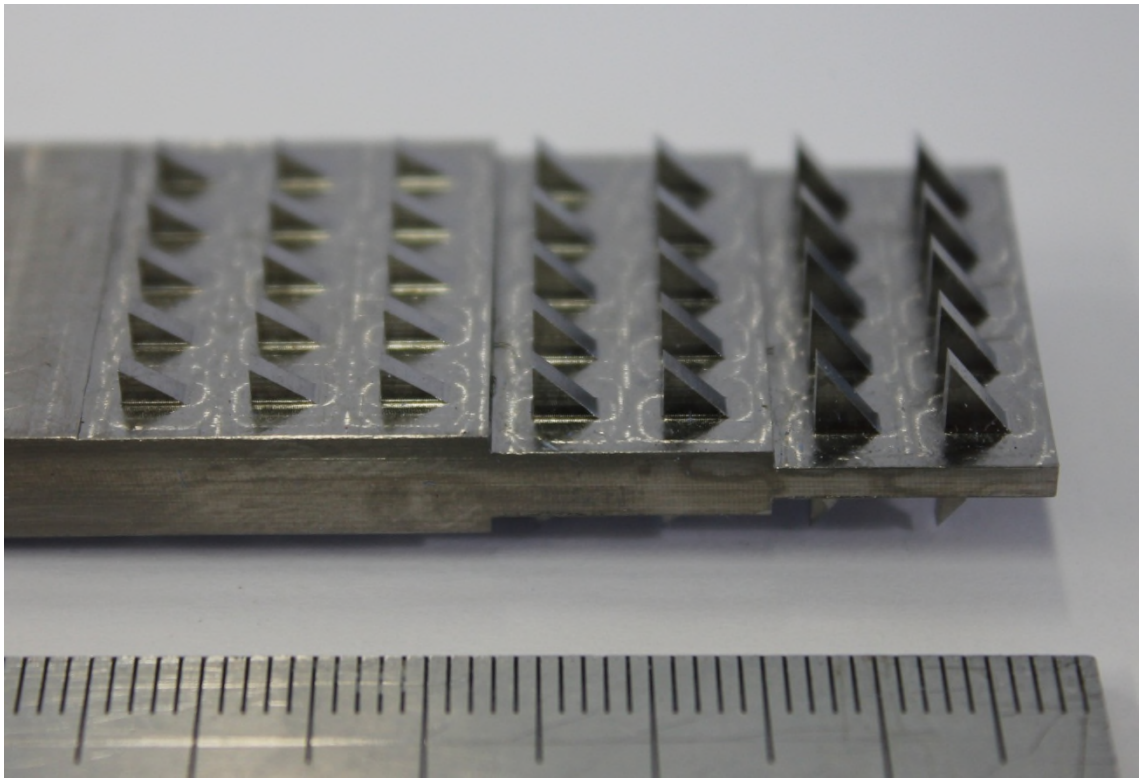

Figure 3-9 Details of double-stepped joint with shark teeth shape pins

3.1.4 Double-Scarf joint with surface features

Figure 3-10 describes the control configuration of a double-scarf joint. The main dimensions of the titanium plate are comparable with the stepped plate described before: the total length is 120 mm, 25 mm width and a variable thickness ranging from the 6 mm of the plate to the spike tip (figure 3-11).

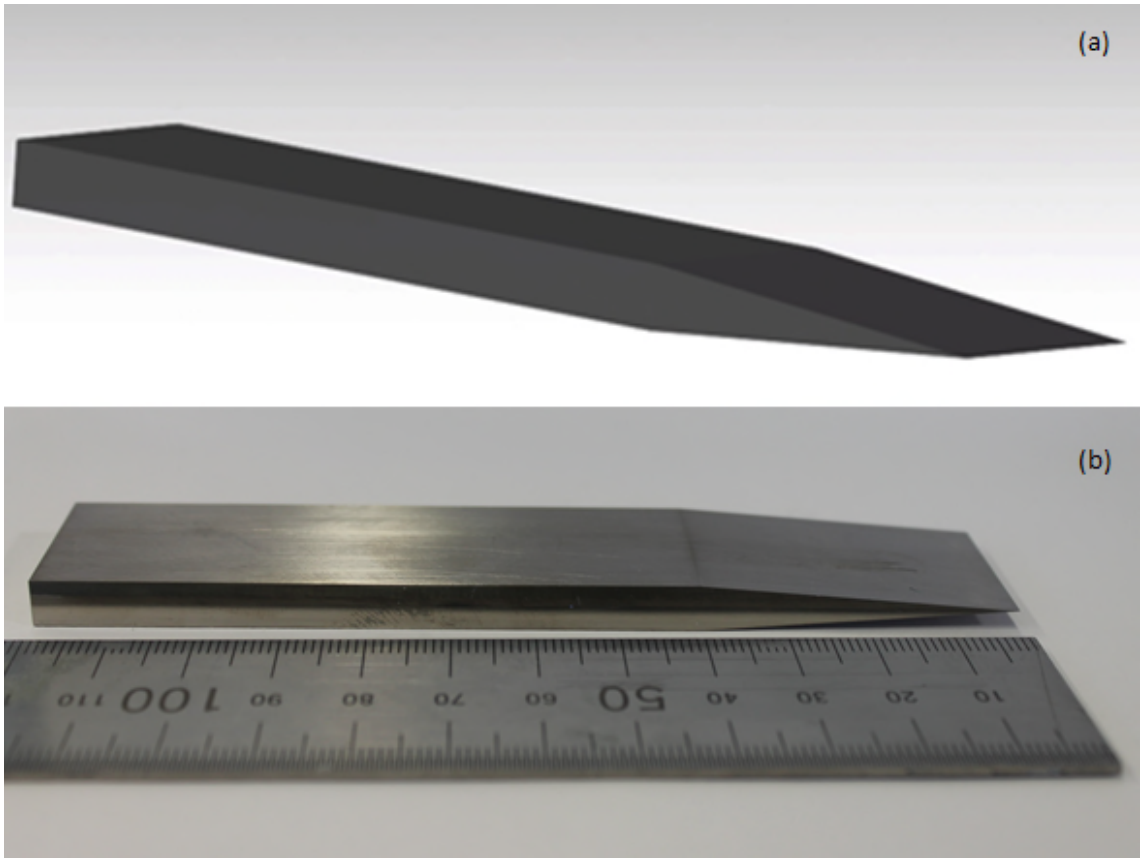

Figure 3-10 Control double-scarf joint: (a) 3D CAD image, (b) micro-machined joint

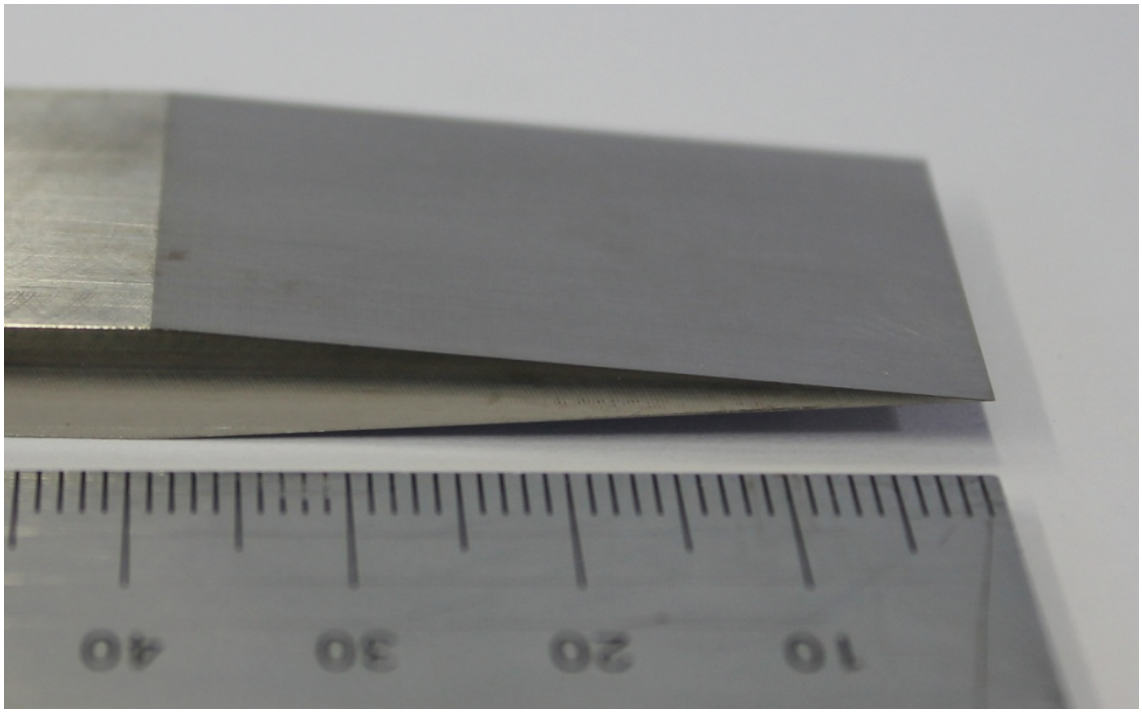

Figure 3-11 Detail of control double-scarf joint

Double-scarf joint with spike pins is described in figure 3-12. The metal reinforcements are arranged in an array of 5 x 7 pins with a pitch of 39.5 x 25 mm. According with the dimension of the stepped plate, this configuration presents the same pin spacing and 1.3 mm pins diameter.

Due to the needed to achieve the same pin height over the entire joint and considering the slope of the joining surface, a gradual variation on pin length from the first row to the tip is provided. The pins are orthogonal to the symmetric axes of the plate providing advantages to the embedding process into the composite (figure 3-13).

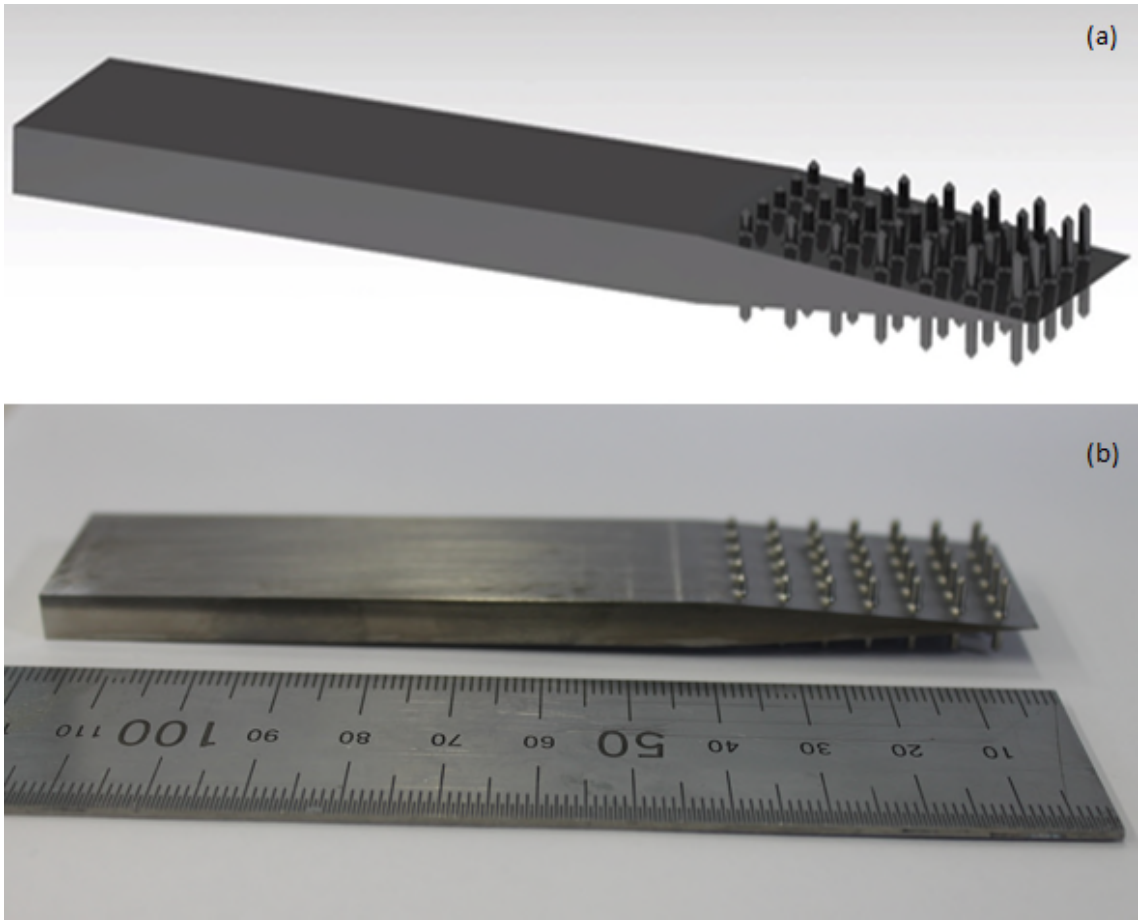

Figure 3-12 Double-scarf joint with spike pins: (a) 3D CAD image, (b) micro-machined joint

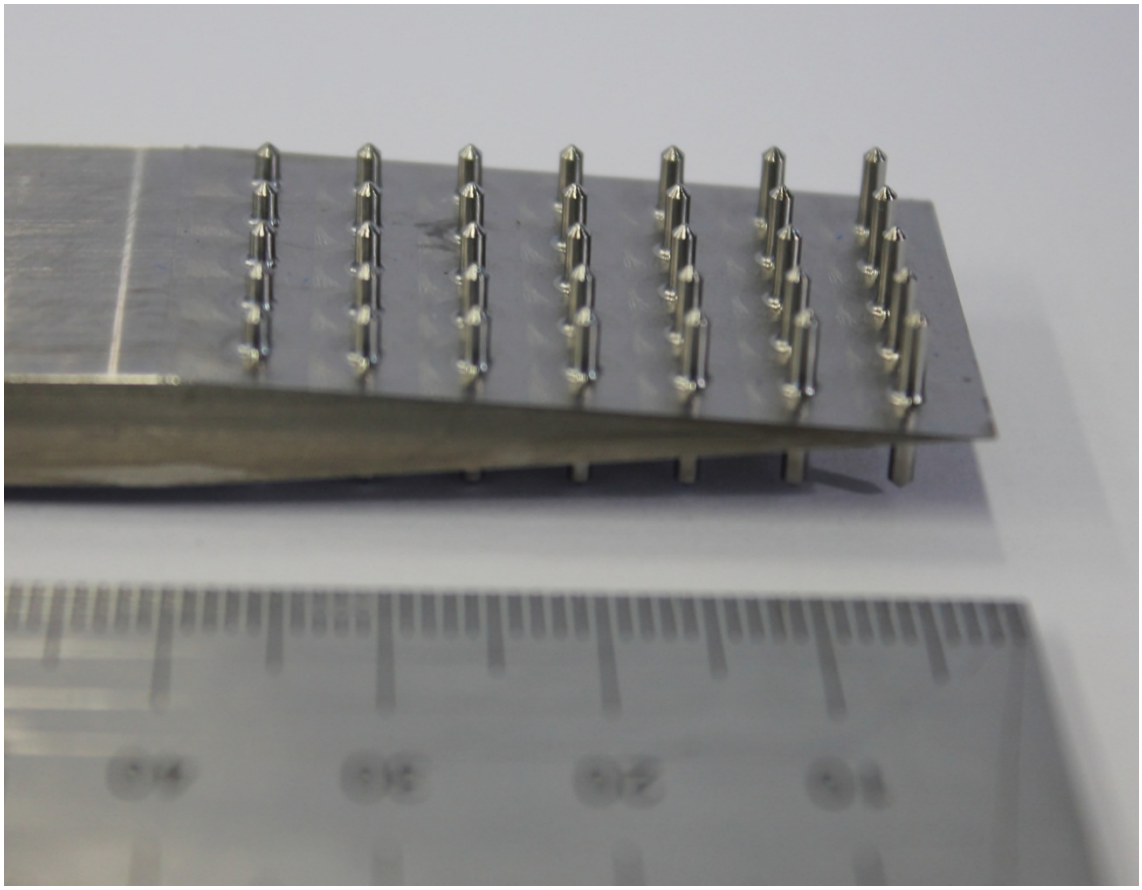

Figure 3-13 Details of Double-scarf joint with spike pins

The shark teeth configuration (figure 3-14) presents the same pin pattern, variable height and orthogonal orientation like the previous scarf configuration with spike pins. The differences are only on the pin shape and dimensions. The shark teeth pins have a 3 mm length base while the thickness is comparable with the pins diameter (figure 3-15).

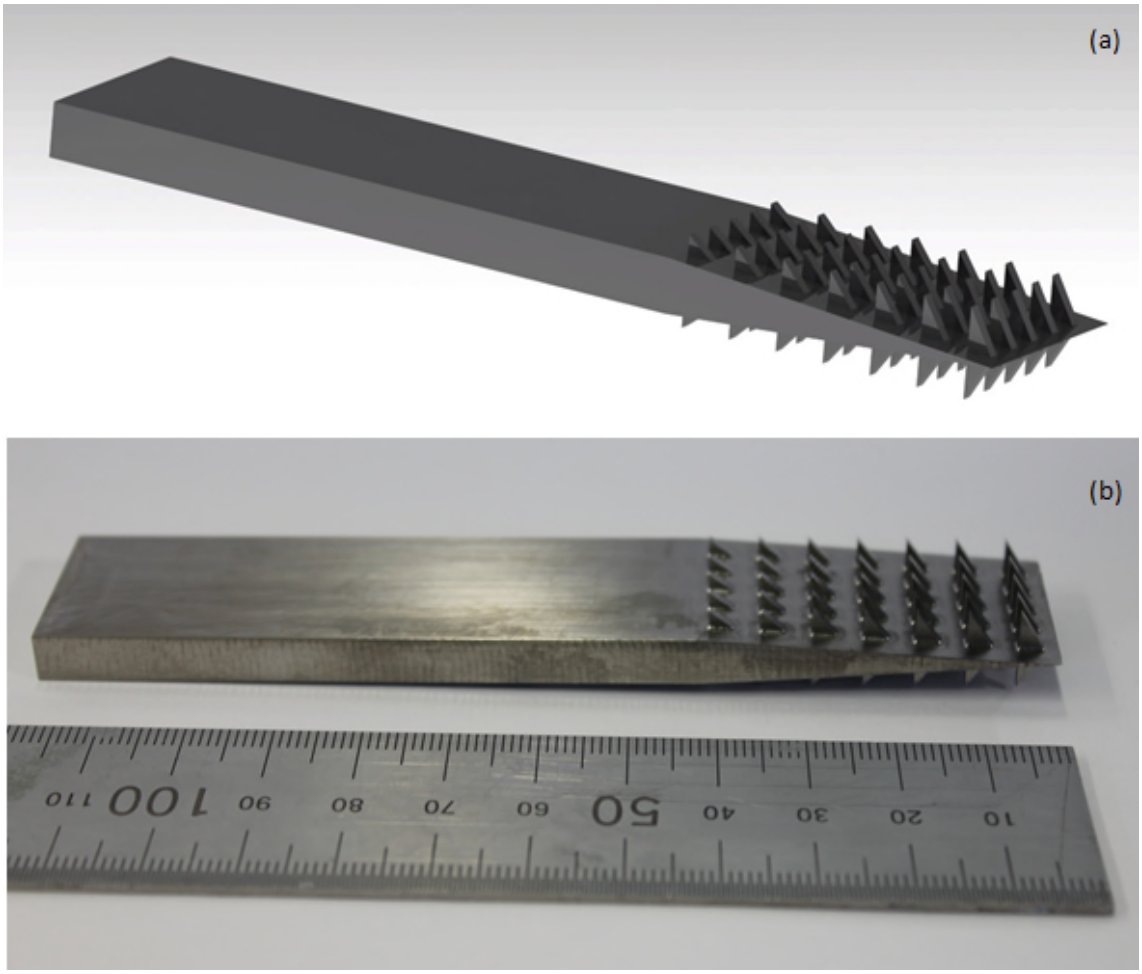

Figure 3-14 Shark teeth double-scarf joint: (a) 3D CAD image, (b) micro-machined joint

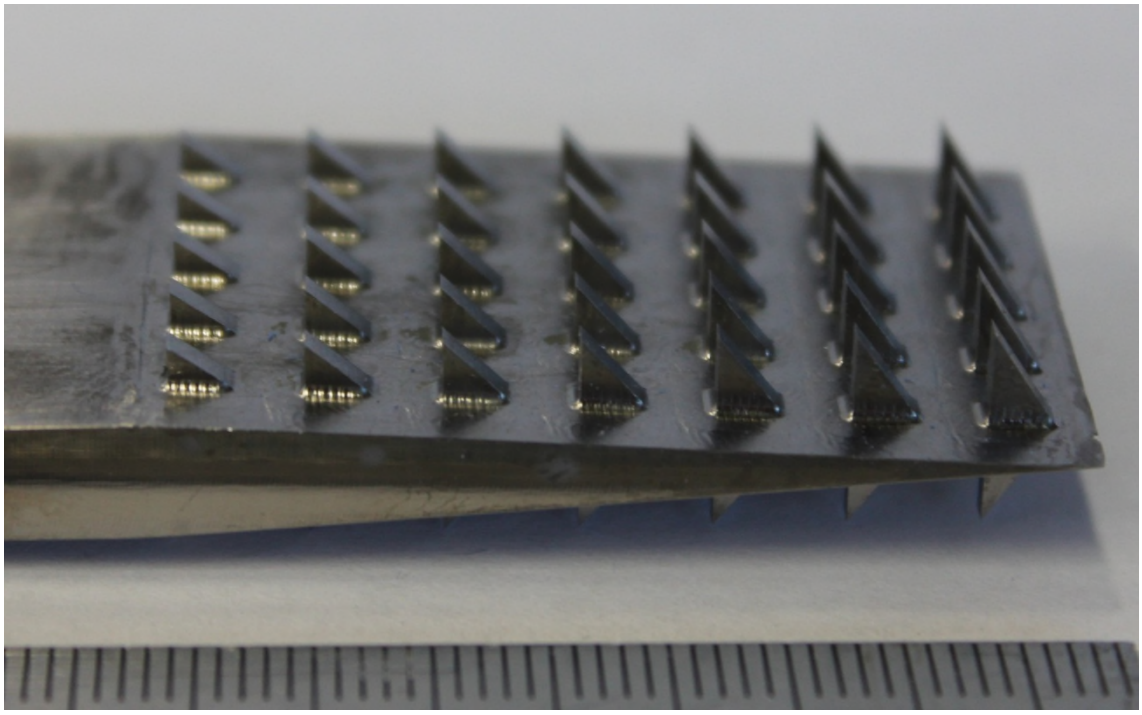

Figure 3-15 Detail of shark teeth double-scarf joint

Moreover, for more details it is possible to refer to Appendix A that contains the CAD drawings and fully describes the geometry of the several configurations proposed.

3.2 Manufacturing process

3.2.1 Lay-up procedure

The lay-up process influences the mechanical properties of the laminate. An accurate procedure is recommended to manufacture the joint.

Due to the symmetry of both plates, double-stepped and scarf, it will be described the procedure for one side of the joint while the other one will be made symmetrically.

To obtain a perfect alignment of the fibres in the different orientations it is recommended to lay-up 4 plies per time and debulk to ensure removal of air trapped during the lay-up process.

For double-stepped lap the lay-up is divided in 4 main parts according with the three steps of the plate and the fillet part. Each part has a different length: the first one corresponding at the first step has a total length of 170 mm and is composed by 10 plies; the second is composed by 4 plies of 144 mm length and is located into the second step while the third one composed by 4 plies of 131 mm length corresponds at the tip step. The fillet part is made with 4 plies of 118 mm length (figure 3-16).

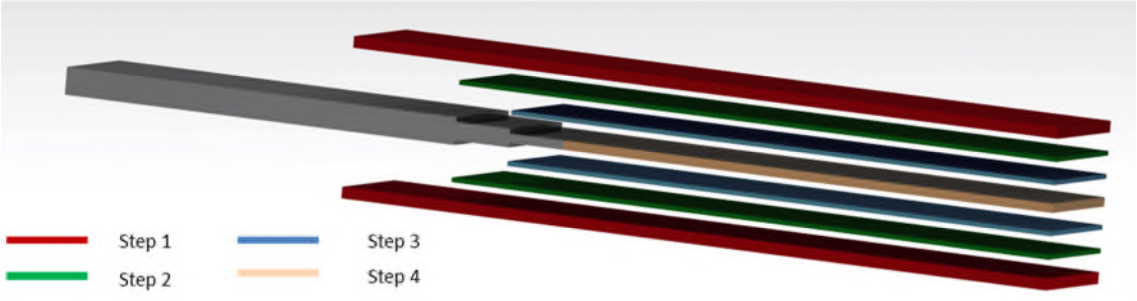

Figure 3-16 Lay-up steps

Compared with the double-stepped, the lay-up procedure for double-scarf joint presents more difficulties and working hours due to the necessity to provide a profile that follows the slope of the metal plate.

To provide this slope each ply is cut at different length, then stacked together 4 plies per time and debulked obtaining several sub-parts comparable with the main parts of the stepped joint. A 0° extra layer is first attached to the metal joint area to ensure a fibre distribution and continuity between the metal surface and the rest of the laminate (figure 3-17).

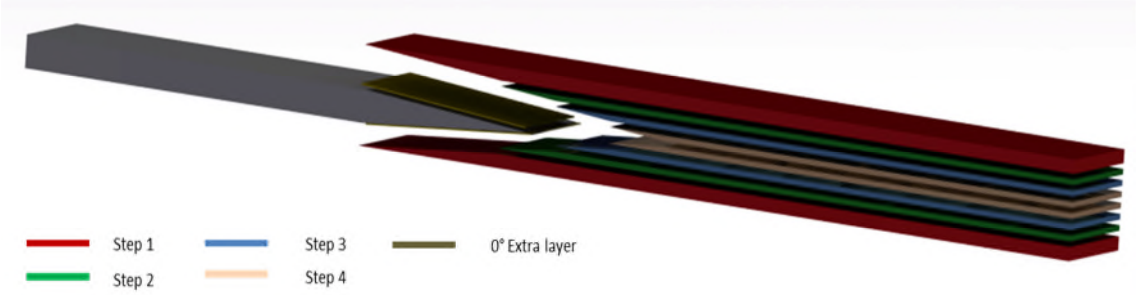

Figure 3-17 Double-scarf lay-up

The final step for both configurations consists of stacking together the sub-parts during the embedding process. This process requires a check on pin insertion to ensure control of fibre alignment and interface matching between metal plate and composite materials.

3.2.2 Metal plate insertion

The challenge is to understand the pin behaviour during joint loading and their contribution to joint strength. Testing of (adhesive bond) released and co-cured joints show respectively the strength of pins only and the strength of the whole bonded and pinned joint.

Because the MM process provides a smooth surface finishes a shot blasting treatment and degrease using acetone are applied to increase the roughness of MM metal fittings.

While for all configurations of co-cured joints the titanium fittings do not require any additional treatment before embedding, to manufacture a released joint (EBM or MM) a PTFE film is attached on the surface of all joint configurations to release the plate. In this way only the pins are locked into the composite and the load of the tensile test is supported only by the pins without any adhesive strength (figure 3-18).

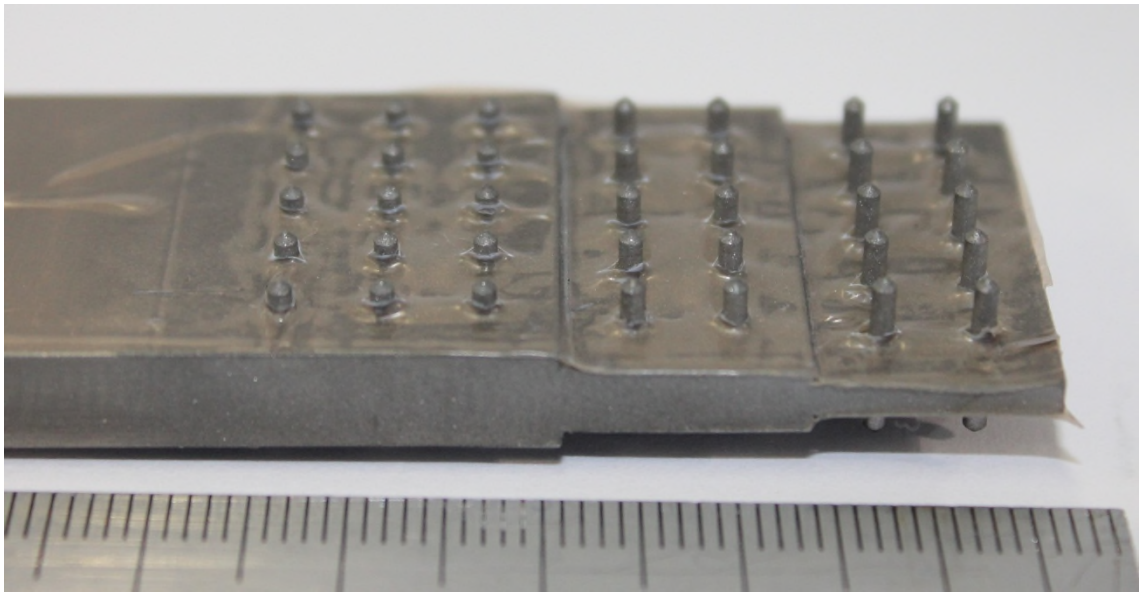

Figure 3-18 Released joint

The titanium plate is embedded into the carbon fibre prepreg by means of an ultrasonic hammer and a gantry system to joint metal to composite (figure 3-19): it applies a pressure on the stacking sequence of pre-pregs, inserting the surface features into the carbon fibre.

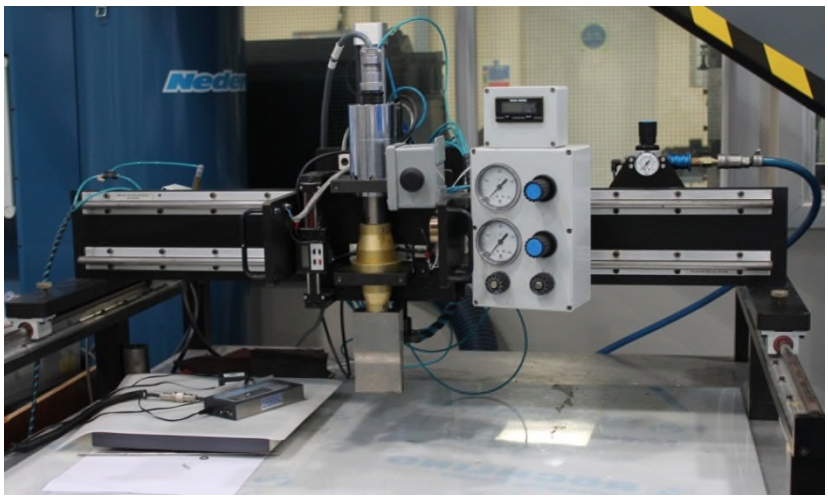

Figure 3-19 Ultrasonic hammer

Before the insertion each sub-part is put in the oven and heated up at the temperature range between 40°C and 50°C to soften the material and facilitate this process.

Moreover, according with the plate geometry, the embedding procedure is developed in several stages proceeding from the tip to the first step of each face of the double-stepped and double-scarf joints (figure 3-20).

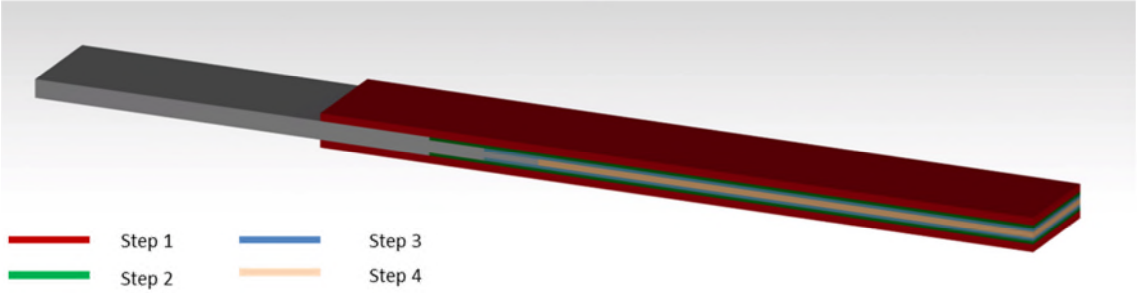

Figure 3-20Plate insertion:embedded plate

3.2.3 Joint Cure

Autoclave processing of the composite is a vacuum bag technique that provides high pressure and high temperature to cure the composite materials.

The composite part is enclosed in a vacuum bag where full or partial vacuum is drawn within the bag. Then, within the autoclave a gas pressure greater than atmospheric is applied on the exterior of the bag exerting mechanical forces on the unconsolidated composite. The high pressure increases the efficiency of transport of volatiles to the vacuum port and causes increased wetting and flow of the resin.

The temperature is raised to initiate cure of polymer reducing the viscosity of the polymer and helping wetting of the reinforcement and consolidation of the composite. The volume of the trapped air and released volatile is reduced proportionally to the applied pressure vacuum at the given temperature [63].

The joints cure process consists of 60 minutes at the temperature of 150 °C and 120 minutes at the temperature of 180 °C with a pressure of 7 bars (figure 3-21).

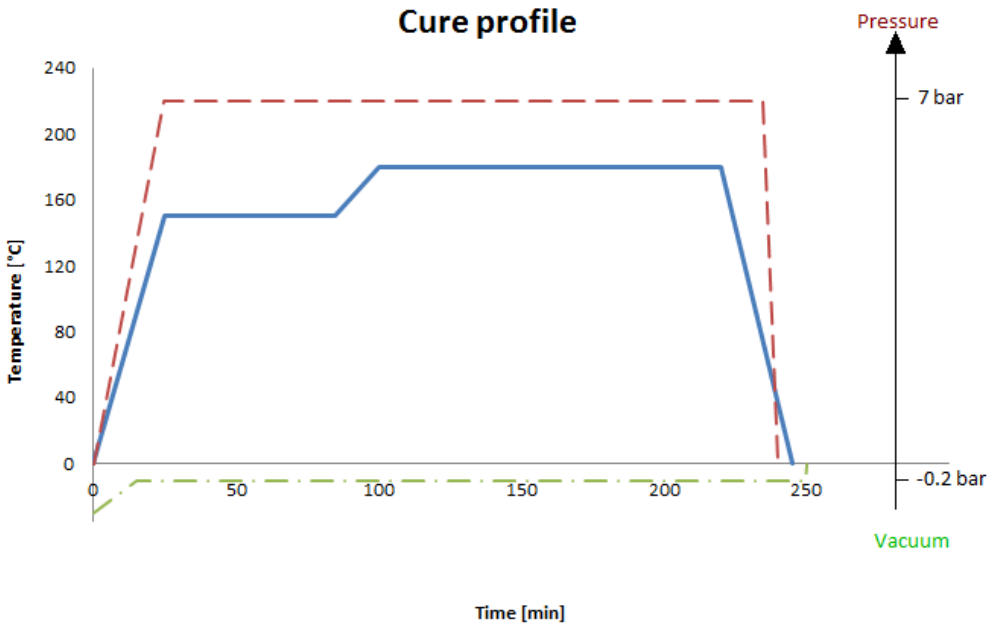

Figure 3-21 Cure profile

The joint is then painted in the thickness dimension to evaluate the strain at the interface between composite and metal plate with DIC analysis. A white paint is used as a background to provide contrast while the facets are made with black paint (figure 3-22). More details on DIC technology are explained in section 4.1.2

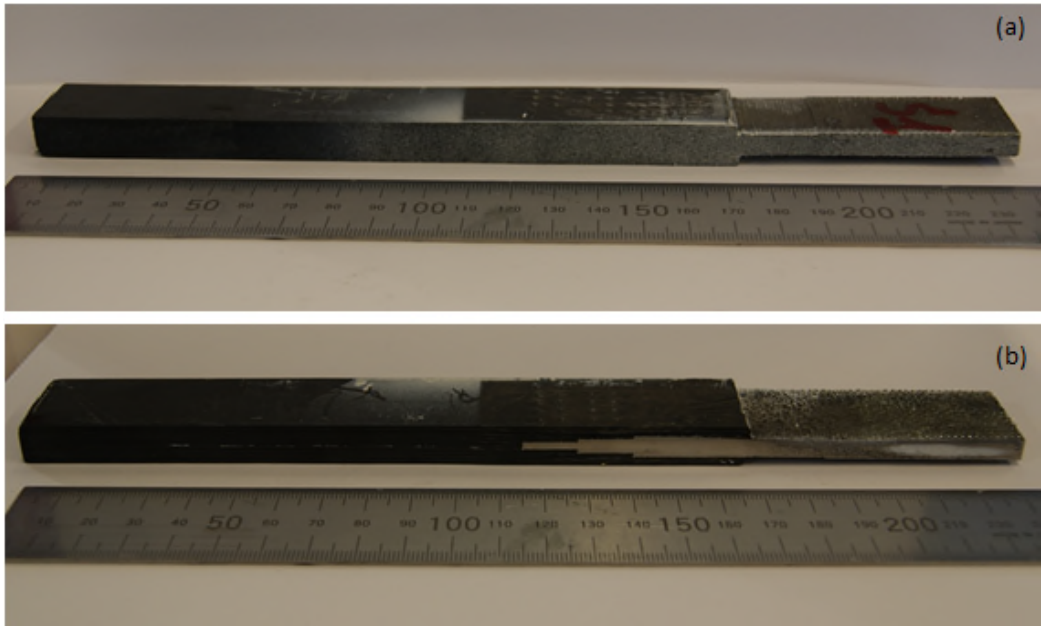

Figure 3-22Cured joint: (a) frontal view, (b) rear view

3.3 Tensile testing

3.3.1 Testing frame setup including test procedure

Tensile testing is carried out using the electromechanical load frame Instron 5500 fitted with a 100 kN load cell. The load on the specimens is driven by the downwards movement of a crosshead at the speed of 1 mm/min. The sample is clamped vertically with the laminate part in the lower grip and the titanium plate in the upper grip.

Two cameras are installed in front of the tensile machine in order to analyse the specimen deformation during the test with the Digital Image Correlation technique. The DIC control system is connected with the Instron system to obtain load and crosshead displacement data (figure 3-23).

More details about DIC technique and setting parameters are explained in Appendix B.

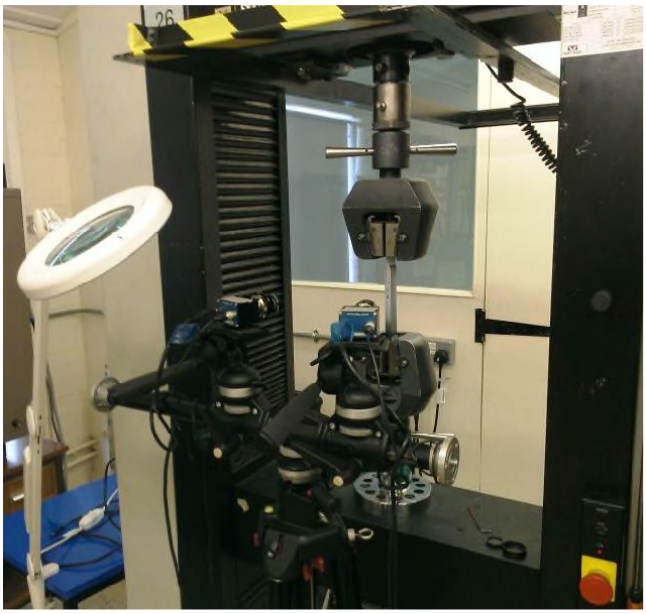

Figure 3-23 Testing frame setup with DIC system

4 RESULTS AND DISCUSSION

4.1 Specimen nomenclature

The specimen is classified with a code of 7 letters that describes the design properties. To explain the classification code consider the code that describes the baseline double-stepped joint C-St.Bc-1.A

The first letter (**C**-St.Bc-1.A) defines the test configuration (table 4-1) highlighting if the test is carried out to evaluate the joint strength (cocured) or the strength of surface features only (released).The following two letters (C-**St**.Bc-1.A) indicate the plate geometry. Three different options are available and summarised in table 4-2: double-stepped, double-scarf and double-lap joint. The second couple of letters (C-St.**Bc**-1.A) describe the surface feature shape: baseline, spike or shark teeth pins (table 4-3). The number in the classification code(C-st.Bc-**1.**A) refers to the different lay-up proposed (table 4-4) while the last letter (C-st.Bc-1.**A**) is used to identify the specimens with the same geometrical characteristics.

Code	Test configuration
R	Released
C	Cocured

Table 4-1Test configuration

Code	Plate description
St	Double-stepped joint
Sc	Double-scarf joint
Dl	Double-lap joint

Table 4-2 Plate design

Code	Pin description
Bc	Control baseline
Sp	Spike pin
Sh	Shark teeth pin

Table 4-3 Pin shape

Code	Lay-up description
1	First lay-up
2	Second lay-up

Table 4-4 Lay-up stacking sequence

4.2 Mechanical test results

4.2.1 Double-Stepped joint-Tensile test result

The baseline control double-stepped joints were tested in tension until failure in order to evaluate the dependence of mechanical properties on the two composite lay-up configurations. The graph in figure 4-1 describes the tensile behaviour of stepped baseline joints. Both prepreg lay-up configurations exhibit the same behaviour: they reach the maximum load and then have a catastrophic failure.

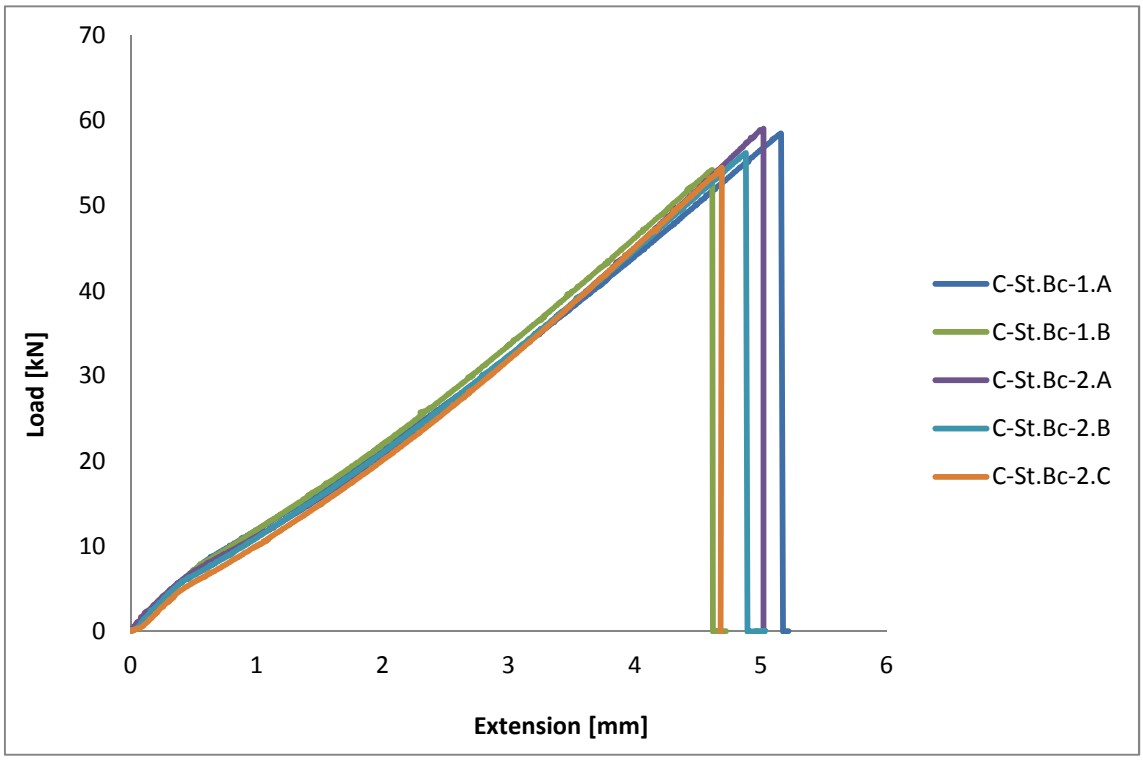

Figure 4-1Baseline double-stepped joint tensile test results

The ultimate load values and the corresponding ultimate tensile strength obtained by the two different configurations are summarised in the following tables (table 4-5, 4-6). The averages of these values are 56.49 kN for the ultimate tensile load and 22.60 MPa for ultimate shear strength respectively.

Joint	Ultimate tensile load [kN]	Ultimate shear strength [MPa]
C-St.Bc-1.A	58.49	23.40
C-St.Bc-1.B	54.22	21.69
C-St.Bc-2.A	59.06	23.62
C-St.Bc-2.B	56.21	22.48
C-St.Bc-2.C	54.46	21.79

Table 4-5 Baseline double-stepped joint tensile results

	Ultimate tensile load [kN]	Ultimate shear strength [MPa]
Average	56.49 ± 2.23	22.60± 0.89

Table 4-6 Summary of double-stepped control results

The small difference in tensile results shown in the table 4-5 is justified by previous work where the dependence of mechanical properties with the number of 0° plies is exposed. Moreover, because this difference in mechanical properties is small and the adhesive strength is more affected by interface fibre orientation; both lay-ups can be selected in terms of bonding strength.

This assumption is confirmed by the analysis of the surface of the metal plates after failure (figure 4-2). In fact the first ply of composite (with the fibre in the load direction) is still attached on the metal plate, showing how the crack is propagated into the composite causing an interplay failure.

This means that there is one free parameter to use in hybrid joint design: it is possible to choose the second lay-up that provides better mechanical performance with metal insertion as suggested by Gay [62].

Once it was selected, all the specimens with surface features were manufactured with this lay-up.

Figure 4-2Baseline double-stepped joint failure

Four co-cured and four released EBM double-stepped joint with spike pins made by Sheffield University (Mercury Centre) are tested in tension to quantify the pin interlocking benefits when compared with the control configuration.

Figure 4-3 shows the results of cocured specimens: the presence of pins increase the strength of joint (75kN compared with the baseline value of 56kN) and a considerable load is achieved before catastrophic failure (table 4-7).

However two tests failed losing the tabs that connect the samples to the machine grips (C-St.St-2.A & C.St.Sp-2.C) at the load of 68 kN without showing any failure in the joint as confirmed even from the microscopy analysis.

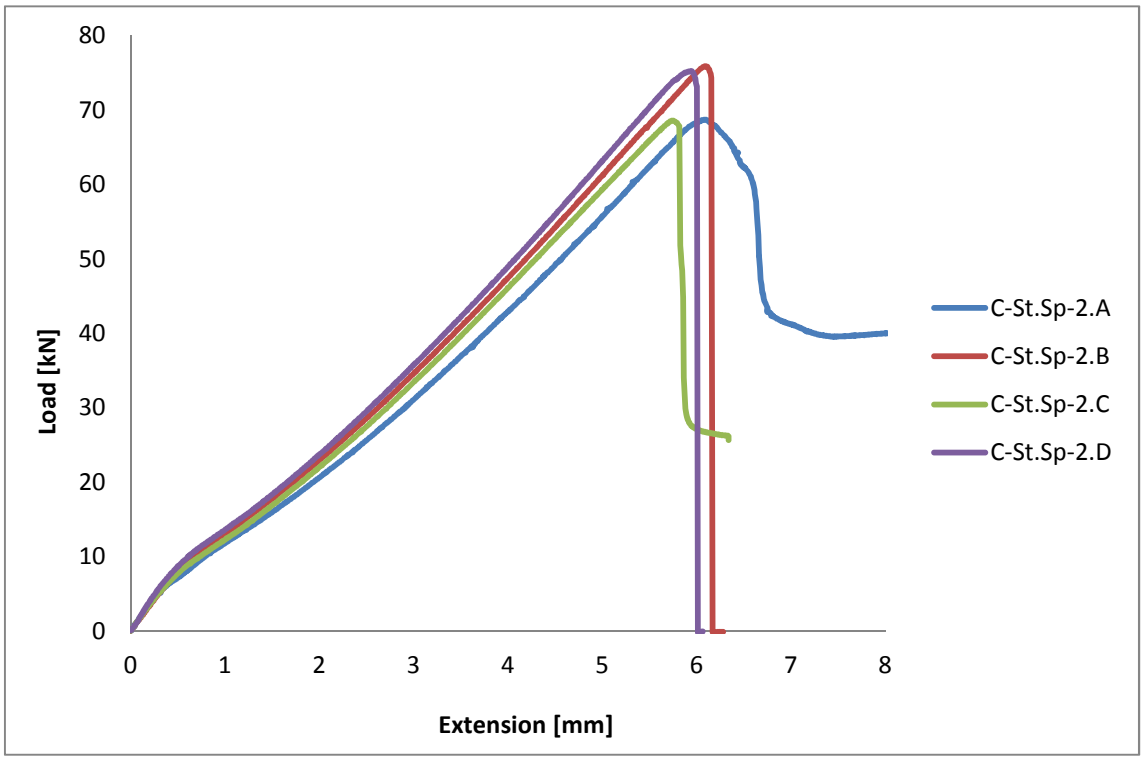

Figure 4-3 Cocured EBM double-stepped joint tensile test results

Joint	Ultimate tensile load [kN]	Ultimate shear strength [MPa]
C-St.Sp-2.A	68.70 (failed)	27.48
C-St.Sp-2.B	75.89	30.36
C-St.Sp-2.C	68.60 (failed)	27.44
C-St.Sp-2.D	75.25	30.10

Table 4-7 Cocured EBM double-stepped joint with spike pins tensile results

The averages of ultimate tensile load and shear strength are revealed in table 4-8. Comparing these results with the same results of the baseline configuration illustrates the benefits of pins: the average of the ultimate tensile load for the

pinned joint (calculated only on the two samples that completed the test) is 75.57kN while the baseline achieves 56.49 kN (table 4-6) which corresponds to an increase of 34 % in joint strength.

	Ultimate tensile load [kN]	**Ultimate shear strength [MPa]**
Average	75.57± 0.46	30.22± 0.18

Table 4-8 Summary of cocured EBM double-stepped joint with spike pins tensile results

Tensile testing carried out on released EBM joints provided results revealed in figure 4-4. Pins are able to support a maximum load of 41.15 kN before catastrophic failure. The consistency of the results is summarised in table 4-9.

Moreover this analysis of the released joint offers additional information to be used during joint design, providing a safety parameter for the composite structure. Because a degree of uncertainty is always present for bonded joints due to the difficulty in assessing the quality of the adhesive joint, the use of pins can provide a lower threshold value where the joint is supposed to fail: the strength of pins only represents this value when it is supposed that the contribution of adhesive strength is equal to zero. For this configuration manufactured with EBM technology the joint shear strength without adhesive contribution corresponds at 16.46 MPa (table 4-10).

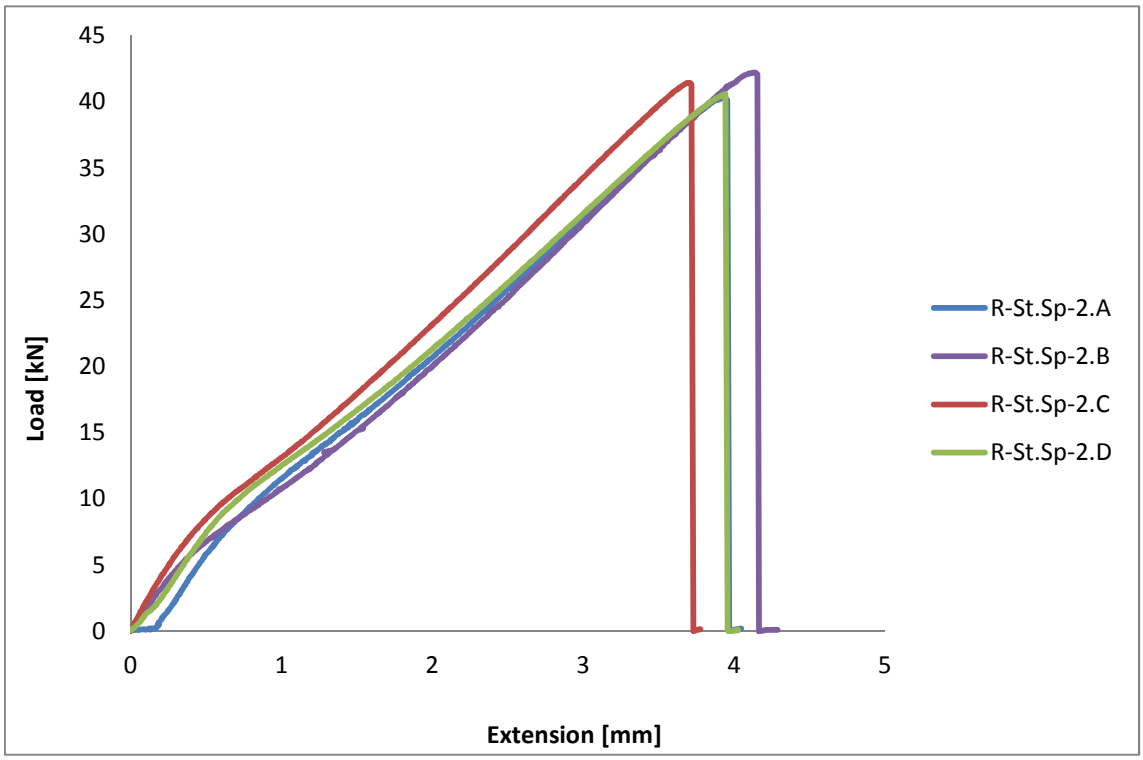

Figure 4-4 Released EBM double-stepped joint tensile test results

Joint	Ultimate tensile load [kN]	Ultimate shear strength [MPa]
R-St.Sp-2.A	40.35	16.14
R-St.Sp-2.B	42.20	16.88
R-St.Sp-2.C	41.44	16.58
R-St.Sp-2.D	40.59	16.24

Table 4-9 Released EBM double-stepped joint with spike pins tensile results

	Ultimate tensile load [kN]	Ultimate shear strength [MPa]
Average	41.15 ± 0.85	16.46 ± 0.34

Table 4-10 Summary of released EBM double-stepped joint with spike pins tensile results

The micro-machined (MM) double-stepped joints made by Nottingham University are tested adopting the same test procedure of the EBM joints. A first batch of 4 cocured MM samples are tested in tension to identify the performance of the joint while a second batch of 4 released MM samples are tested to evaluate the quality of surface features. The results are compared with the same results obtained from EBM joint in order to provide a guideline to select the right manufacturing process for the embedded plate.

The graphic on figure 4-5 describes the behaviour of MM cocured double-stepped joint with spike pins during the tensile test demonstrating a linear increment in the load/extension until catastrophic failure.

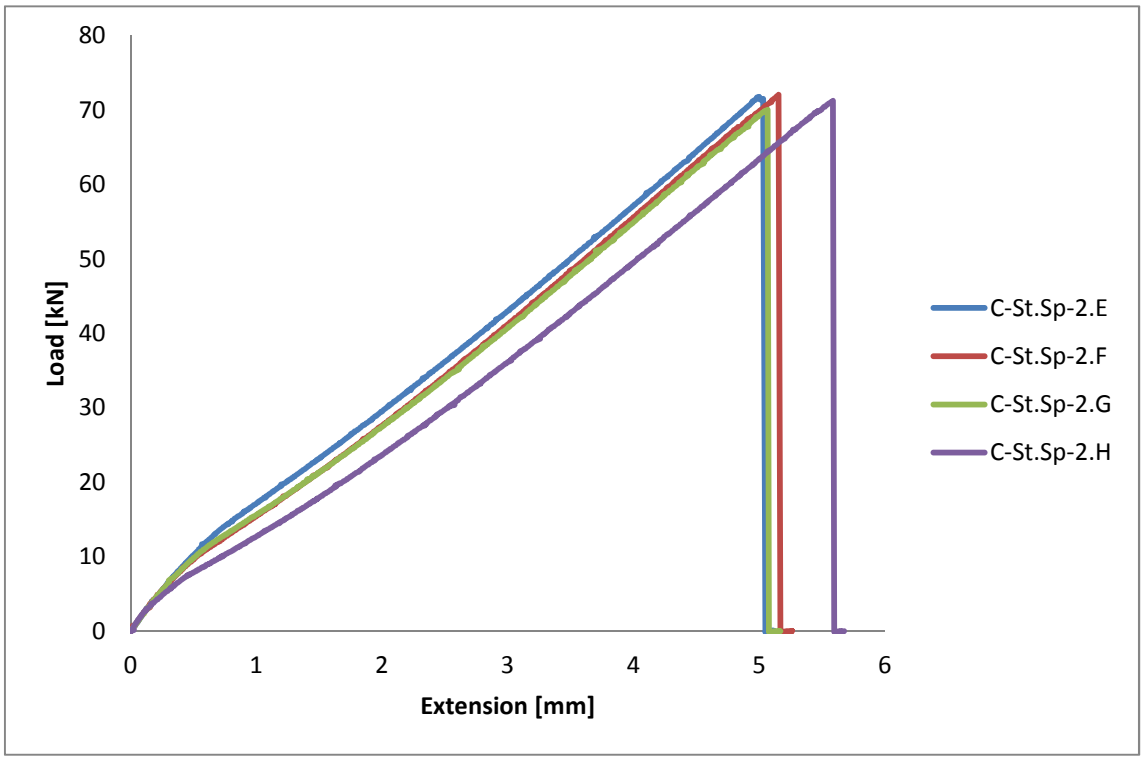

Figure 4-5 Cocured micro-machined double-stepped joint with spike pins

The averages of MM joint mechanical properties are: 71.28 kN maximum load and 28.51 MPa for shear strength (table 4-12). Comparing these results with the mechanical properties of the baseline (table 4-6) the benefits of surface features are underlined with an increase of 26% in failure load.

More interesting deductions are obtained comparing the consistency of MM results (table 4-11) with the results of EBM joint (table 4-7). The maximum load and the shear strength of MM and EBM joints are similar: a difference about only 6% in maximum load (71.28 kN for MM against 75.57 kN for EBM) highlights the principal role of design on joint strength instead of selected manufacturing processes.

Figure 4-6 shows the quality of manufacturing process of double-stepped joint with EBM (figure (a)) and MM (figure (b)) technology. Despite the micro-machining manufacturing process being more accurate in terms of geometric

details when compared with EBM (better surface finishes, better details of surface features such as base fillet, tip shape etc),the mechanical properties are basically the same for both joints because the main dimensions (pin diameters and spacing, plate size, pin length) are comparable in both configurations. This aspect gives two important deductions: first the EBM technology that manufactures parts from metal powder provides a high quality structured part comparable with the wrought product, secondly the manufacturing process (EBM or MM) does not affect joint strength significantly and the process choice can be made on economic grounds (which process is cheapest).

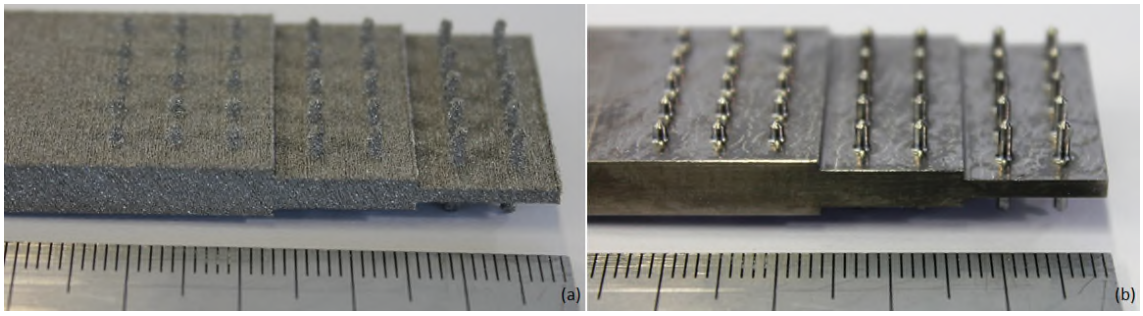

Figure 4-6 (a) EBM double-stepped joint, (b) MM double-stepped joint

Joint	Ultimate tensile load [kN]	Ultimate shear strength [MPa]
C-St.Sp-2.E	71.78	28.71
C-St.Sp-2.F	72.06	28.82
C-St.Sp-2.G	70.05	28.02
C-St.Sp-2.H	71.24	28.50

Table 4-11 Cocured micro-machined double-stepped joint with spike pins tensile results

	Ultimate tensile load [kN]	Ultimate shear strength [MPa]
Average	71.28 ± 0.89	28.51 ± 0.36

Table 4-12 Summary of cocured micro-machined double-stepped joint with spike pins tensile results

The results of released MM joint under tensile loading are revealed in figure 4-7 and table 4-13. The MM pins are able to stand a maximum load of 43.25 kN, that corresponds at total shear strength of 17.30 MPa, before a catastrophic failure (table 4-14).

These results match up to the results obtained for released EBM joints: the slightly higher difference about of 5% revealed for MM pins when compared with the EBM (table 4-10) verified the assumption above that both technologies can be used to manufacture the embedded joints and a more accurate selection can be undertaken based on production factors such as costs and production time.

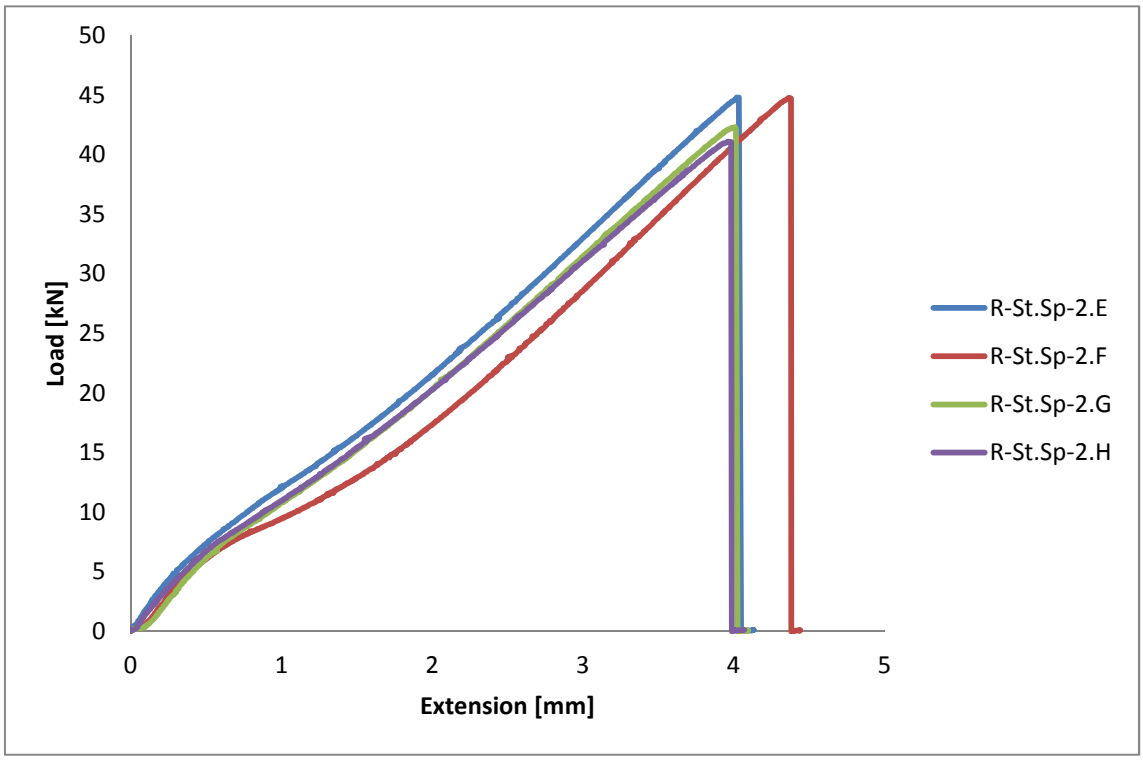

Figure 4-7 Released micro-machined double-stepped joint with spike pins

Joint	Ultimate tensile load [kN]	Ultimate shear strength [MPa]
R-St.Sp-2.E	44.81	17.92
R-St.Sp-2.F	44.76	17.90
R-St.Sp-2.G	42.32	16.93
R-St.Sp-2.H	41.10	16.44

Table 4-13 Released micro-machined double-stepped joint with spike pins tensile results

	Ultimate tensile load [kN]	Ultimate shear strength [MPa]
Average	43.25 ± 1.84	17.30 ± 0.74

Table 4-14 Summary of released micro-machined double-stepped joint with spike pins tensile results

After the evaluation of manufacturing technologies through the analysis of a single joint design presented above, the second aspect investigated is the influence of design concepts on joint strength. The several permutations proposed, all made with MM technology by Nottingham University, are tested under tensile loading.

The MM double-stepped joint with shark teeth pins represents the first permutation tested to quantify the influence of the pins shape on joint properties.

The load/extension curve of cocured MM double-stepped joint with shark teeth is revealed in figure 4-8. These curves can be divided in three main parts: a first one with a linear trend where the load increases, a transition area characterized by several drop/increase of load and the last area with a linear trend until catastrophic failure.

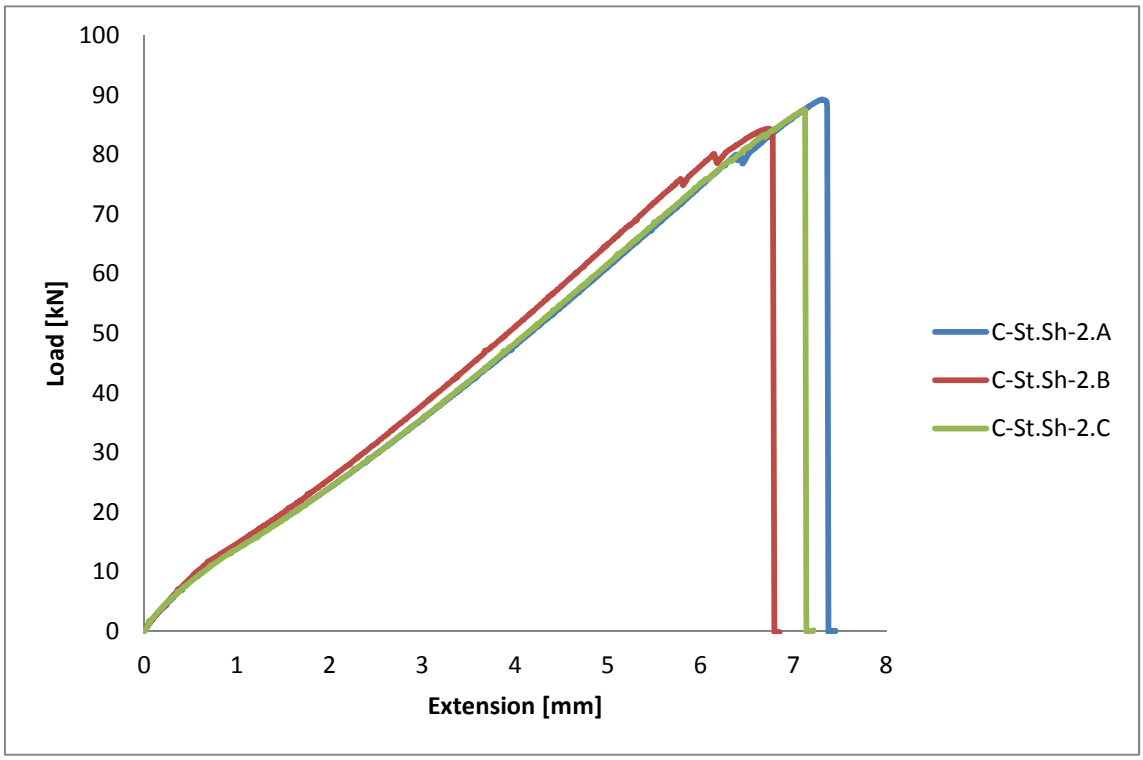

Figure 4-8 Cocured micro-machined double-stepped joint with shark teeth pins

Table 4-15 displays the mechanical properties of these cocured joints underlining the advantages of shark teeth in terms of ultimate load and shear strength.

The cocured double-stepped lap with shark teeth pins, in fact, is able to support a maximum load of 87.08 kN and a shear strength of 34.83 MPa (table 4-16) that corresponds to an increase of 22% on ultimate load of previous double-stepped joint with spike pins (87.08 kN vs 71.28 kN) and an increase of 55% if compared with the baseline (87.08 kN vs 56.49).

Joint	Ultimate tensile load [kN]	Ultimate shear strength [MPa]
C-St.Sh-2.A	89.30	35.72
C-St.Sh-2.B	84.41	33.76
C-St.Sh-2.C	87.53	35.01

Table 4-15 Cocured micro-machined double-stepped joint with shark teeth pins tensile results

	Ultimate tensile load [kN]	Ultimate shear strength [MPa]
Average	87.08 ± 2.48	34.83 ± 0.99

Table 4-16 Summary of cocured micro-machined double-stepped joint with shark teeth pins tensile results

The enhanced mechanical properties of shark teeth pins are illustrated analysing the transition area of the load/extension curve (figure 4-8). However the magnification of one of the sample results (figure 4-9) shows two consistent drops that corresponding at failure of adhesive between metal and composite laminate before the failure of all joint. The first drop is experienced at the same failure load of cocured double-stepped joint with spike pins. It describes the difference in fracture mechanism between spike and shark teeth pins: the spike design is able to support a load up to the point of the failure of the adhesive and the surface features (failure occurs at the same moment) while the shark teeth design, with stronger mechanical interlocking performances, is able to support a higher load even after the failure of the adhesive.

Moreover due the presence of shark teeth pins the failure of the adhesive does not occur in one stage only: the pins modify the load distribution in the plate and the adhesive between two closed pins can resist longer until the second drop

where the load intensity is able to complete the failure of adhesive. This failure mechanism is clearly described by figure 4-10 (a) and (b) that show the failure of the adhesive at interface between the composite and the embedded plate.

At this stage the shark teeth pins of the joint withstand the increasing load until the catastrophic failure characterized by production of sparks due to the high fracture energy released and the friction between the titanium features and the carbon fibre laminate.

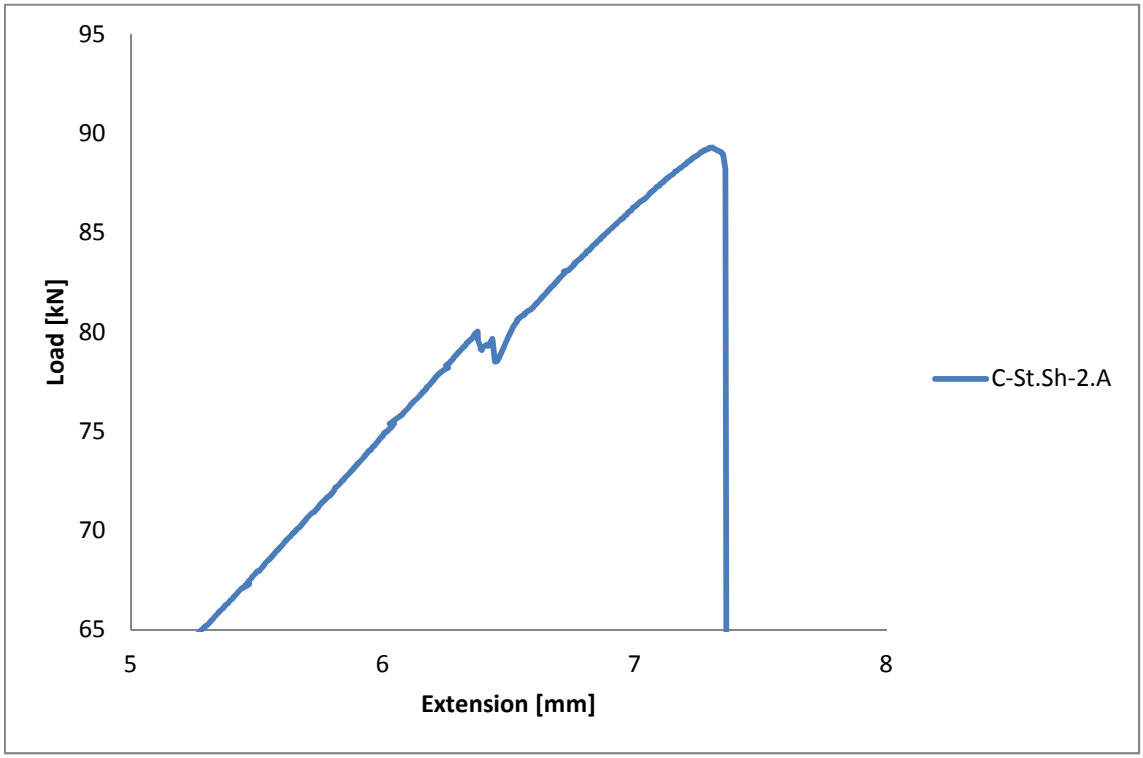

Figure 4-9 Magnification of Cocured micro-machined double-stepped joint with shark teeth pins

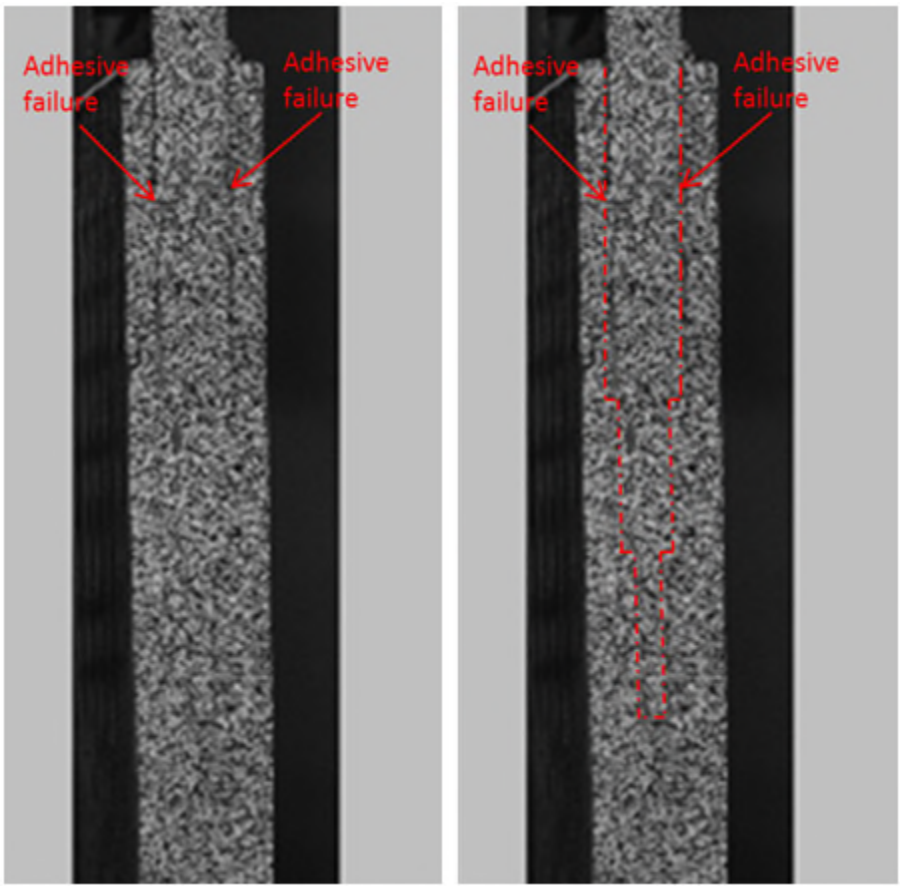

Figure 4-10(a) Adhesive failure on MM joint with shark teeth, (b) overlaid metal plate geometry corresponds at adhesive failure

The load/extension curves of released double-stepped joint with shark teeth pins describe the behaviour of surface features under tensile loading. The linear trend of the curves shows the capability of pins to stand a growing load until catastrophic failure (figure 4-11).

The results on the two samples tested in this configuration are presented in table 4-17. As summarised in table 4-18 the release joint is able to support a tensile load of 79.69 kN before failure. Comparing this result with the same results of cocured joint (table 4-16) with shark teeth pins it is possible to highlight the marginal role of adhesive in the joint strength. In fact the cocured joint can support a maximum load higher by about 9% more than the released one (87.08 vs 79.69). This result confirms the assumption that the shark pins

are able to support the great part of the load and the joint fails after the adhesive failure.

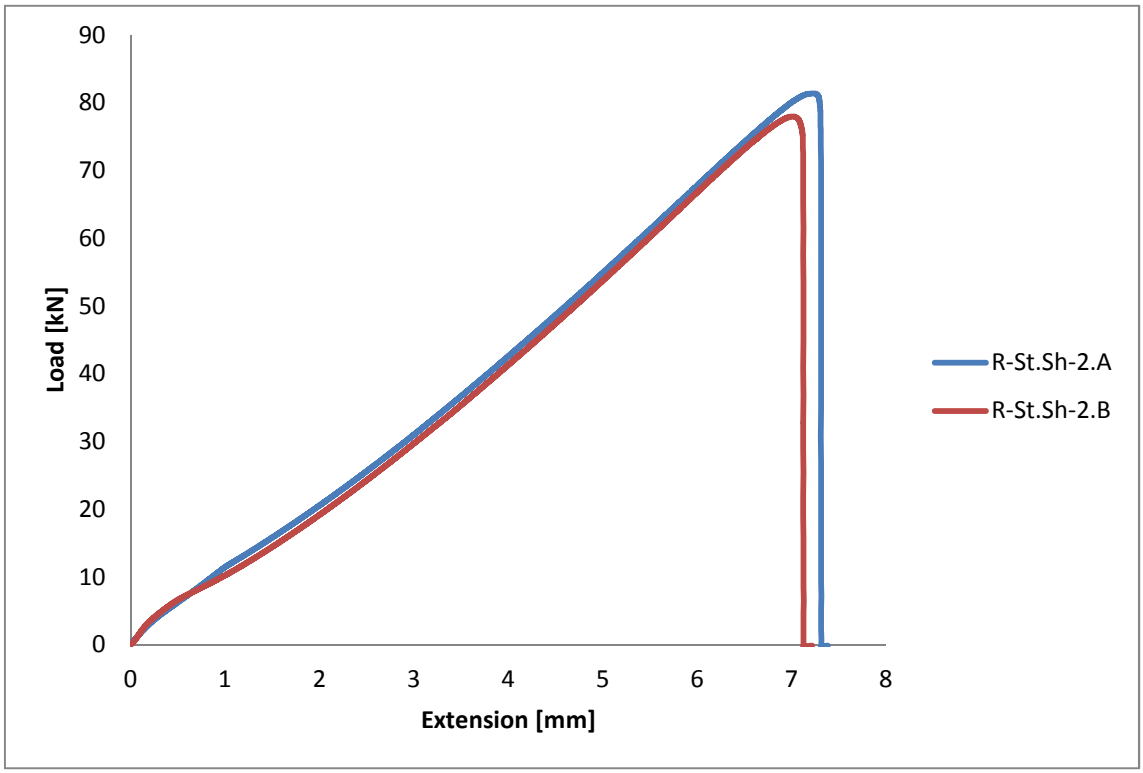

Figure 4-11 released MM double-stepped joint with shark teeth pins testing results

Joint	Ultimate tensile load [kN]	Ultimate shear strength [MPa]
R-St.Sh-2.A	81.40	32.56
R-St.Sh-2.B	78.00	31.20

Table 4-17 Released micro-machined double-stepped joint shark teeth pins tensile results

	Ultimate tensile load [kN]	Ultimate shear strength [MPa]
Average	79.69 ± 2.42	31.88 ± 0.96

Table 4-18 Summary of released micro-machined double-stepped joint shark teeth pins tensile results

The influence of surface feature design on joint strength is enhanced comparing the results of released double-stepped joint with spike pins (table 4-14) with the same joint with shark teeth pins (table 4-18). Because all the other factors are the same (same plate geometry, same lay-up, no influence of bonding process, cured in the same batch)the higher difference in ultimate load is due only on the pin shape. For these reasons the shark teeth pins stand an ultimate load of 79.69 kN compared with the failure load of spike pins (43.25 kN), representing an increase of 84% in ultimate load.

4.2.2 Double-Scarf joint-Tensile test results

It is proposed that the joint strength is the result of plate and surface feature design combination. To investigate the plate design a configuration with double-scarf plate and several surface features are proposed.

Tensile tests are performed on all scarf configurations (baseline, spike pins and shark teeth pins) to evaluate the dependence of mechanical properties on the design concepts.

The figure 4-12 shows the behaviour of the baseline double-scarf joints until failure: all the samples reached the maximum load (table 4-19) and experienced a catastrophic failure.

The averages of values for this configuration without any additional surface features are about 46.84 kN for ultimate load of and 18.73 MPa for shear strength respectively (table 4-20).

This double-scarf joint configuration, if compared with the double-stepped baseline joint, shows lower mechanical properties (46.84 kN instead of 56.49 kN) due to the lay-up procedure. The necessity to provide a slope comparable with the same slope of the metal plate increases the numbers and dimensions of resin rich channels in proximity of the joining area, between the extra layer at 0 degree attached on the metal surface and the rest of the laminate (figure 3-17). However the joint under tension fails exactly at interface between the layer at 0 degree and the rest of the composite laminate (figure 4-13) where these weaker points are located.

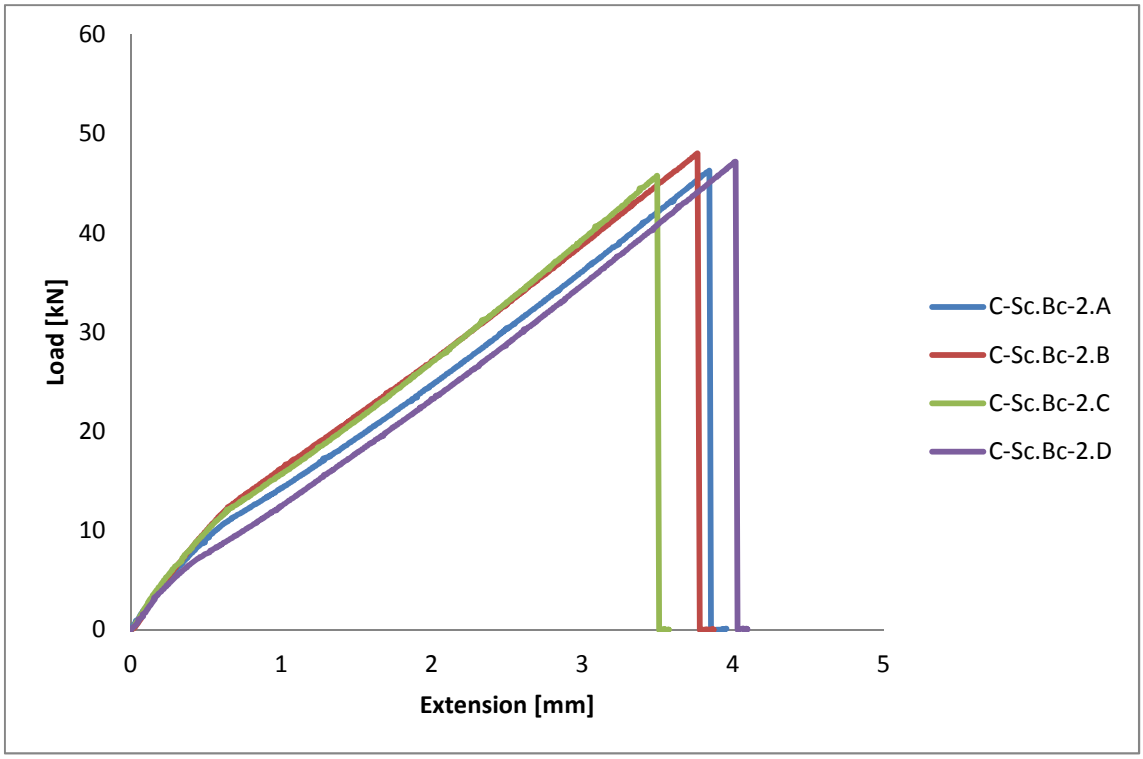

Figure 4-12 Baseline micro-machined double-scarf joint

Joint	Ultimate tensile load [kN]	Ultimate shear strength [MPa]
C-Sc.Bc-2.A	46.32	18.53
C-Sc.Bc-2.B	48.04	19.22
C-Sc.Bc-2.C	45.78	18.31
C-Sc.Bc-2.D	47.21	18.88

Table 4-19 Baseline double-scarf joint tensile results

	Ultimate tensile load [kN]	Ultimate shear strength [MPa]
Average	46.84 ± 0.99	18.73 ± 0.40

Table 4-20Summary of double-scarf control joint results

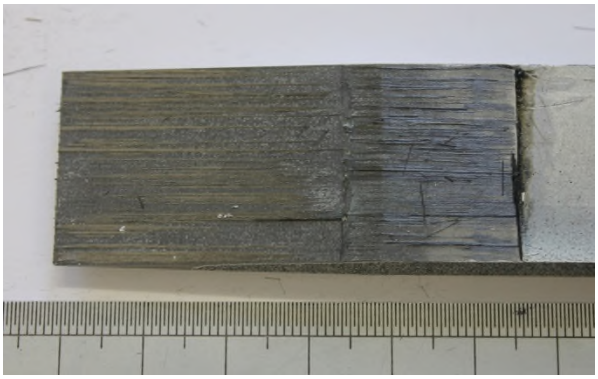

Figure 4-13Baseline double-scarf joint failure

Three co-cured and two released MM double-scarf joint with spike pins are tested in tension to quantify the pin interlocking benefits when compared with the control configuration (figure 4-14).

Table 4-21 describes the results of the tensile tests on cocured specimens. The average of failure load is 70.31 kN (table 4-22) compared with the corresponding value of double-stepped configuration (table 4-12) reveals a difference about 1%.

This result confirms how joint strength depends on pins geometry: although the scarf baseline is weaker than the double stepped baseline, the use of spike pins in both configurations allowed them to achieve the same maximum load. It means that despite a dissimilar load distribution in the joining area, due to the different plate design, the pins are able to support this higher load while the role of the plate design is eclipsed.

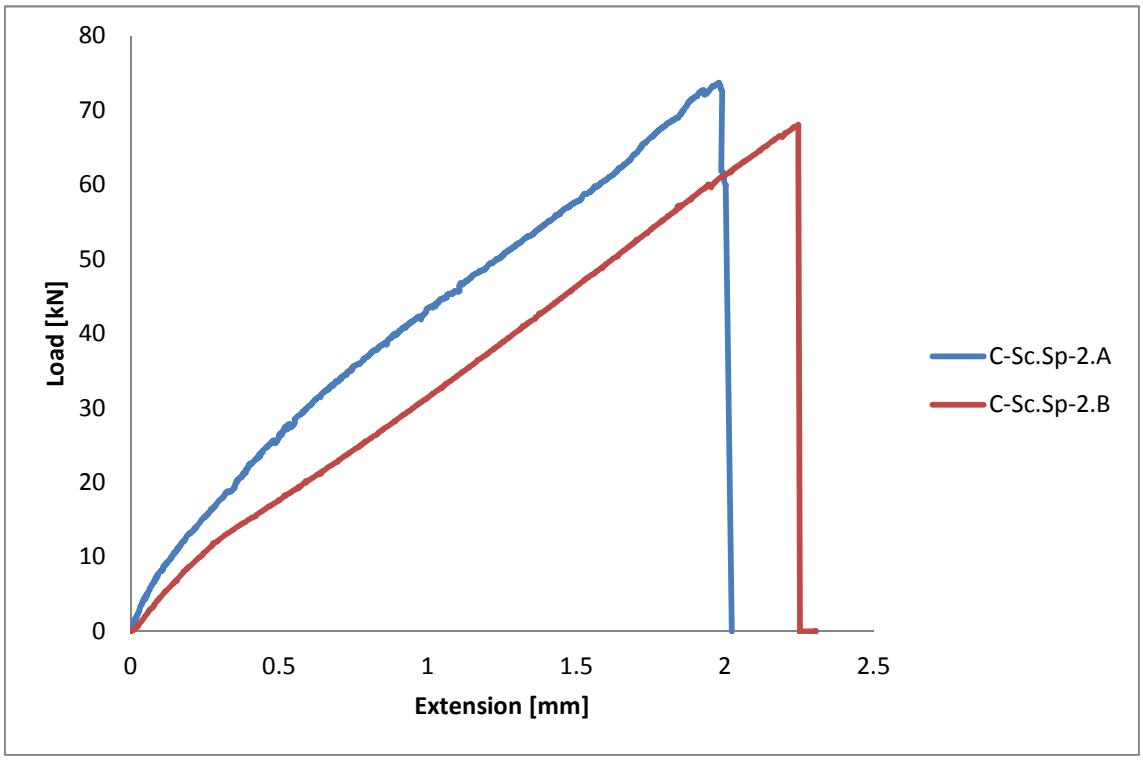

Figure 4-14Cocured micro-machined double-scarf joint with spike pins

Joint	Ultimate tensile load [kN]	Ultimate shear strength [MPa]
C-Sc.Sp-2.A	73.61	29.44
C-Sc.Sp-2.B	68.07	27.23
C-Sc.Sp-2.C	69.26	27.70

Table 4-21 Cocured micro-machined double-scarf joint with spike pins tensile results

	Ultimate tensile load [kN]	Ultimate shear strength [MPa]
Average	70.31 ± 2.92	28.12 ± 1.17

Table 4-22 Summary of cocured micro-machined double-scarf joint with spike pins tensile results

The figure 4-15 describes the behaviour of released double-scarf joint with spike pins. The curves behaviour present the same trend revealed in the other released configuration with spike pins.

However mechanical performance of these released joint are highlighted in table 4-23. The released configuration is able to withstand a maximum load of 46.39 kN before failure.

Comparing this result with the other released configurations with spike pins (table 4-14 & 4-10) a small difference in maximum load about 7% is obtained. This higher value in joint strength for the double-scarf configuration (46.39 kN vs 43.25 kN for MM and 41.15 kN for EBM double-steeped) is expected and confirms that a scarf design reduces the peel stress.

This confirms the consistency of the dissimilar manufacturing processes and the dependence of pin strength on pin shape and geometry.

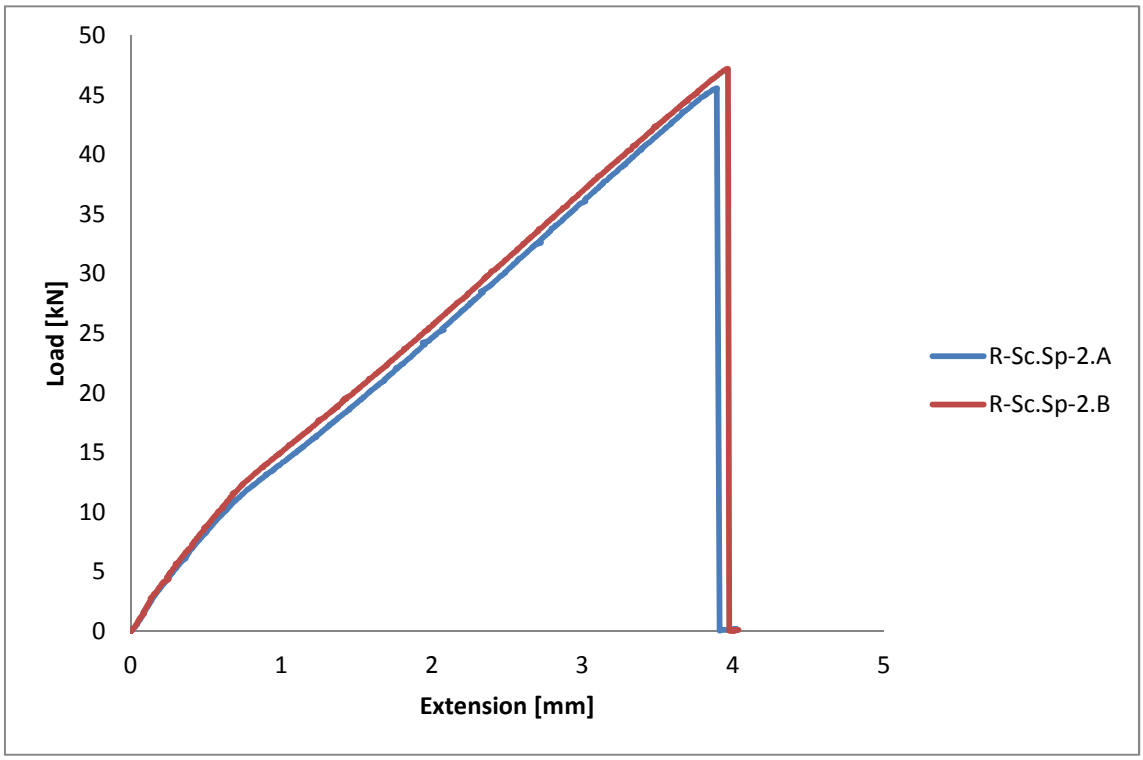

Figure 4-15 Released micro-machined double-scarf joint with spike pins

Joint	Ultimate tensile load [kN]	Ultimate shear strength [MPa]
R-Sc.Sp-2.A	45.57	18.23
R-Sc.Sp-2.B	47.21	18.88

Table 4-23 Released micro-machined double-scarf joint with spike pins tensile results

	Ultimate tensile load [kN]	Ultimate shear strength [MPa]
Average	46.39 ± 1.16	18.57 ± 0.46

Table 4-24 Summary of released micro-machined double-scarf joint with spike pins tensile results

The double-scarf with shark teeth pins represents the last joint configuration proposed. The following section shows the results of the two cocured and two released joint tested.

The cocured joints have behaviour similar to the cocured double-stepped configuration with the same surface features. The fracture mechanism of the joint is divided in two main steps: a first one characterized by the debonding of the interface between metal and the second one with the failure of the joint. The adhesive failure occurs at the same load of the cocured stepped and seems to be related on the mechanical properties of the resin (figure 4-16). Moreover, after adhesive failure, the shark teeth pins support the increasing load until the failure.

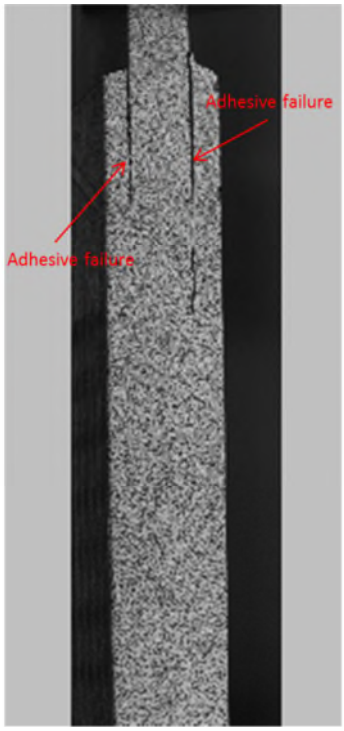

Figure 4-16 Adhesive failure on double-scarf joint with shark teeth pins

Table 4-25 shows the results of tensile tests. The first sample tested (C-Sc.Sh-2.A) achieved the limit of the mechanical facilities and the test was stopped before the sample failure.

To verify the ultimate load failure of this configuration a 250 kN tensile machine is used for samples C-Sc.Sh-2.B and C-Sc.Sh-2.C (figure 4-17).The average of failure load (evaluated only with the last two joints tested) provides a value of 105.00 kN (table 4-26).Comparing this result with the corresponding double-stepped joint (105 vs 87.08 kN) the increase of 20% in ultimate load shows how for high loading condition a better stress distribution (obtained with the scarf plate design) can improve the mechanical properties of the joint.

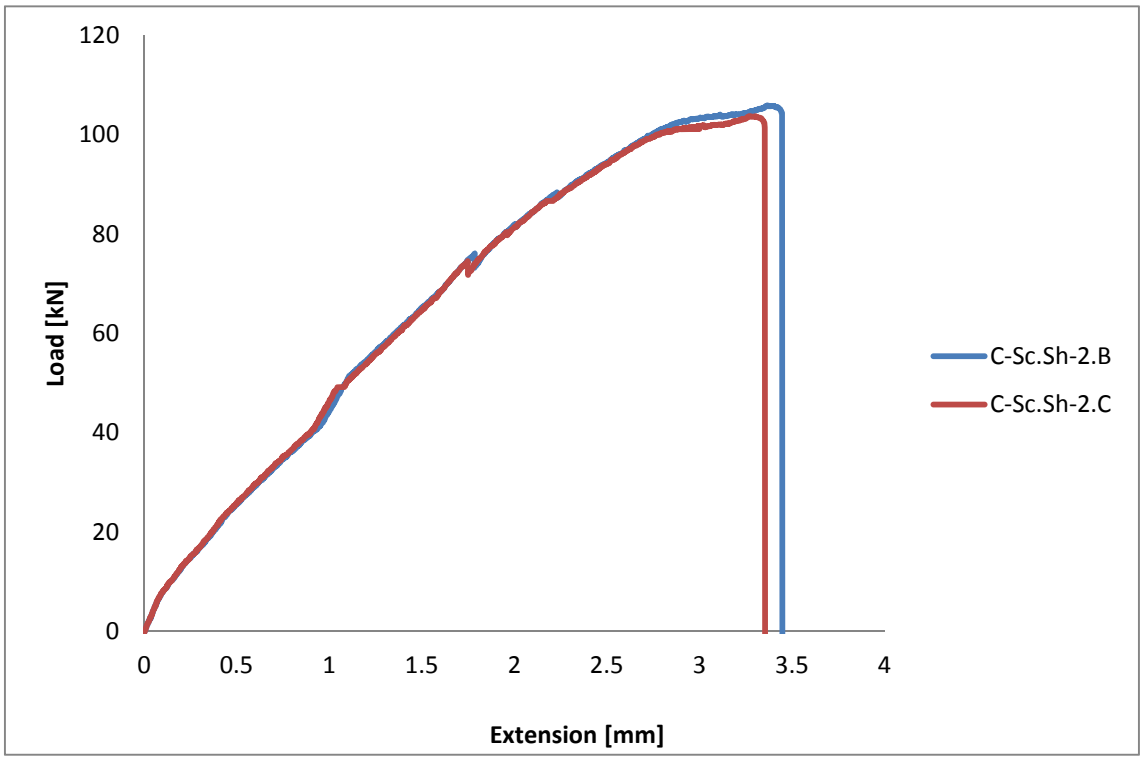

Figure 4-17 Cocured micro-machined double-scarf joint with shark teeth pins

Joint	Ultimate tensile load [kN]	Ultimate shear strength [MPa]
C-Sc.Sh-2.A	97.94	39.18
C-Sc.Sh-2.B	105.91	42.36
C-Sc.Sh-2.C	104.08	41.63

Table 4-25 Cocured micro-machined double-scarf joint with shark teeth pins tensile results

	Ultimate tensile load [kN]	Ultimate shear strength [MPa]
Average	105.00 ± 1.29	41.06 ± 1.67

Table 4-26 Summary of Cocured micro-machined double-scarf joint with shark teeth pins tensile results

Testing the released double-scarf joint it is confirmed the role of the metal plate at high load (figure 4-18). This assumption is confirmed by results presented in table 4-27. The failure load of 91.77 kN for the released configuration with double-scarf plate represents an increase of 15% on joint strength when compared with the double-stepped joint. The better load distribution provided by a scarf design, in fact, allows the joint to achieve a higher load before failure, presumably because the peel stress has been reduced.

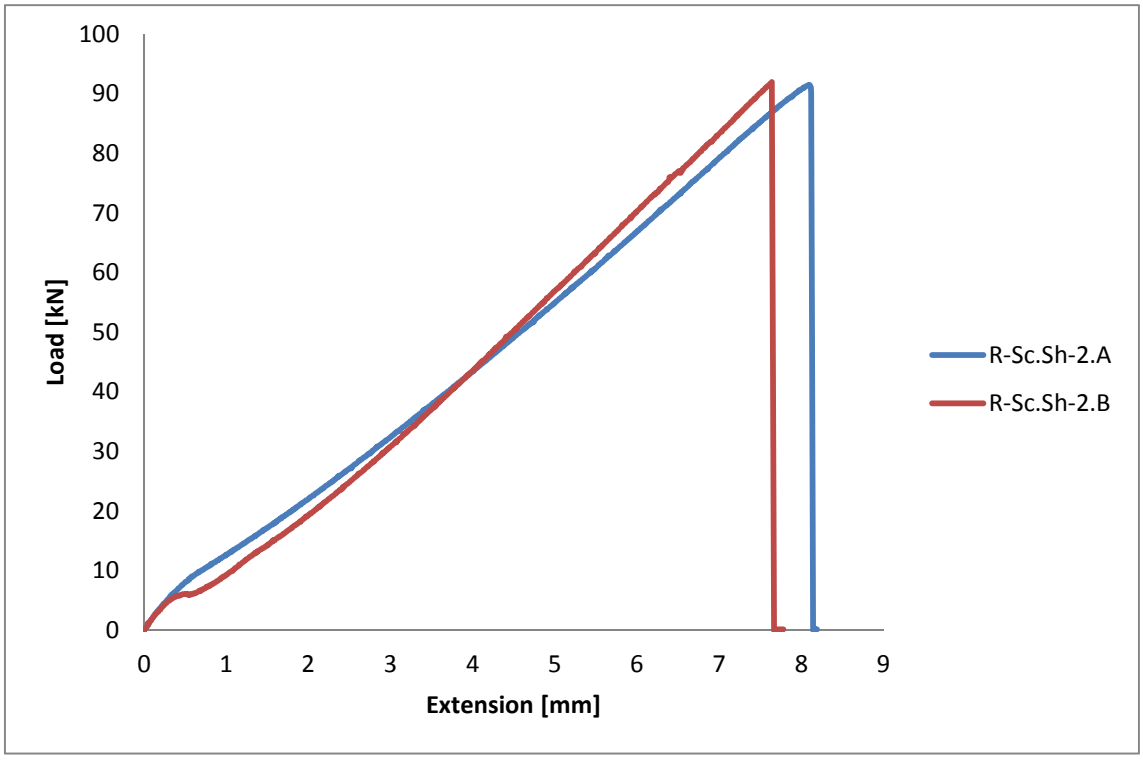

Figure 4-18 Released micro-machined double-scarf joint with shark teeth pins

Joint	Ultimate tensile load [kN]	Ultimate shear strength [MPa]
R-Sc.Sh-2.A	91.54	36.62
R-Sc.Sh-2.B	92.00	36.80

Table 4-27 Released micro-machined double-scarf joint with shark teeth pins tensile results

	Ultimate tensile load [kN]	Ultimate shear strength [MPa]
Average	91.77 ± 0.33	36.71 ± 0.13

Table 4-28 **Summary of released micro-machined double-scarf joint with shark teeth pins tensile results**

4.3 Digital Image Correlation (DIC)

4.3.1 DIC analysis for double-stepped joint

Digital Image Correlation is used as a non-contact method for measuring deformation and strain. It is used in this work to identify the regions in the joint which exhibit higher strains and hence determine the main failure mechanism. Relevant considerations on the control double-stepped joint failure are obtained analysing the DIC results at loading failure.

Figure 4-19 shows the local strain across the joint (in the main directions X and Y) at the ultimate load of 58.50 kN and provide more details to understand the failure mechanism of the joint.

As expected, the main factor that involves the joint failure is represented by local strain in the X direction where a maximum value of 130 mm/m is achieved. This local strain (peel) is higher at the edges of the overlaps while across the body of the sample no relevant changes are highlighted.

Moreover, the maximum value of local strain in the Y direction (45 mm/m) is three times lower than the component in the X axis: the areas with higher values on Y direction are the tip and the thresholds of the steps due to the discontinuity between the metal plate and the carbon fibre (figure 4-19(b)).

This analysis confirms how the failure mechanism of the unpinned joint is mostly related to peel stress: the crack, due to the peel opening mechanism, moves instantaneously from the edge across the joint causing a catastrophic failure.

Moreover, the DIC analysis offers an additional point of view to develop the design of the joint: because of the failure mechanism of bonded joint depends on peel stress the use of pins might reduce this factor and enhances the joint strength.

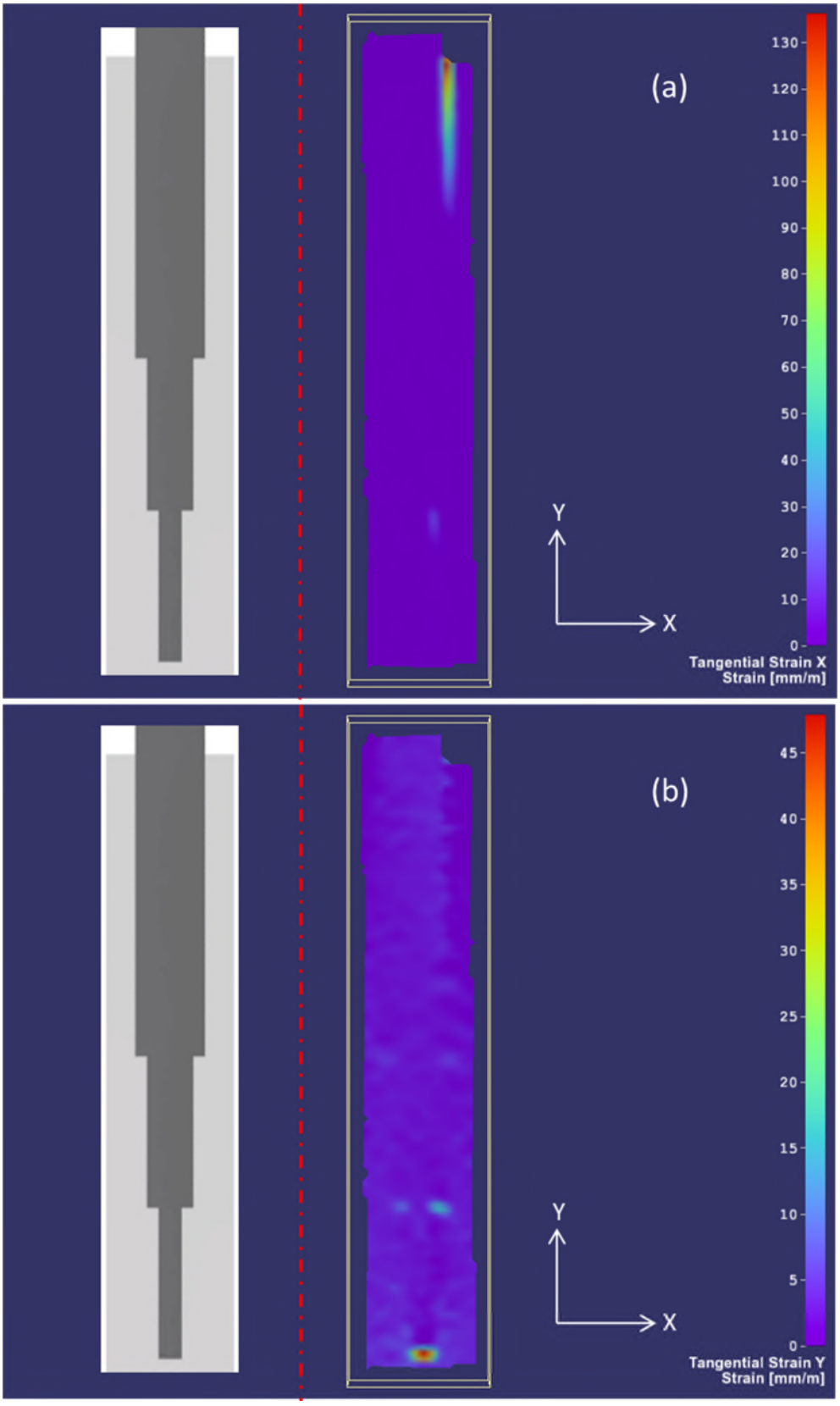

Figure 4-19 Baseline double-stepped joint at 58.50 kN: (a) tangential strain X, (b) tangential strain Y

The DIC analysis of EBM cocured double-stepped joint with spike pins confirms, in addition to the results of tensile testing, how the use of surface features enhances the joint strength.

For this joint, focusing on the strain distribution in the main directions X (figure 4-20(a)) and Y (figure 4-20(b)) at the loading failure of the control specimen (58.50 kN), the predominant role of pins is revealed.

A severe reduction of about 93% on local strain in X direction is observed comparing the maximum value of this parameter for EBM pinned joint (8mm/m) with the corresponding value of control joint (130 mm/m). This effect is due to the presence of pins: locked inside the laminate they provide a compressive force that reduces the moment to the edge of the overlap area of the carbon fibre and consequently reduces the peel stress.

However pins provide benefits even for the strain in the Y direction (figure 4-20(b)): the tip of the metal plate experiences a reduction of local strain in the Y direction of about 66% if compared with the bonded joint (from 45 mm/m for the control joint to 15 mm/m of the pinned one).In fact the pins, preventing the opening mechanism of the overlap edges, reduce even the displacement between the thresholds of the several steps and the composite laminate causing the strain reduction in Y direction described above.

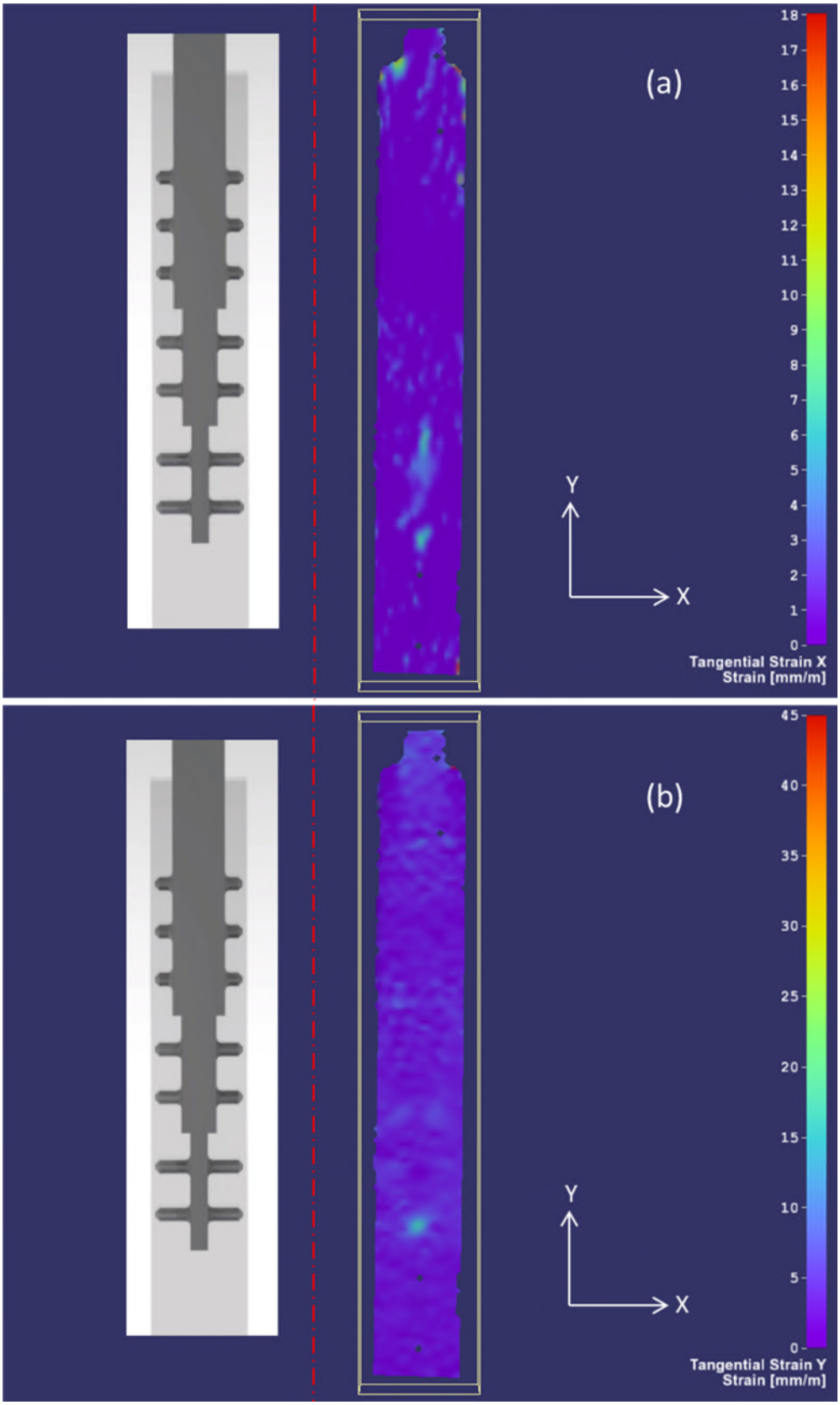

Figure 4-20 EBM cocured double-stepped joint at 58.50 kN:(a) tangential strain X, (b) tangential strain Y

According with the tensile testing results the EBM cocured double-stepped joint with spike pins experiences a failure load of 75.50 kN. The DIC analysis carried out in proximity of failure load (74.30 kN) describes the strain distribution across the joint and the failure mechanism (figure 4-21).

The two components of the local strain in both directions X and Y (figure 4-21(a),(b)), if compared with the control specimen, point out an increment in the maximum strain at the respective loading failure of about 83% for the X and 100% for Y direction.

These higher values of local strain across the specimen underline the role of pins in joint strength. The cracks start to propagate across the joint from the run-out of the overlap (as expected by the opening mechanism of peel stress) finding the first row of pins. Now the crack, forced to stop by pins, has to increase the amount of fracture energy to the value required to break the pins. As soon as the first row is overtaken the crack propagates until the following row of pins where it is forced to stop again and the energy loading begins. It is the energy absorbed by pins fracture during this start/stop failure mechanism that allows the pinned joint to stand these higher intensity strain distribution.

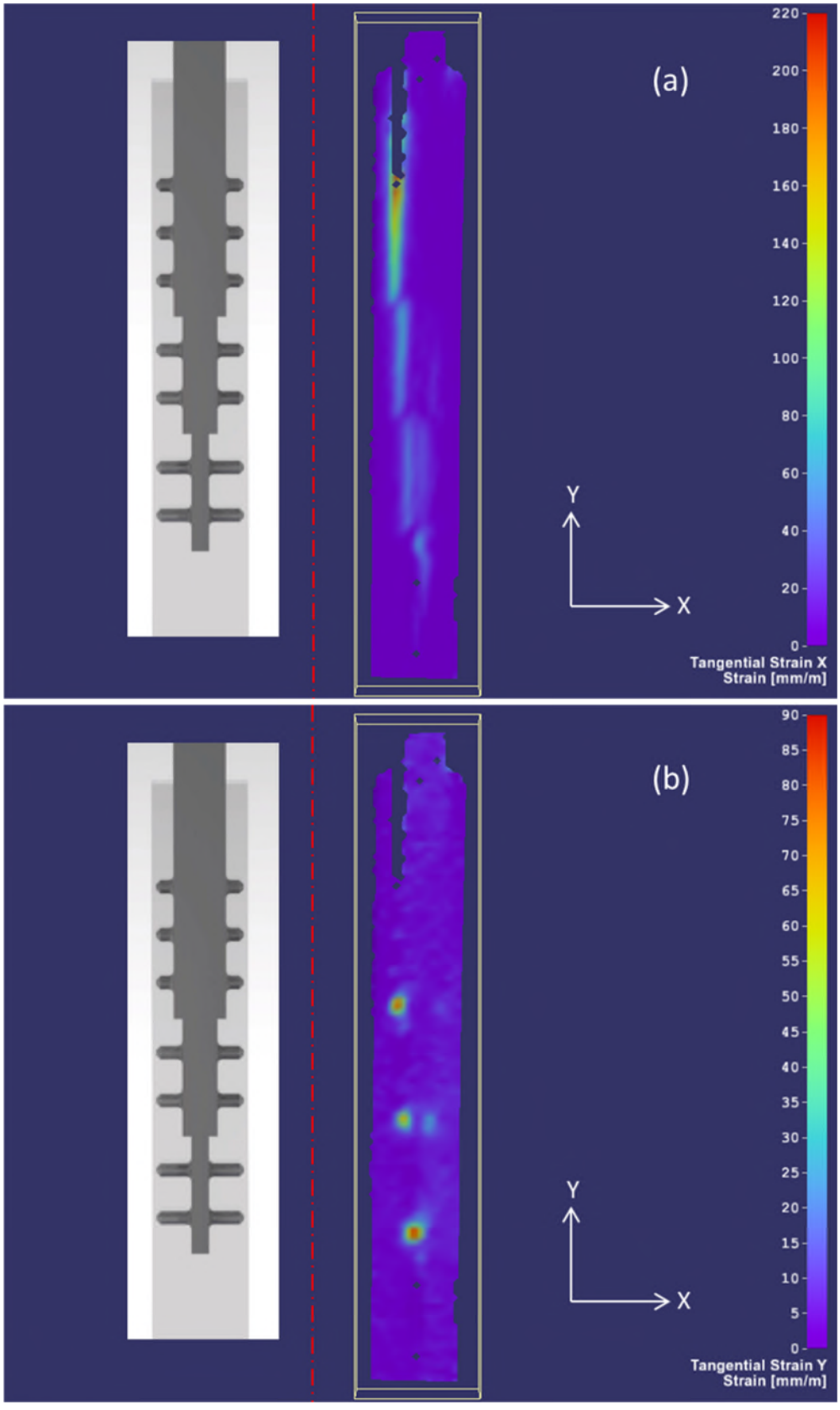

Figure 4-21 EBM cocured double-stepped joint at 74.30 kN: (a) tangential strain X, (b) tangential strain Y

The substantial analogies on mechanical properties of MM double-stepped joint with spike pins with the EBM joint (same geometry) are confirmed by DIC analysis. Figures 4-22 confirms the positive effects of surface features on joint strength: the severe reduction on local strain in X direction (at load of 58.50 kN) is quantified on 92% if referred on baseline configuration (figure 4-19), confirming the same behaviour presented for the EBM joint.

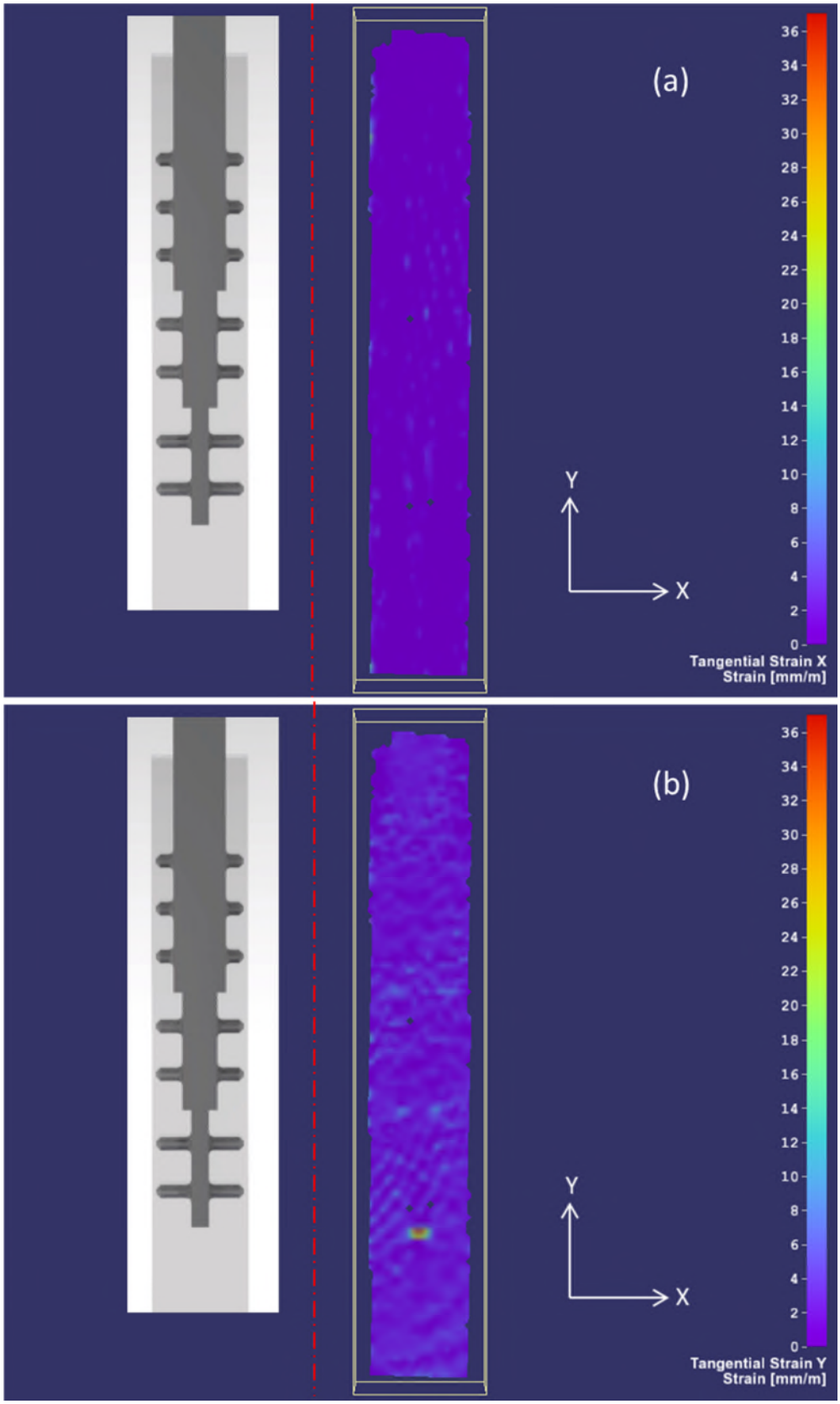

Figure 4-22 MM cocured double-stepped joint at 58.50 kN: (a) tangential strain X, (b) tangential strain Y

The instantaneous failure of pinned joint is confirmed by figure 4-23(a) and figure 4-23(b) and all the considerations about failure mechanism proposed for the EBM joint are still valid for this MM joint.

The local strain is progressively increasing in the run-out of the overlap area and tip of the metal plate with the same magnitude revealed for EBM joint. At this ultimate loading condition a relevant strain distribution is highlighted on all the steps of the metal plate (figure 4-23): the pins and the adhesive are not able to stand this high load and a catastrophic failure is observed.

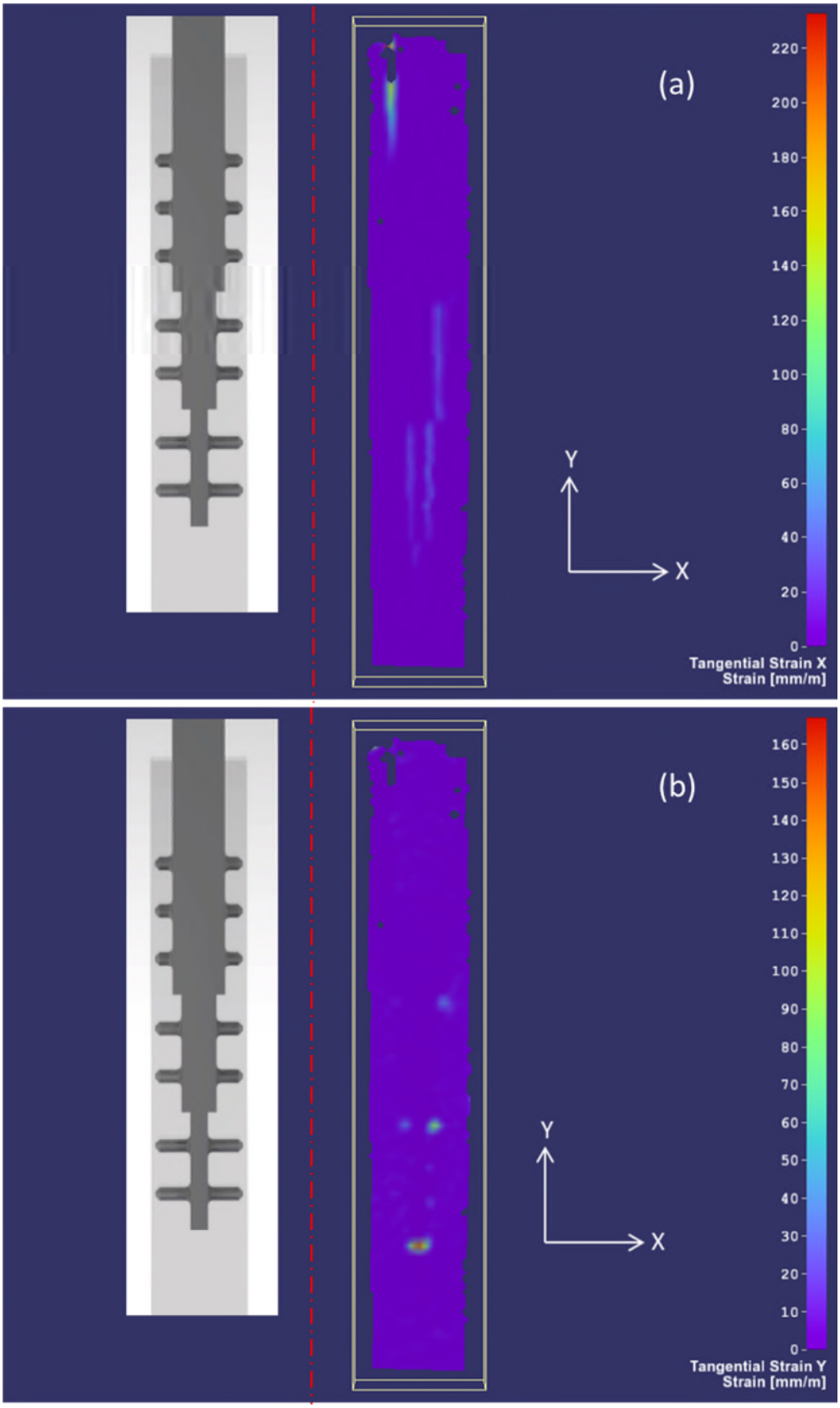

Figure 4-23 MM cocured double-stepped joint at 71.90 kN: (a) tangential strain X, (b) tangential strain Y

The strain distribution on MM double-stepped joint with shark teeth is observed in three different stages of failure process: the first stage (figure 4-24) is evaluated on the loading condition that characterized the baseline failure (58.50 kN). The high interlocking properties of the shark teeth design reduces to zero the local strain in the X direction (figure 4-24(a)) while the discontinuity between the plate tip and the composite laminate enhances the tangential strain in Y direction as evaluated with the others configurations proposed (figure 4-24(b)). Moreover the local strain in X direction is still predominant to characterize the failure of the joint.

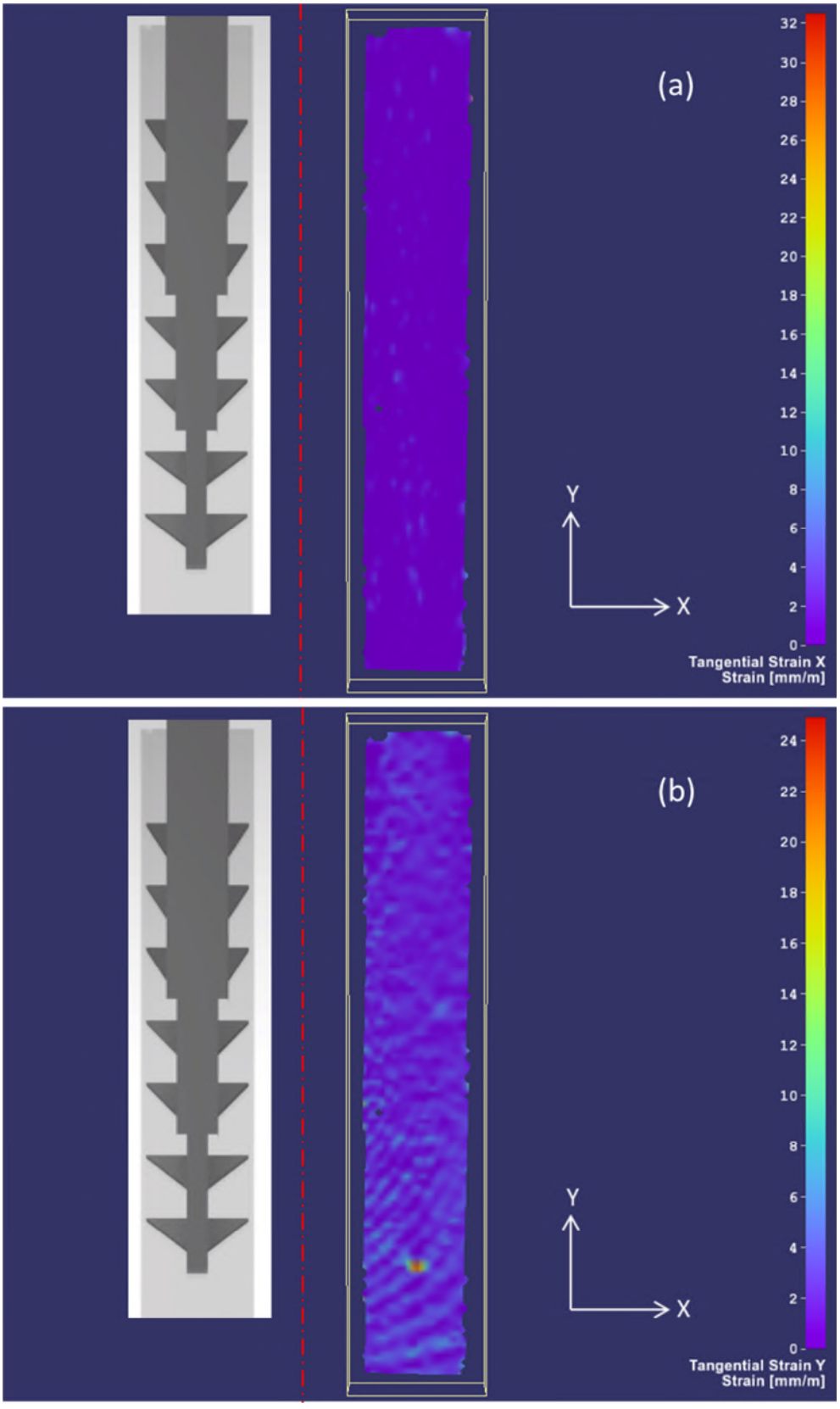

Figure 4-24 MM cocured double-stepped joint with shark teeth pins at 58.50 kN: (a) tangential strain X, (b) tangential strain Y

The advantages in using the shark teeth design instead of spike pins are highlighted at the higher load.

The local strain in the X direction, evaluated at loading condition of 71.90 kN (value of fracture for the spike pins configuration), is represented in figure 4-25. The local strain on the run-out of the overlap achieves a maximum value of 110 mm/m while for the spike configuration an interface failure is observed (figure 4-23). Moreover the high strength of the shark pins erases any local strain in X direction across the joint body enhancing the joint strength.

Focusing on the tip region, a lower reduction effect on the local strain in the Y direction (figure 4-25(b)) of about 75% is observed when compared with the spike configuration (figure 4-23(b)).This expected result has to be connected to the nature of the mechanical interlocking behaviour of pins: the compressive force developed by the surface feature increase the strength in the X direction but has low effects in the Y direction.

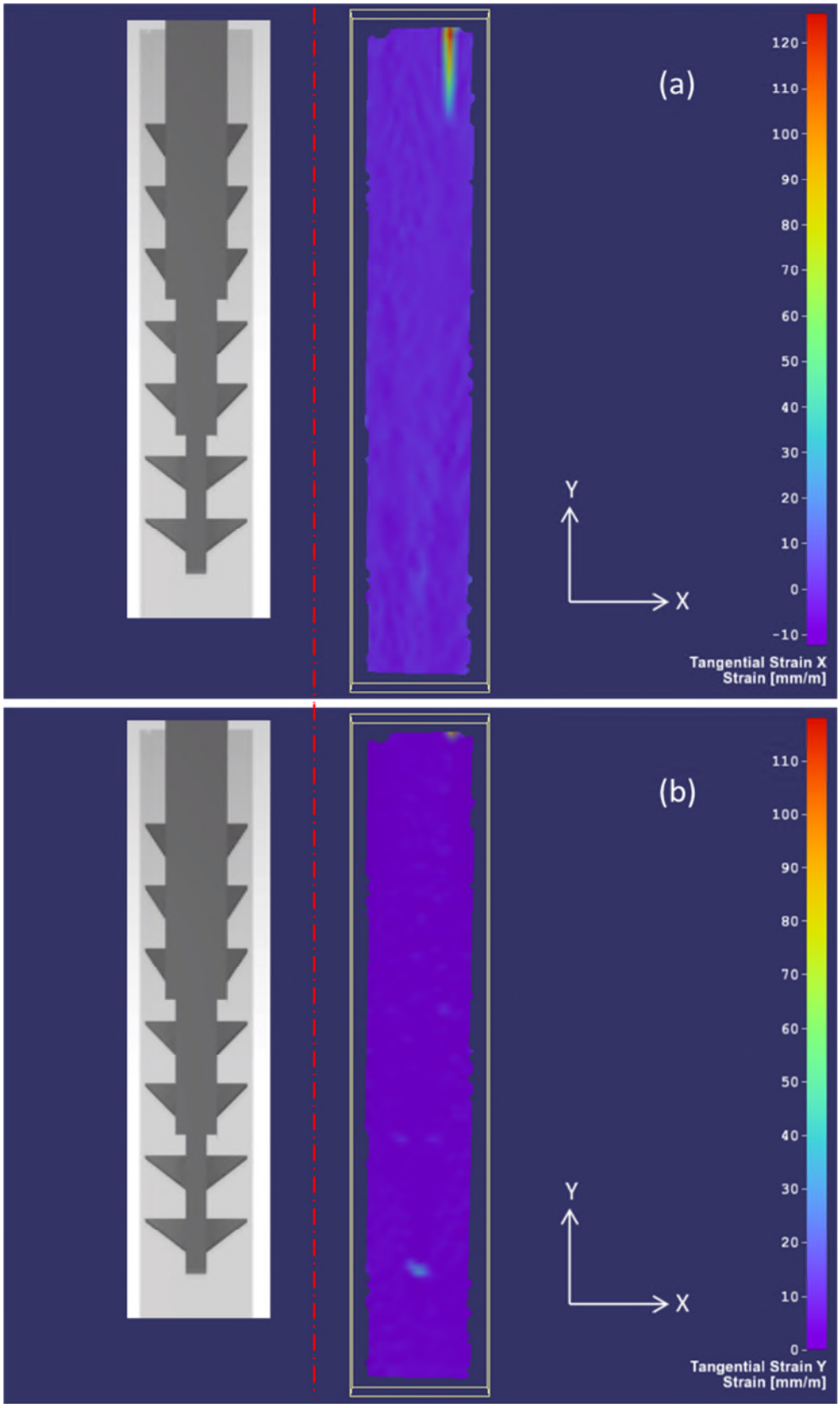

Figure 4-25 MM cocured double-stepped joint with shark teeth at 71.90 kN: (a) tangential strain X, (b) tangential strain Y

The relevant load drop described in the magnification of the load/extension curve is associated with the failure of the adhesive between the composite and the metal plate (figure 4-10). To confirm this theory an investigation with the DIC is carried out. Figure 4-26(a) shows the local strain distribution in X direction at the peak load before the drop. A local strain distribution is observed across the joint steps with a maximum value of 300 mm/m in proximity if the run-out of the overlap where is pointed out the beginning of debonding mechanism.

For the Y direction (figure 4-26(b)) the maximum value is observed in proximity if the tip threshold with a value of 150 mm/m.

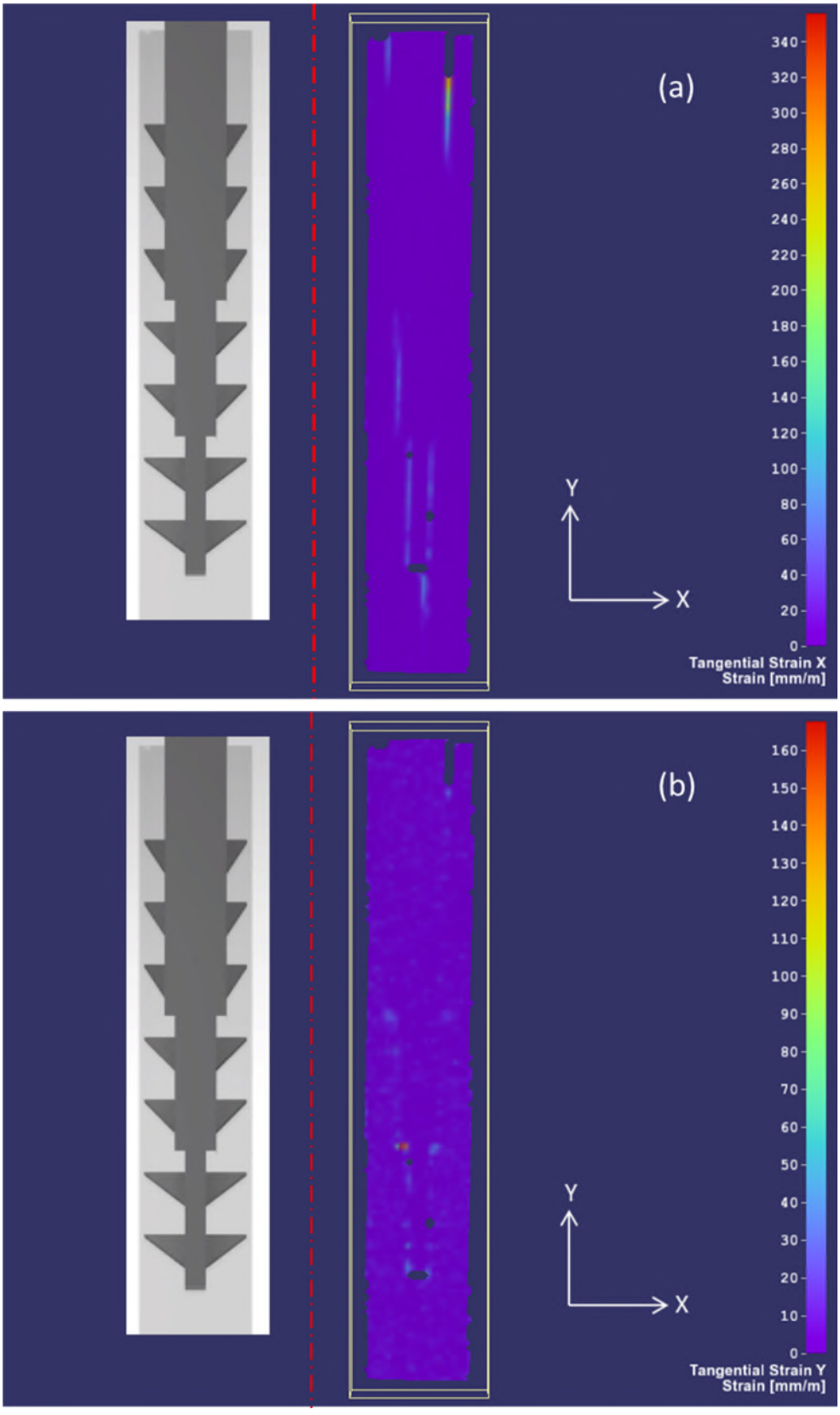

Figure 4-26 MM cocured double-stepped joint with shark teeth at 79.50 kN: (a) tangential strain X, (b) tangential strain Y

However the DIC images at load of 84.50 kN confirm the failure mechanism: the interface debonding is clearly described by the displacement between the metal plate and the composite laminate (figure 4-27(a) & (b)), while now the increasing load is completely transferred on the shark teeth pins until the ultimate failure.

While the adhesive failure reduces the capability of DIC to define the local strain distribution across the joining area, a considerable local strain in X direction is illustrated starting from the tip of the plate extending into the composite laminate (figure 4-27(a)). The magnitude and the orientation of this local strain can be associated with interlaminar crack propagation across the laminate.

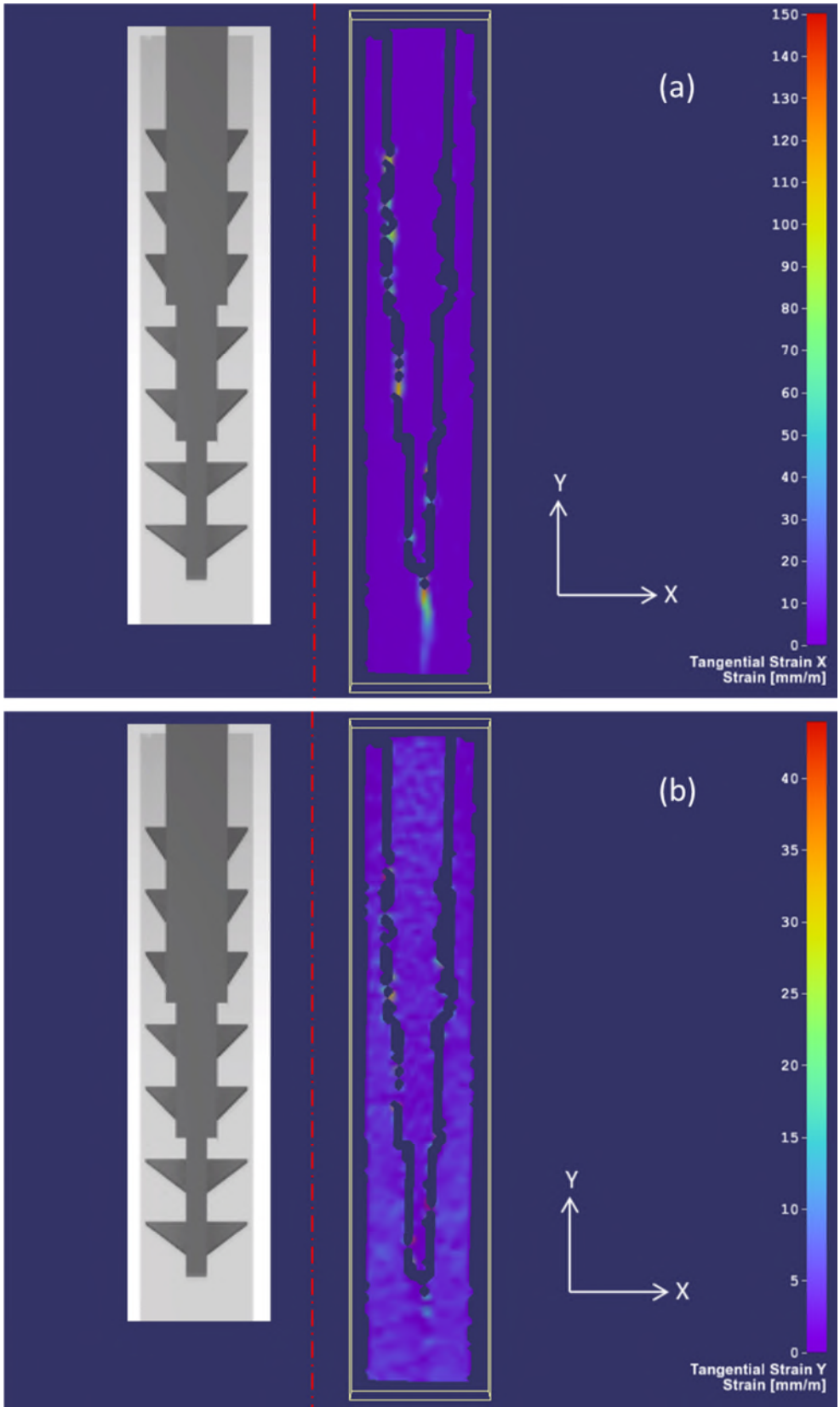

Figure 4-27 MM cocured double-stepped joint with shark teeth at 84.50 kN: (a) tangential strain X, (b) tangential strain Y

4.3.2 DIC analysis for double scarf-lap joint

The figure 4-28(a) & figure 4-28(b), at a loading condition of 48 kN, illustrate the catastrophic nature of the double-scarf bonded joint failure. As evaluated in the previous configurations, the local strain in the X direction (peel) is the factor that characterizes the joint failure. Moreover the DIC analysis shows how the area affected by high local strain represents a small percentage of the joining surface: the crack starts to propagate from the run-out of the overlap, due to the peel stress, and grows rapidly causing the instantaneous failure of the joint.

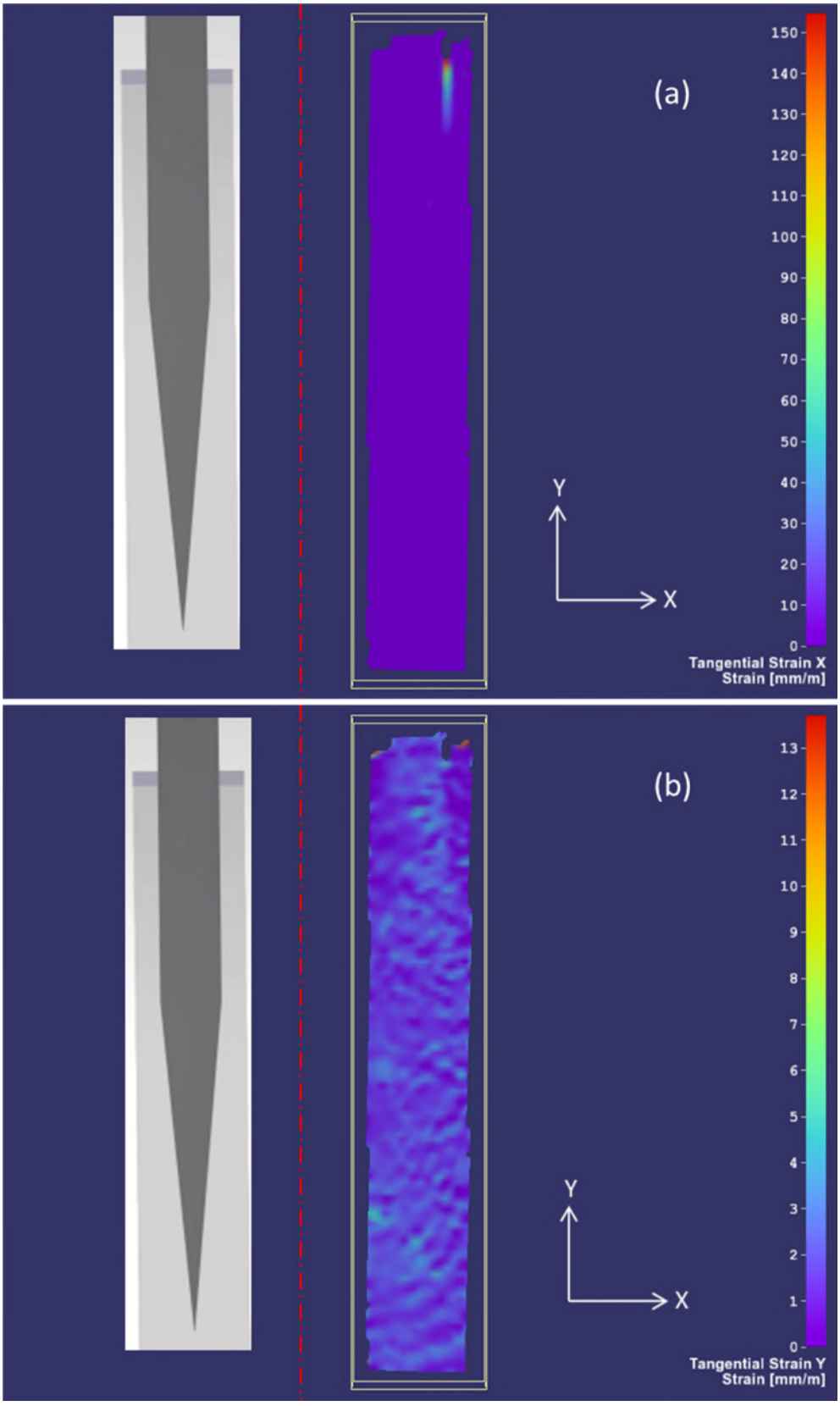

Figure 4-28 MM baseline double-scarf joint at 48 kN: (a) tangential strain X, (b) tangential strain Y

The strain distribution on a double-scarf joint with spike pins is evaluated for two different loading conditions: the first one at 48 kN to define the benefits of spike pins when compared with the control configuration, while the second condition shows the strain distribution at ultimate load for spike configuration (68 kN).

The local strain distribution at 48 kN described in figure 4-29 highlights how the local strain in X direction governs the failure of the joint.

Comparing the baseline configuration and the pinned one several analogies are pointed out: first of all the crack starts to propagate from the end of the overlap area into the joint. Secondly the magnitude of the local strain in this unpinned part is the same of the baseline (figure 4-28(a) vs figure 4-29(a)).

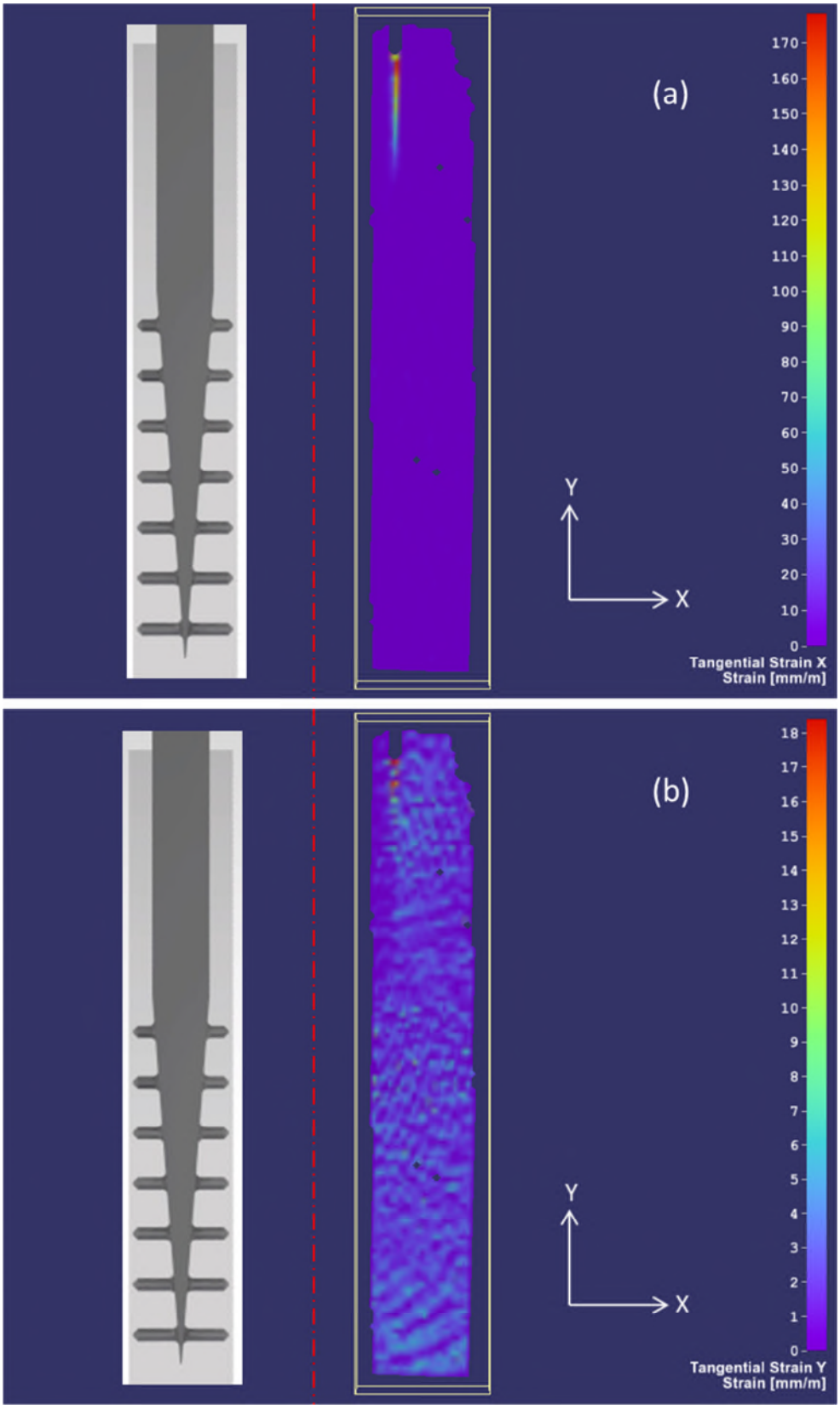

Figure 4-29 MM cocure double-scarf joint with spike pinsat 48 kN: (a) tangential strainX, (b) tangential strain Y

The local strain in Y direction for the two configurations (pinned and unpinned) appears to be limited and considerable lower than the X direction (5 mm/m vs 140 mm/m) confirming the dependence of the joint failure on the peel stress (figure 4-29(b) vs figure 4-28(b)).

The DIC images at failure loading (68 kN) show the increment of local strain across the joint body. While the pinned area experienced a local strain in X direction of 40 mm/m the tip presents a higher value of the same parameter about 80 mm/m due to the absence of pins (figure 4-30(a)).

At this loading condition the local strain at Y direction achieves the value of 25 mm/m (figure 4-30(b)).

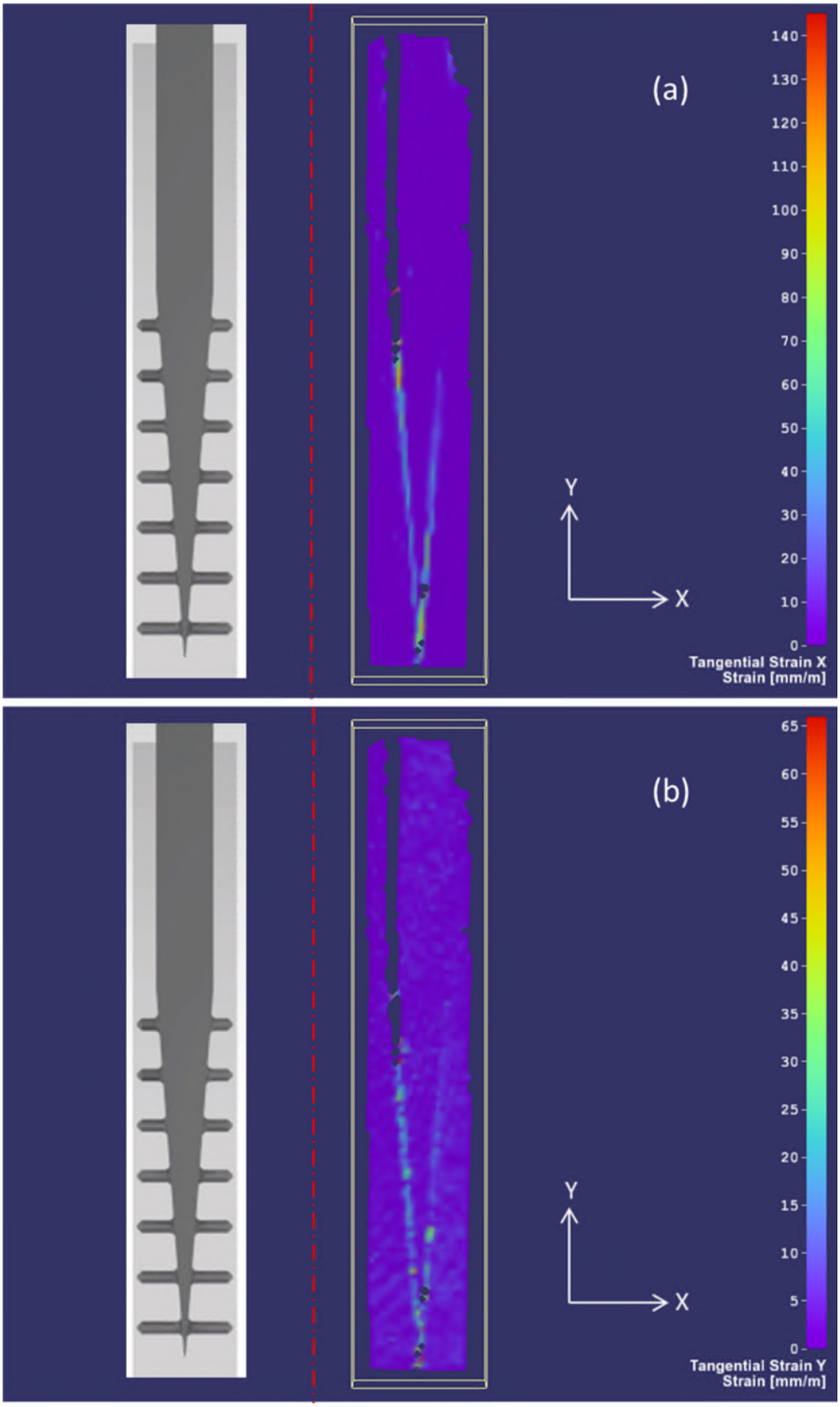

Figure 4-30 MM cocure double-scarf joint with spike pins at 68 kN: (a) tangential strain X, (b) tangential strain Y

According to the mechanical tests the double-scarf joint with shark teeth pins seems to be the most promising joint configuration, being able to support loads up to 105 kN.

The advantages on the shark teeth design are confirmed by DIC analysis at different loading stages.

Figure 4-31(a) and figure 4-31(b) show the strain distribution of double-scarf joint with shark teeth pins at 48 kN loading condition (load at which the control joint fails). The mechanism of failure is confirmed even in this configuration, pointing out the disbonding in the run-out of the overlap.

Focusing on the local strain in X direction (figure 4-31(a)) a severe reduction of the strain is observed if compared with the control specimen and the pinned one. The shark teeth pins in fact are able to reduce the local strain up to 65 mm/m that represents 44% of the pinned configuration (65 mm/m vs 150 mm/m).

At this loading stage the local strain in Y direction presents a maximum value of 4 mm/m, when compared with the component in the other direction this strain is basically negligible (figure 4-31(b)).

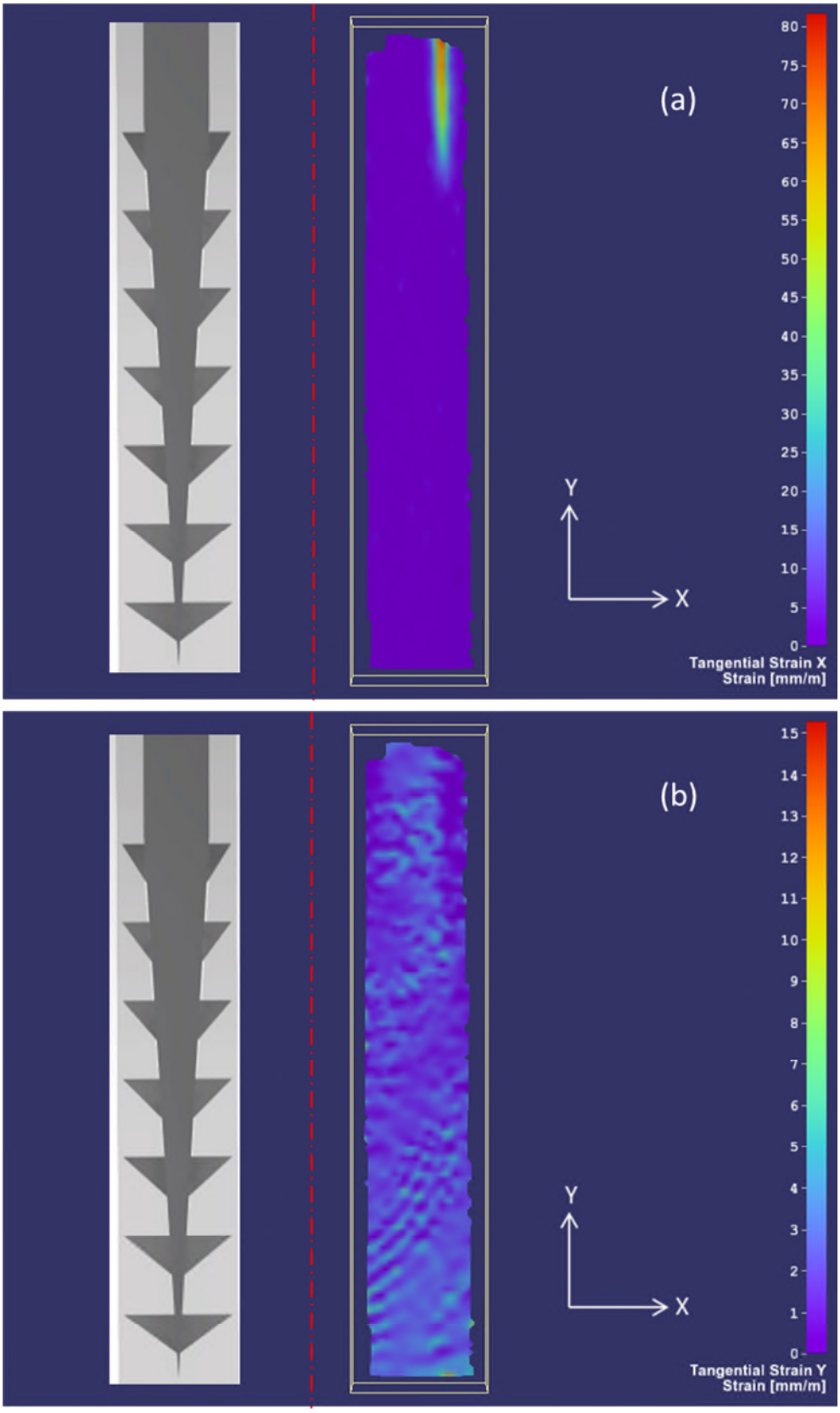

Figure 4-31 MM cocured double-scarf joint with Shark teeth pins at 48 kN: (a) tangential strain X, (b) tangential strain Y

At 68 kN, loading condition where the spike pins configuration fails, whereas the local strain distribution is reduced by the use of shark teeth pins. This surface feature design is able to stand higher load conditions and to prevent the joint failure. Comparing the figure 4-32(a) with figure 4-32(b) the difference explained above is highlighted: for the spike configuration all the joining area is observed a high value of local strain (especially at the tip) while for the shark design (figure 4-32(a)) the only part interested on local strain is represented by the end of the overlap (the tip does not experience any considerable local strain). The maximum value of local strain in X direction is about 150 mm/m.

The positive effects on strain reduction are obtained even for the local strain in Y direction where the higher value obtained is about 5 mm/m that represents a reduction of 80% from the same value for the spike pin configuration (figure 4-32(b)).

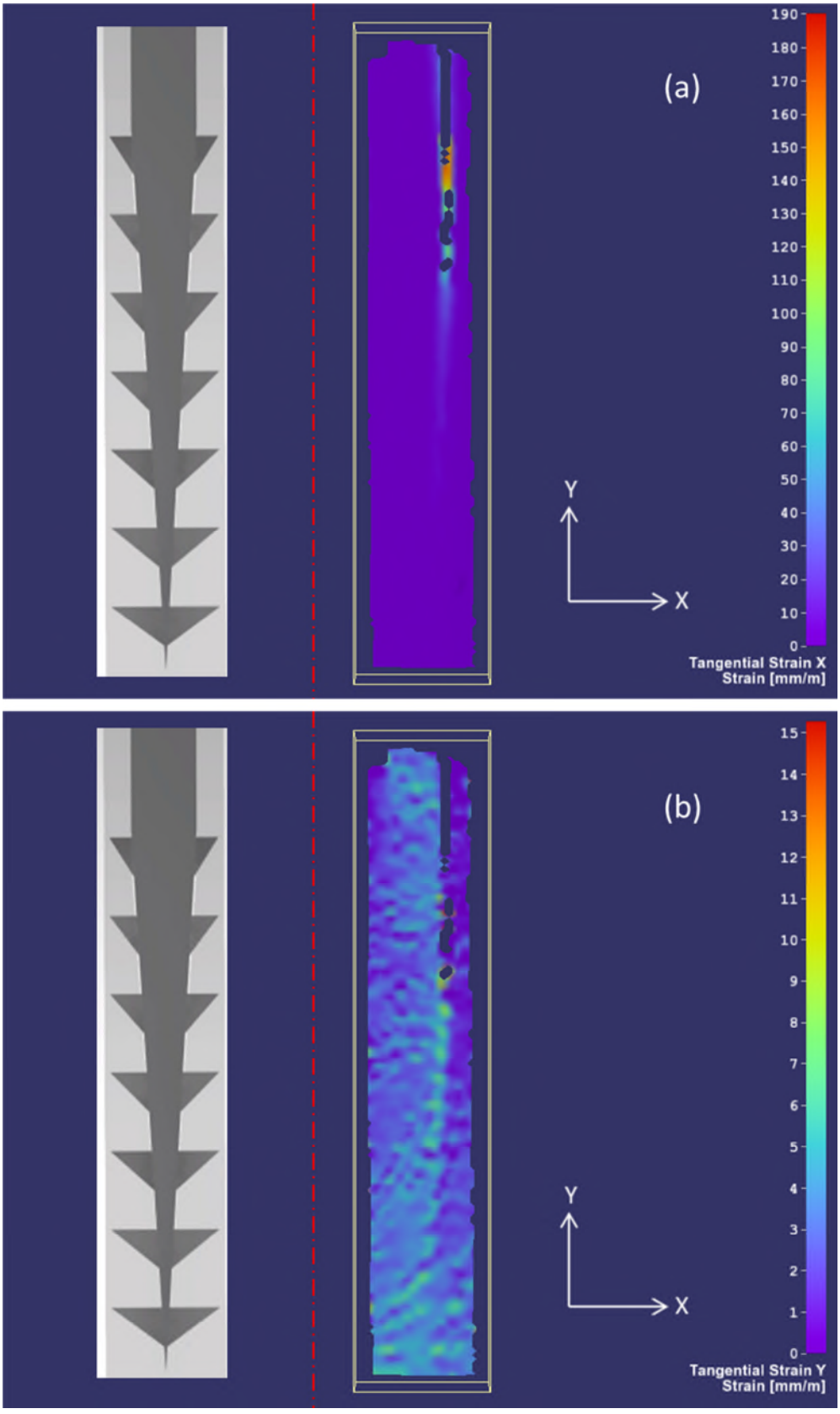

Figure 4-32 MM cocured double-scarf joint with Shark teeth pins at 68 kN: (a) tangential strain X, (b) tangential strain Y

This joint configuration supports load up to 105 kN. The DIC analysis at loads of 98 kN describes the failure process of the joint. Focusing on the local strain in the X direction (figure 4-33(a)), it is demonstrated that the joint failure mechanism is failure of the adhesive first and then the opening mechanism from the run-out of the overlap.

The maximum value of 190 mm/m of local strain (X direction) proves that the shark teeth pins support this high strain providing a higher joint strength. This loading condition determines a local strain distribution across all the joining area to the tip of the plate.

The local strain in the Y direction (figure 4-33(b)) presents a maximum value about 30 mm/m that corresponds to 16% of the maximum strain in the X direction and confirming how the main factor that characterize the joint failure is represented by the local strain in the X direction that is strongly connected with the peel stress.

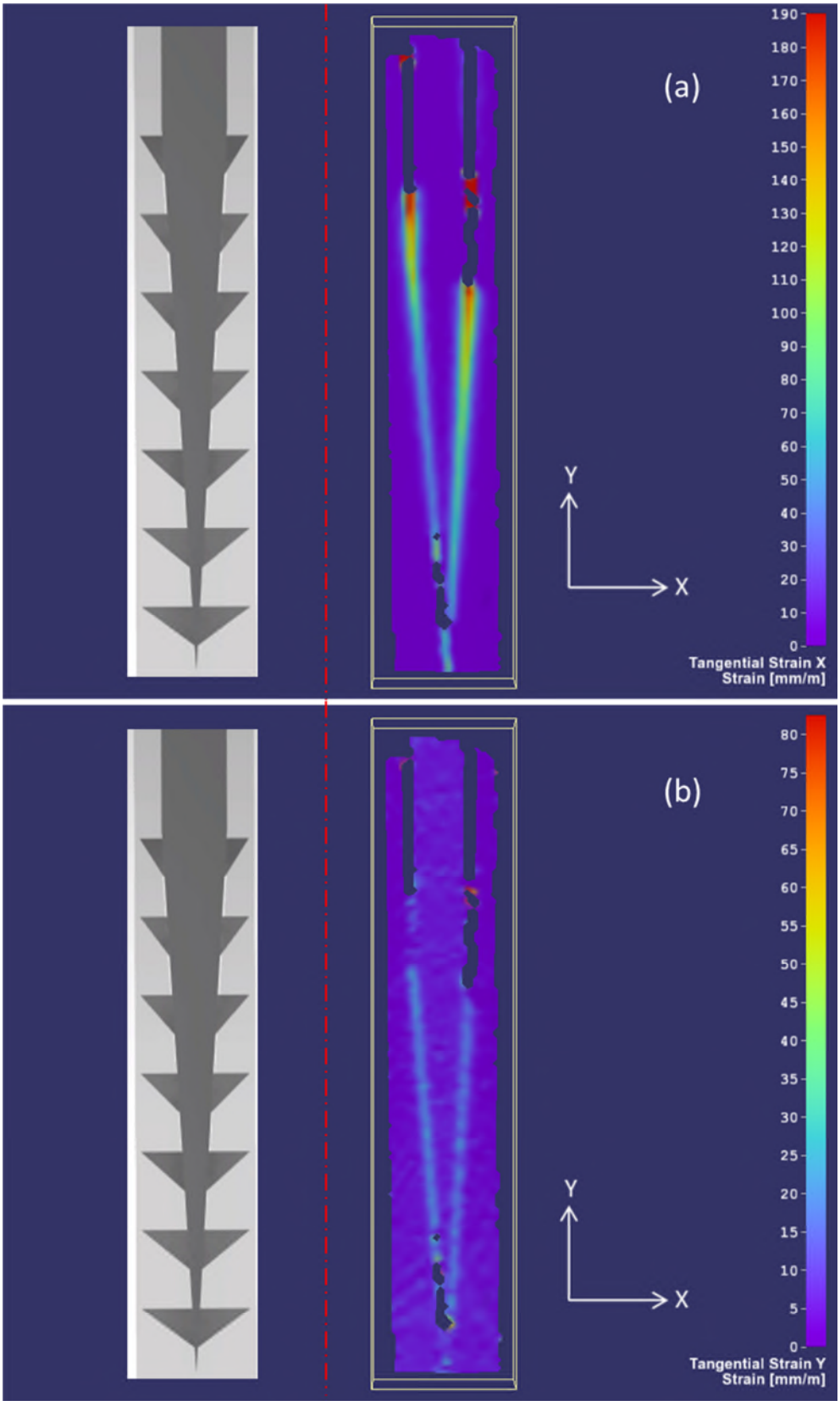

Figure 4-33 MM cocured double-scarf joint with Shark teeth pins at 98 kN: (a) tangential strain, (b) tangential strain Y

4.4 Post-mortem microscopy

4.4.1 Microscope characterization for EBM and MM pins

The manufacturing process selection represents one of the most important challenges of the research project. Despite the joint strength being widely analysed with mechanical tests, this is not enough to provide the right choice in terms of the manufacturing process.

A microscopy investigation is largely required to investigate the limits of the different manufacturing routes to produce the surface features. The investigation is developed focusing on the pin geometry details that represent the most critical part in the plate design and manufacturing.

Figure 4-34 describes a section of a double-stepped joint with spike pins made by EBM technology: the successful lay-up and curing processes are revealed by the right fibre alignment in the joining area.

Figure 4-34Post-mortem section of released EBM double-stepped joint with spike pins

Because the EBM is a layer by layer additive manufacturing process the pin is characterized by a rough surface finish. The microscopy (figure 4-35) underlines how it is impossible to ensure a homogeneous pin shape and dimension: the

pin body is bumpy and the diameter dimension is not constant. Moreover, due to these manufacturing limits, the EBM technology seems not able to clearly produce the required fillet at the base and the spike of the pin.

Figure 4-35 EBM spike pin detail

A better defined pin shape is obtained with MM technology (figures 4-36 and 4-37). The benefits of that manufacturing route in fact provide a constant diameter across the pin body; with the tip spike and fillet at the base of pins being manufactured in greater detail.

Figure 4-36 Post-mortem section of released MM double-stepped joint with spike pins

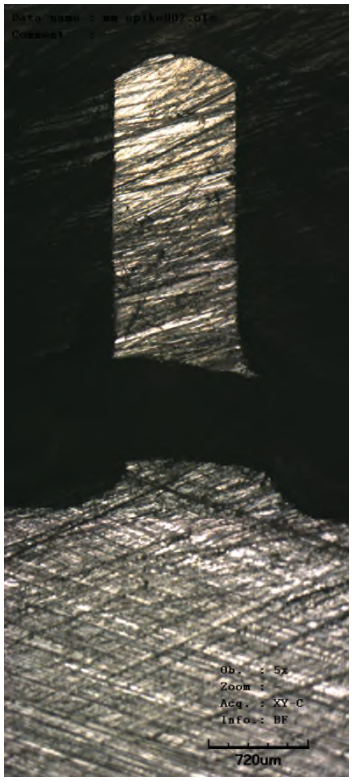

Figure 4-37 MM spike pin detail

Moreover, the MM technology is also able to manufacture the shark teeth pin design (figure 4-38).

Figure 4-38 Post-mortem section of released MM double-scarf joint with shark teeth pins

One of the main issues of this design is connected with the embedding process: the shape of shark teeth might cause a higher fibre disruption during insertion if the surface finish is not smooth.

It is observed how the slope of this MM shark teeth pin is well defined such as a smooth surface finish is provided. Both of these parameters permit a good quality of embedding with a reduction in resin rich channels (figure 4-39).

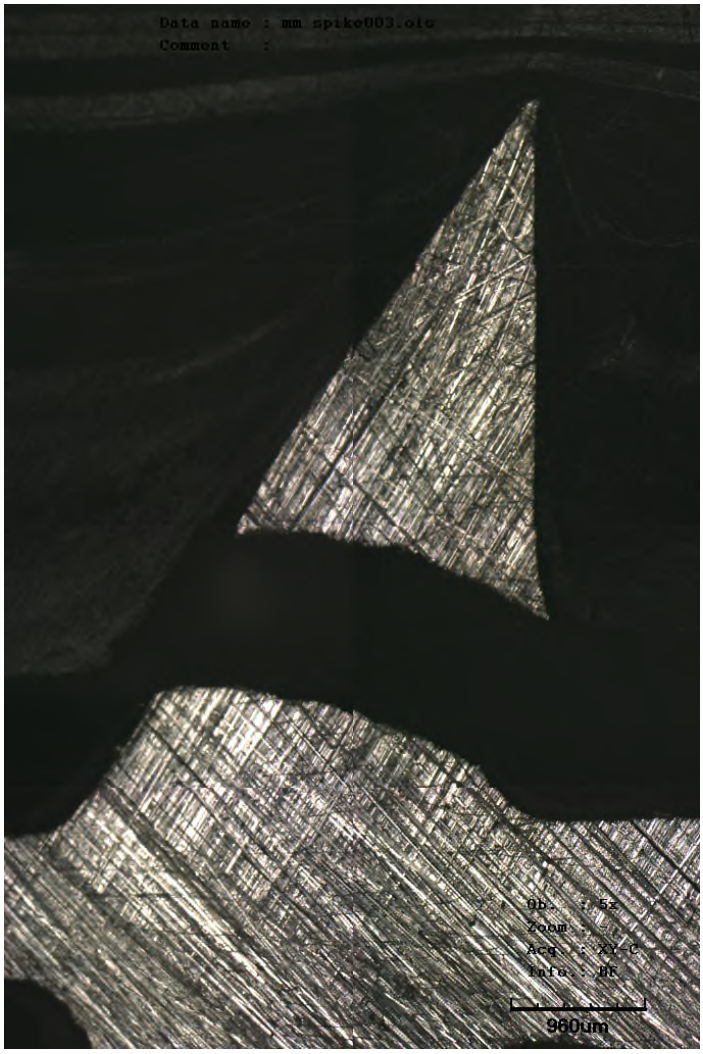

Figure 4-39 MM shark teeth pin detail

5 CONCLUSION AND FUTURE WORKS

5.1 Conclusions

- Surface features improve the mechanical performance of the bonded joint
- Different plate and surface feature designs can be used for different loading cases
- Surface structured adhesive joint design benefits from reduced weight and reduced fibre disruption when compared with a standard mechanically fastened (bolted) joint
- The strength of the pins represents a safety parameter (guaranteed minimum joint strength) if the adhesive strength is compromised during joint manufacture

High strength and damage resistant novel joints are being developed for applications such as Formula 1 suspension and aircraft landing gear parts. Metallic fittings with spikes which are embedded in the carbon fibre composite parts are key components of these joints.

The quality of the metallic/composite joints has been determined using tensile test results.

The undeniable surface feature positive effects on joint strength for double-stepped joint are summarised in figure 5-1. The increase in ultimate load ranges from 26%, for the micro-machined joint with spike pins, to 54%, for the shark teeth pins, when compared with the control configuration. The manufacturing route to produce the spikes, Electron Beam Melting or Micro-Machining, does not significantly affect the ultimate joint strength. Therefore, if this joint geometry is required, the manufacturing route will be strongly influenced by economic factors.

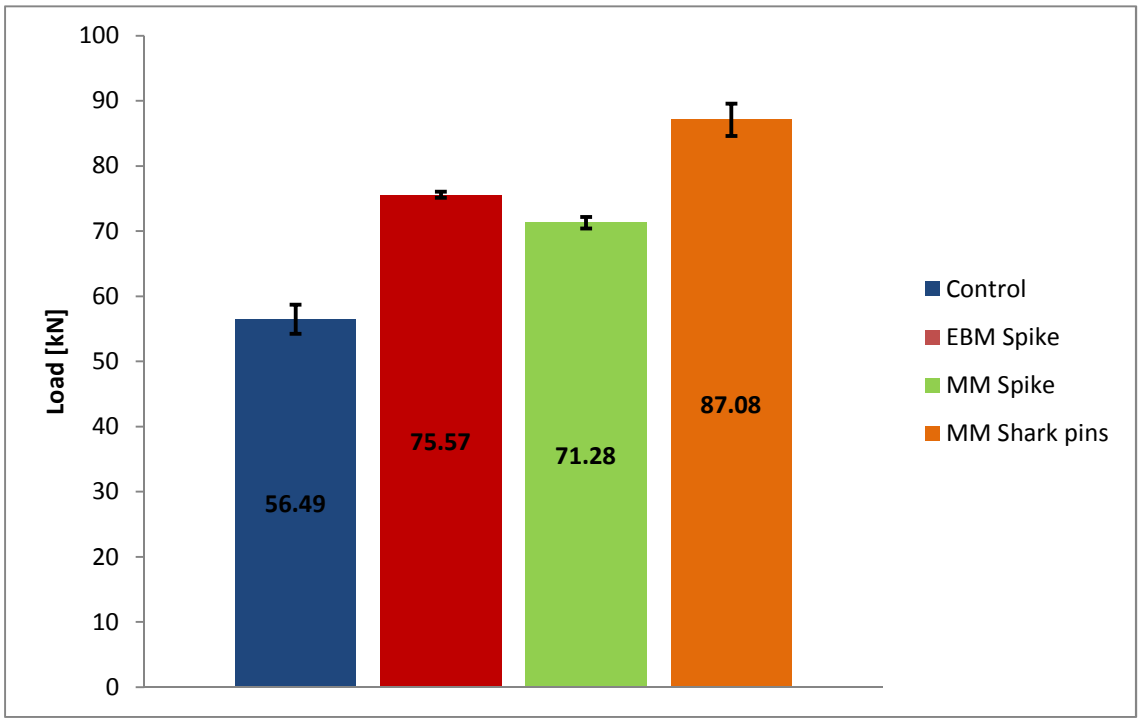

Figure 5-1 Double-stepped joint: ultimate load summary

For double-scarf joints the two pinned configurations present an increase in failure load of 50% for the spike pins and 124% for the shark teeth pins respectively when compared with the bonded double-scarf control joint (figure 5-2).

The reduced strength of the double-scarf vs double-stepped baseline joints (46.84 kN vs 56.49 kN) seems to be connected with the lay-up process and the difficulty to provide, for the scarf design, a slope comparable with the same slope of the metal plate.

The fibre alignment mismatching of this lay-up procedure increases the numbers and dimensions of resin rich channels in proximity of the joining area which represent the weak points for the laminate.

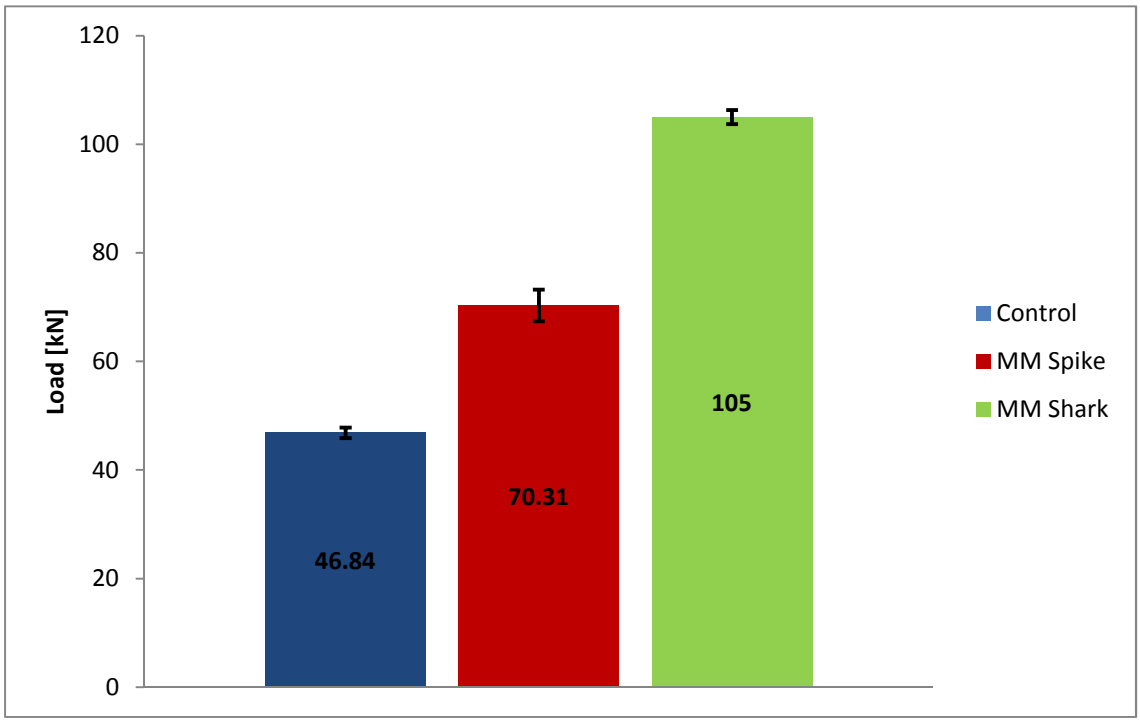

Figure 5-2 Double-scarf joint: ultimate load summary

Both configurations, double-stepped and double-scarf, with spike pins experienced a catastrophic failure where the pins and the adhesive fail together.

The double-stepped and double-scarf joints have the same trend up to the failure of the first [26] while the main role of surface features is to withstand and transfer the load to the joint plate reducing the peel stress and consequently increasing the joint strength in terms of failure load.

The shark teeth pins are able to support higher load as confirmed by mechanical tests. The failure mechanism of double-stepped and double-scarf joints with shark teeth pins can be divided in two main parts: in the first part the joint supports the load until the failure of the adhesive in the interface between composite and metal plate and a second part where the joint withstands the load until catastrophic failure with pins only.

The difference in ultimate load between double-stepped and double-scarf joint with shark teeth is due to the different plate design. After adhesive failure, the plate's role is highlighted: the scarf design provides better stress distribution on the surface features improving the pins efficiency and consequently the joint strength.

In addition the analysis of mechanical properties of surface features only provides interesting results to be used in the design process (figure 5-3 and figure 5-4).

The results of EBM and MM spike pins (figure 5-3) confirmed how the mechanical properties of surface features are ruled by the pin geometry more than the manufacturing process. The influence of the pin shape on the mechanical properties of the joint is reiterated by shark teeth pins results (figure 5-4). The strength of surface features is enhanced by more than 84% comparing the strength of MM spike pins with the MM shark teeth pins.

Moreover, these results enhanced the pin interlocking properties concept and the possibility to use small surface features to improve the strength of the joining area without a severe fibre disruption and increase of weight (as imposed when bolted fasteners are used).

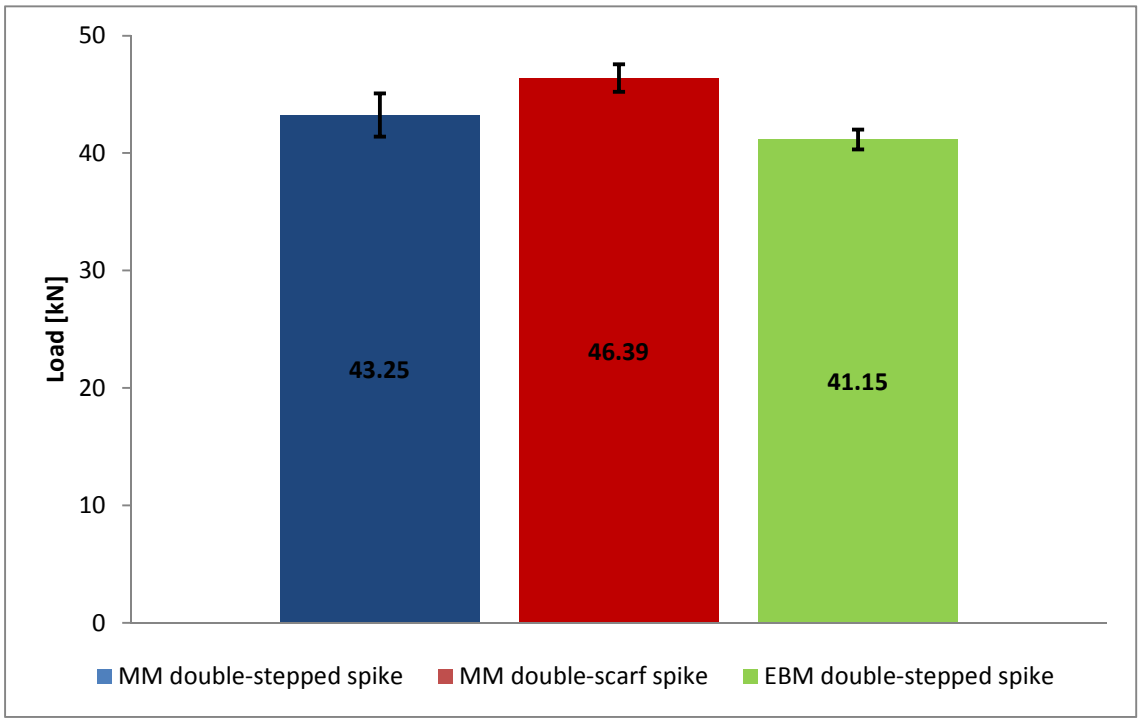

Figure 5-3 Released joint: spike pins strength

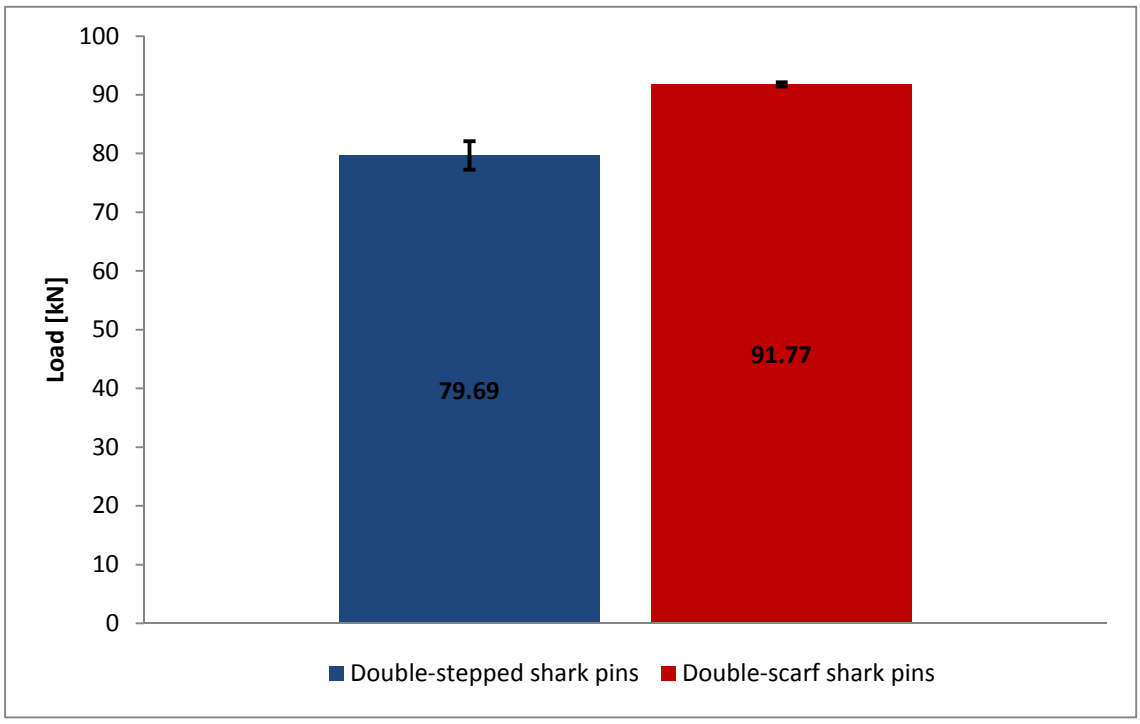

Figure 5-4 Released joint: shark teeth pins strength

5.2 Future works

Several aspects of this successful joining technique have to be investigated further to provide a joint design ready for industrial applications.

The effect of adhesive (type and bondline thickness) and surface preparation in conjunction with (macro) surface features are parameters which could significantly affect joint strength and require investigations to support the work reported here.

It is also important to optimise the design of surface features and metal plate in accordance with all the different loading conditions such as compressive force, mixed modes and fatigue. For the shark teeth pin, for example, it might be interesting to investigate different pin orientation and spacing to support a compressive loading mode.

This study has focussed solely on the use of prepreg for joint manufacture. It is not expected that a resin infusion route to manufacture would alter the general findings with respect to joint performance. However, investigations using alternative manufacturing routes should be considered.

From a manufacturing point of view an analysis on technique for inserting metallic fittings is necessary. This would include assessments to ensure minimal damage to the carbon fibre prepreg or preform, characterising the force required inserting pins, characterising the disturbance in fibres/ fabric/ preform and determining the effect on structural implications –knowledge of the microstructure at the joint is mandatory.

Also the mould tool design to locate and secure the fitting during the autoclave or oven processing stage has to be selected especially to provide a full scale component.

REFERENCES

[1] S.D. Thoppul, J. Finegan, R.F. Gibson, Mechanics of mechanically fastened joints in polymer-matrix composite structures - A review, Composites Sci. Technol. 69 (2009) 301-329.

[2] P.P. Camanho, F.L. Matthews, Stress analysis and strength prediction of mechanically fastened joints in FRP: A review, Composites Part A: Applied Science and Manufacturing. 28 (1997) 529-547.

[3] P.P. Camanho, M. Lambert, A design methodology for mechanically fastened joints in laminated composite materials, Composites Sci. Technol. 66 (2006) 3004-3020.

[4] M. Dano, E. Kamal, G. Gendron, Analysis of bolted joints in composite laminates: Strains and bearing stiffness predictions, Composite Structures. 79 (2007) 562-570.

[5] V. Kradinov, E. Madenci, D. Ambur, Application of genetic algorithm for optimum design of bolted composite lap joints, Composite structures. 77 (2007) 148-159.

[6] T. Ireman, T. Nyman, K. Hellbom, On design methods for bolted joints in composite aircraft structures, Composite Structures. 25 (1993) 567-578.

[7] J. Whitney, R. Nuismer, Stress fracture criteria for laminated composites containing stress concentrations, J. Composite Mater. 8 (1974) 253-265.

[8] R. Nuismer, J. Labor, Applications of the average stress failure criterion: Part II—Compression, J. Composite Mater. 13 (1979) 49-60.

[9] F. Chang, R.A. Scott, G.S. Springer, Strength of mechanically fastened composite joints, J. Composite Mater. 16 (1982) 470-494.

[10] S. Yamada, C. Sun, Analysis of laminate strength and its distribution, J. Composite Mater. 12 (1978) 275-284.

[11] M.D. Banea, L.F.M. Da Silva, Adhesively bonded joints in composite materials: An overview, Proceedings of the Institution of Mechanical Engineers, Part L: Journal of Materials: Design and Applications. 223 (2009) 1-18.

[12] A.J. Kinloch, Adhesion and adhesives: science and technology, Springer, 1987.

[13] M. Davis, D. Bond, Principles and practices of adhesive bonded structural joints and repairs, Int J Adhes Adhes. 19 (1999) 91-105.

[14] P. Molitor, V. Barron, T. Young, Surface treatment of titanium for adhesive bonding to polymer composites: A review, Int J Adhes Adhes. 21 (2001) 129-136.

[15] B.M. Parker, The effect of composite prebond moisture on adhesive-bonded CFRP-CFRP joints, Composites. 14 (1983) 226-232.

[16] B.M. Parker, The strength of bonded carbon fibre composite joints exposed to high humidity, Int J Adhes Adhes. 10 (1990) 187-191.

[17] B.M. Parker, Some effects of moisture on adhesive-bonded CFRP-CFRP joints, Composite Structures. 6 (1986) 123-139.

[18] W. Wright, A review of the influence of absorbed moisture on the properties of composite materials based on epoxy resins, RAE Technical Memorandum (1979).

[19] G. Davis, J. Venables, A. Kinloch, Durability of Structural Adhesives, ed.Kinloch, AJ, Applied Science Publ., London (1983) 43.

[20] J.K. Kim, H.S. Kim, D.G. Lee, Investigation of optimal surface treatments for carbon/epoxy composite adhesive joints, J. Adhes. Sci. Technol. 17 (2003) 329-352.

[21] K. Kim, J. Yoo, Y. Yi, C. Kim, Failure mode and strength of uni-directional composite single lap bonded joints with different bonding methods, Composite Structures. 72 (2006) 477-485.

[22] K.D. Potter, F.J. Guild, H.J. Harvey, M.R. Wisnom, R.D. Adams, Understanding and control of adhesive crack propagation in bonded joints between carbon fibre composite adherends I. Experimental, Int J Adhes Adhes. 21 (2001) 435-443.

[23] M. Qin, Y.A. Dzenis, Analysis of single lap adhesive composite joints with delaminated adherends, Composites Part B: Engineering. 34 (2003) 167-173.

[24] S.B. Kumar, S. Sivashanker, A. Bag, I. Sridhar, Failure of aerospace composite scarf-joints subjected to uniaxial compression, Materials Science and Engineering: A. 412 (2005) 117-122.

[25] S.B. Kumar, I. Sridhar, S. Sivashanker, S.O. Osiyemi, A. Bag, Tensile failure of adhesively bonded CFRP composite scarf joints, Materials Science and Engineering: B. 132 (2006) 113-120.

[26] M.C. Niu, Composite airframe structures: practical design information and data, Adaso Adastra Engineering Center, 1992.

[27] S.M.R. Khalili, A. Shokuhfar, S.D. Hoseini, M. Bidkhori, S. Khalili, R.K. Mittal, Experimental study of the influence of adhesive reinforcement in lap joints for composite structures subjected to mechanical loads, Int J Adhes Adhes. 28 (2008) 436-444.

[28] P.P. Camanho, F.L. Matthews, Bonded metallic inserts for bolted joints in composite laminates, Proceedings of the Institution of Mechanical Engineers Part L: Journal of Materials: Design and Applications. 214 (2000) 33-40.

[29] P.J. Herrera-Franco, G.L. Cloud, Strain-relief inserts for composite fasteners-an experimental study, J. Composite Mater. 26 (1992) 751-768.

[30] S. Nilsson, Increasing strength of graphite/epoxy bolted joints by introducing an adhesively bonded metallic insert, J. Composite Mater. 23 (1989) 642-650.

[31] S.V. Hoa, A. Di Maria, D. Feldman, Inserts for fastening sheet molding compounds, Composite Structures. 8 (1987) 293-309.

[32] P.P. Camanho, C.M.L. Tavares, R. De Oliveira, A.T. Marques, A.J.M. Ferreira, Increasing the efficiency of composite single-shear lap joints using bonded inserts, Composites Part B: Engineering. 36 (2005) 372-383.

[33] B. Kolesnikov, L. Herbeck, A. Fink, CFRP/titanium hybrid material for improving composite bolted joints, Composite Structures. 83 (2008) 368-380.

[34] A. Fink, B. Kolesnikov, Hybrid titanium composite material improving composite structure coupling, Eur Space Agency Spec Publ ESA SP (2005) 843-848.

[35] A. Fink, P. Camanho, M. Canay, A. Obst, Increase of bolted joint performance by means of local laminate hybridization (2007).

[36] P.P. Camanho, A. Fink, A. Obst, S. Pimenta, Hybrid titanium-CFRP laminates for high-performance bolted joints, Composites Part A: Applied Science and Manufacturing. 40 (2009) 1826-1837.

[37] F. Bianchi, X. Zhang, A numerical model for hybrid metal-composite joints with through-thickness reinforcement, Collection of Technical Papers - AIAA/ASME/ASCE/AHS/ASC Structures, Structural Dynamics and Materials Conference (2012).

[38] B. Dance, A. Buxton, An introduction to Surfi-Sculpt® technology–new opportunities, New Challenges (2007).

[39] F. Smith, COMELD™: An innovation in composite to metal joining, Mater. Technol. 20 (2005) 91-96.

[40] W. Tu, P. Wen, F. Guild, The optimization of Comeld™ joints: A novel technique for bonding composites and metal, WCE 2010 - World Congress on Engineering 2010. 2 (2010) 1383-1385.

[41] K. Fronius, Electronic welding apparatus. U.S Patent No 4,521,672.4(1985).

[42] A. Schierl, The CMT - Process - A Revolution in welding technology, Weld.World.49 (2005) 38.

[43] K. Furukawa, New CMT arc welding process–welding of steel to aluminium dissimilar metals and welding of super-thin aluminium sheets, Welding international. 20 (2006) 440-445.

[44] S. Ucsnik, M. Scheerer, S. Zaremba, D.H. Pahr, Experimental investigation of a novel hybrid metal-composite joining technology, Composites Part A: Applied Science and Manufacturing. 41 (2010) 369-374.

[45] M. Fleischmann, J. Tauchner, S. Ucsnik, BENCHMARKING OF A NOVEL LIGHTWEIGHT METAL-COMPOSITE-JOINT TECHNOLOGY.

[46] C.R. Deckard, J.J. Beaman, Recent advances in selective laser sintering (1987) 447-451.

[47] E. Raszmann, A. Paul, THREE-DIMENSIONAL PRINTING HELPS EFFICIENTLY MANUFACTURE AEROSPACE COMPONENTS.

[48] C. Li, Z. Fang, H. Zhao, Investigation into layered manufacturing technologies for industrial applications. 1 (2010) 213-216.

[49] C.K. Chua, K.F. Leong, C.C.S. Lim, Rapid prototyping: principles and applications, World Scientific, 2010.

[50] P. Rochus, J.-.Plesseria, M. Van Elsen, J.-.Kruth, R. Carrus, T. Dormal, New applications of rapid prototyping and rapid manufacturing (RP/RM) technologies for space instrumentation, Acta Astronaut. 61 (2007) 352-359.

[51] J. Hänninen, DMLS moves from rapid tooling to rapid manufacturing, Metal Powder Report. 56 (2001) 24-29.

[52] E.C. Santos, M. Shiomi, K. Osakada, T. Laoui, Rapid manufacturing of metal components by laser forming, Int. J. Mach. Tools Manuf. 46 (2006) 1459-1468.

[53] D.E. Cooper, M. Stanford, K.A. Kibble, G.J. Gibbons, Additive Manufacturing for product improvement at Red Bull Technology, Materials and Design. 41 (2012) 226-230.

[54] G.N. Levy, The role and future of the Laser Technology in the Additive Manufacturing environment, Physics Procedia. 5, Part A (2010) 65-80.

[55] K.A. Mumtaz, N. Hopkinson, Selective Laser Melting of thin wall parts using pulse shaping, J. Mater.Process. Technol. 210 (2010) 279-287.

[56] E.P. De Garmo, J.T. Black, R.A. Kohser, DeGarmo's materials and processes in manufacturing, John Wiley & Sons, 2011.

[57] F.L. Matthews, T.T. Tester, The influence of stacking sequence on the strength of bonded CFRP single lap joints, Int J Adhes Adhes. 5 (1985) 13-18.

[58] G. Meneghetti, M. Quaresimin, M. Ricotta, Influence of the interface ply orientation on the fatigue behaviour of bonded joints in composite materials, Int. J. Fatigue. 32 (2010) 82-93.

[59] W.J. Renton, J.R. Vinson, Fatigue behavior of bonded joints in composite material structures, J. Aircr. 12 (1975) 442-447.

[60] W. De Goeij, M. Van Tooren, A. Beukers, Composite adhesive joints under cyclic loading, Mater Des. 20 (1999) 213-221.

[61] R.B. Heslehurst, Design and Analysis of Structural Joints with Composite Materials, DEStech Publications, Inc, 2013.

[62] D. Gay, S.V. Hoa, S.W. Tsai, Composite materials: design and applications, CRC press, 2002.

[63] E.J. Barbero, Introduction to composite materials design, CRC press, 2011.

[64] P.J. Burt, Local correlation measures for motion analysis: a comparative study (1982).

[65] M. Sutton, W. Wolters, W. Peters, W. Ranson, S. McNeill, Determination of displacements using an improved digital correlation method, Image Vision Comput. 1 (1983) 133-139.

[66] M.A. Sutton, J. Orteu, H.W. Schreier, Image correlation for shape, motion and deformation measurements: basic concepts, theory and applications, Springer, 2009.

[67] P. Reu, Introduction to Digital Image Correlation: Best Practices and Applications, Exp Tech. 36 (2012) 3-4.

[68] P. Reu, Hidden Components of DIC: Calibration and Shape Function ? Part 1, Exp Tech. 36 (2012) 3-5.

[69] P. Reu, Hidden Components of 3D-DIC: Interpolation and Matching ? Part 2, Exp Tech. 36 (2012) 3-4.

[70] P. Reu, Hidden Components of 3D-DIC: Triangulation and Post-processing–Part 3, Exp Tech. 36 (2012) 3-5.

APPENDICES

Appendix A CAD Drawings

A.1 Double-Stepped lap joint

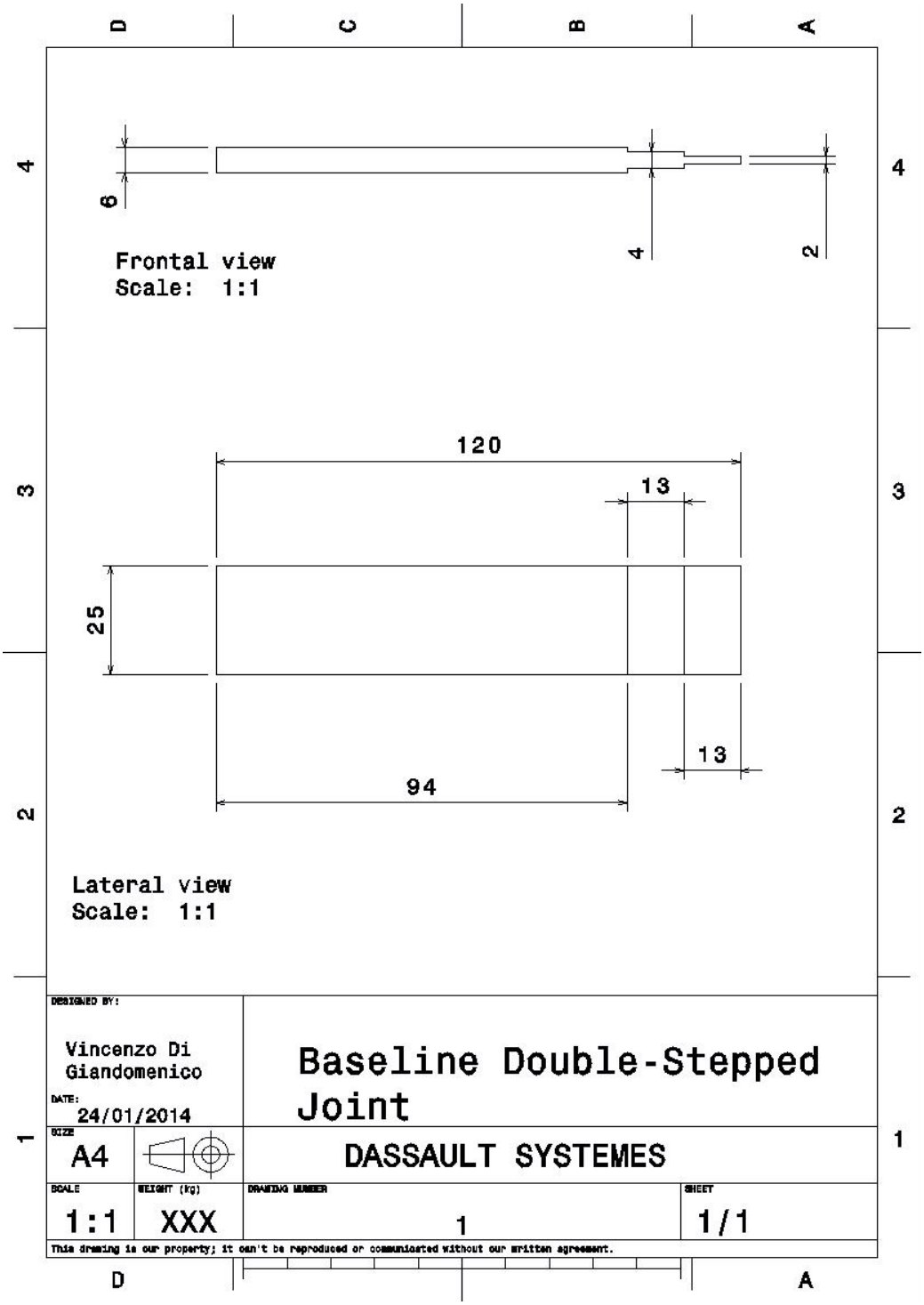

Figure A-1 Baseline Double-Stepped joint

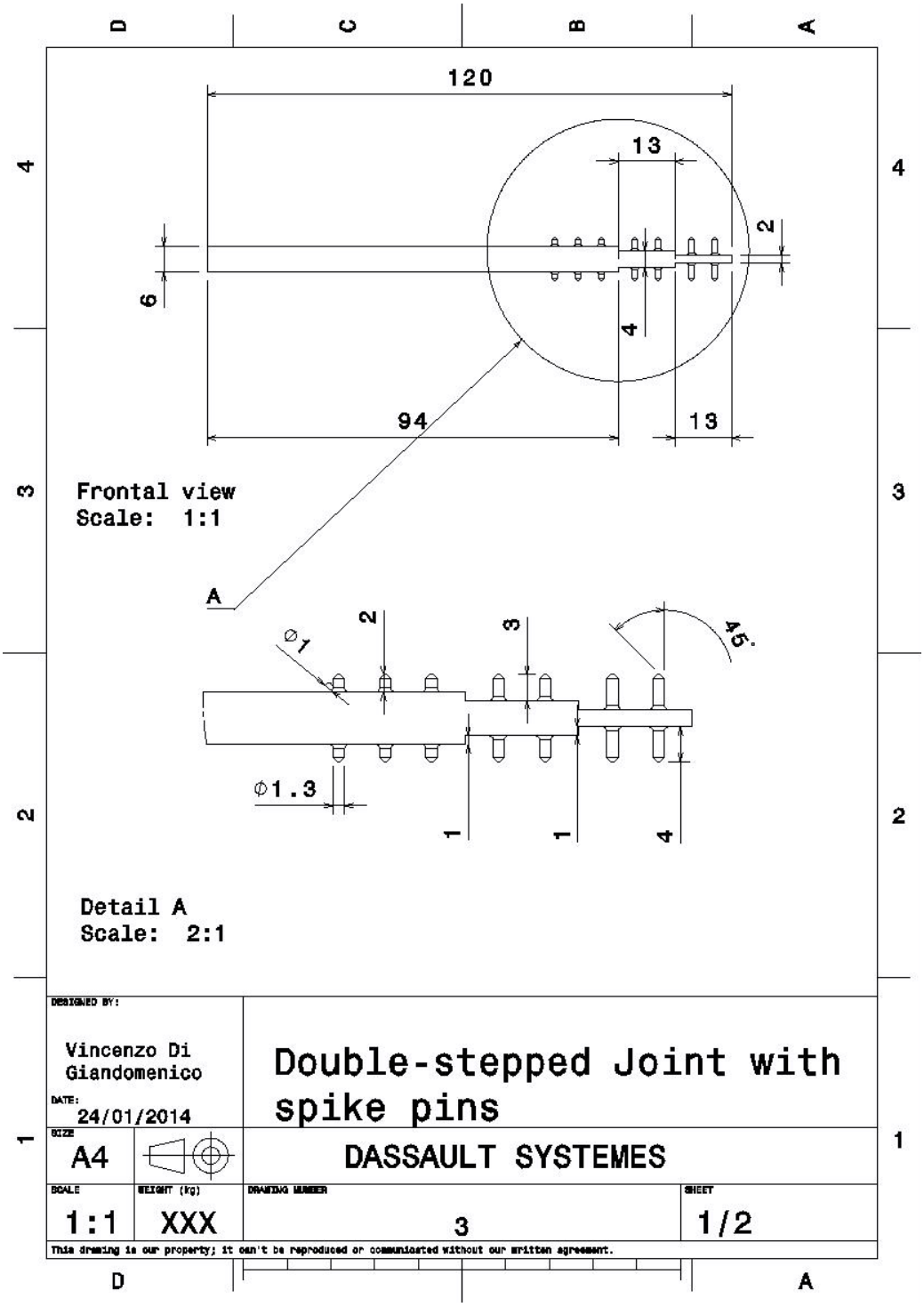

Figure A-2 Double-Stepped joint with spike pins:part 1/2

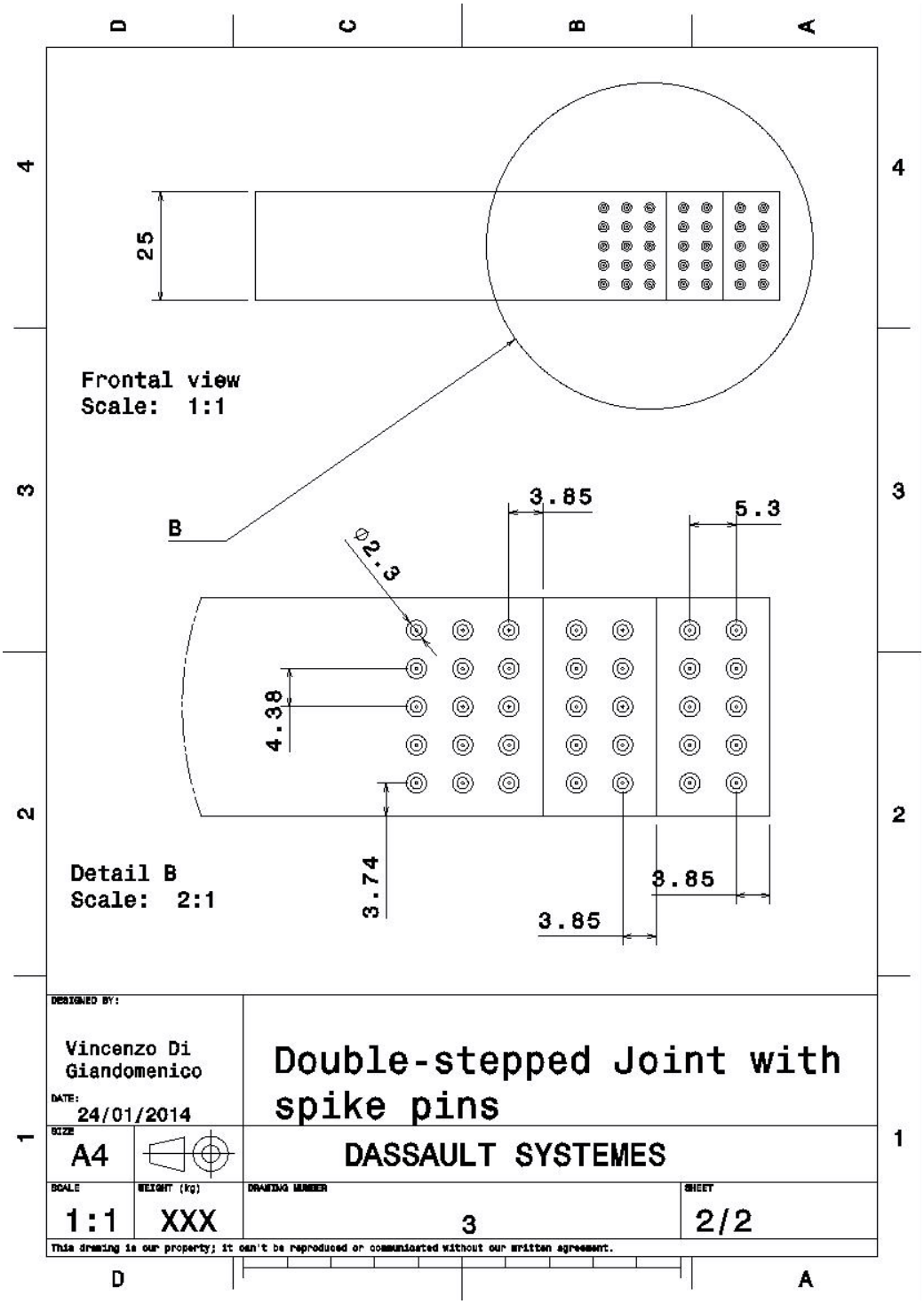

Figure A-3 Double-stepped joint with spike pins:part 2/2

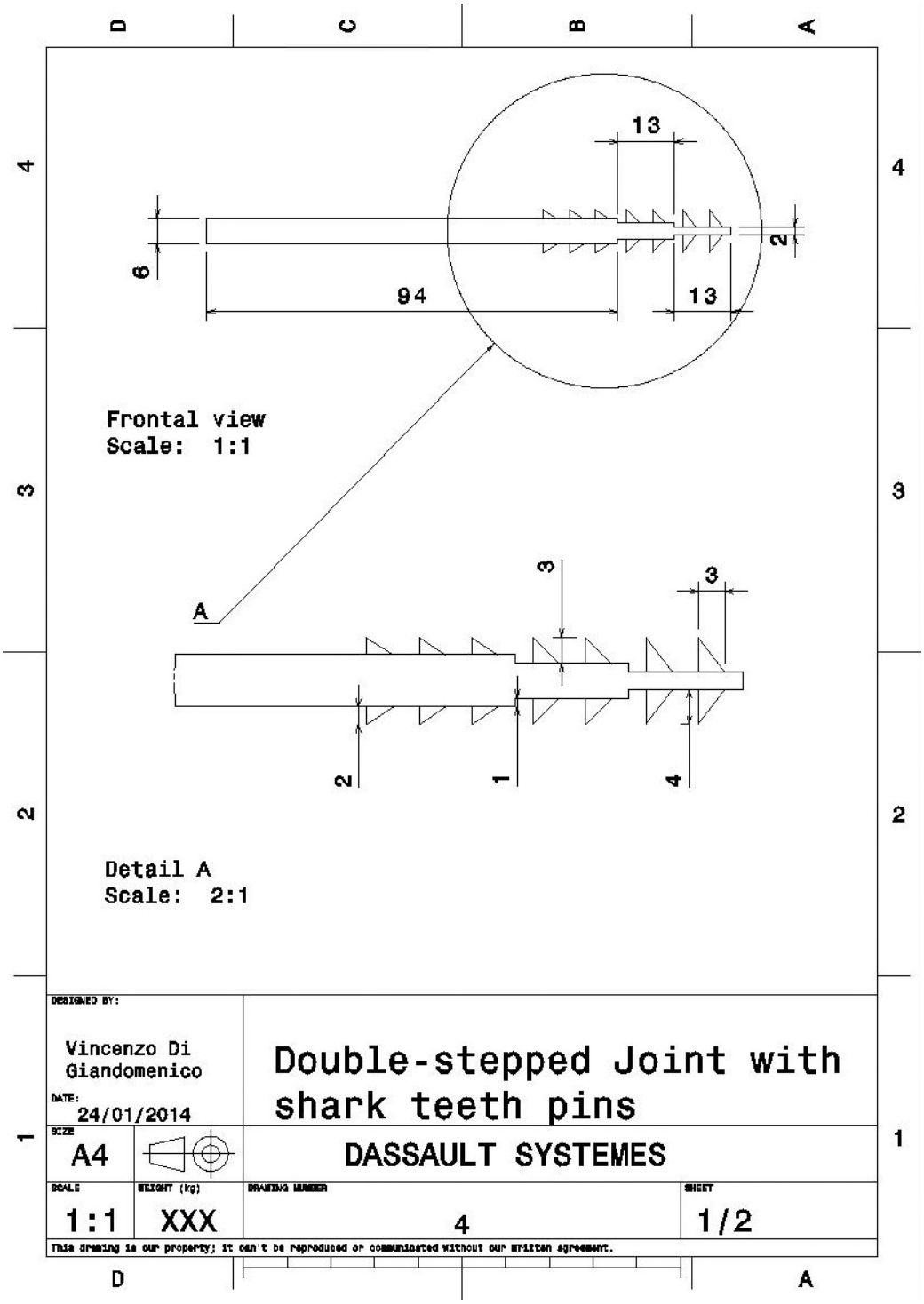

Figure A-4 Double-stepped joint with shark teeth pins:part 1/2

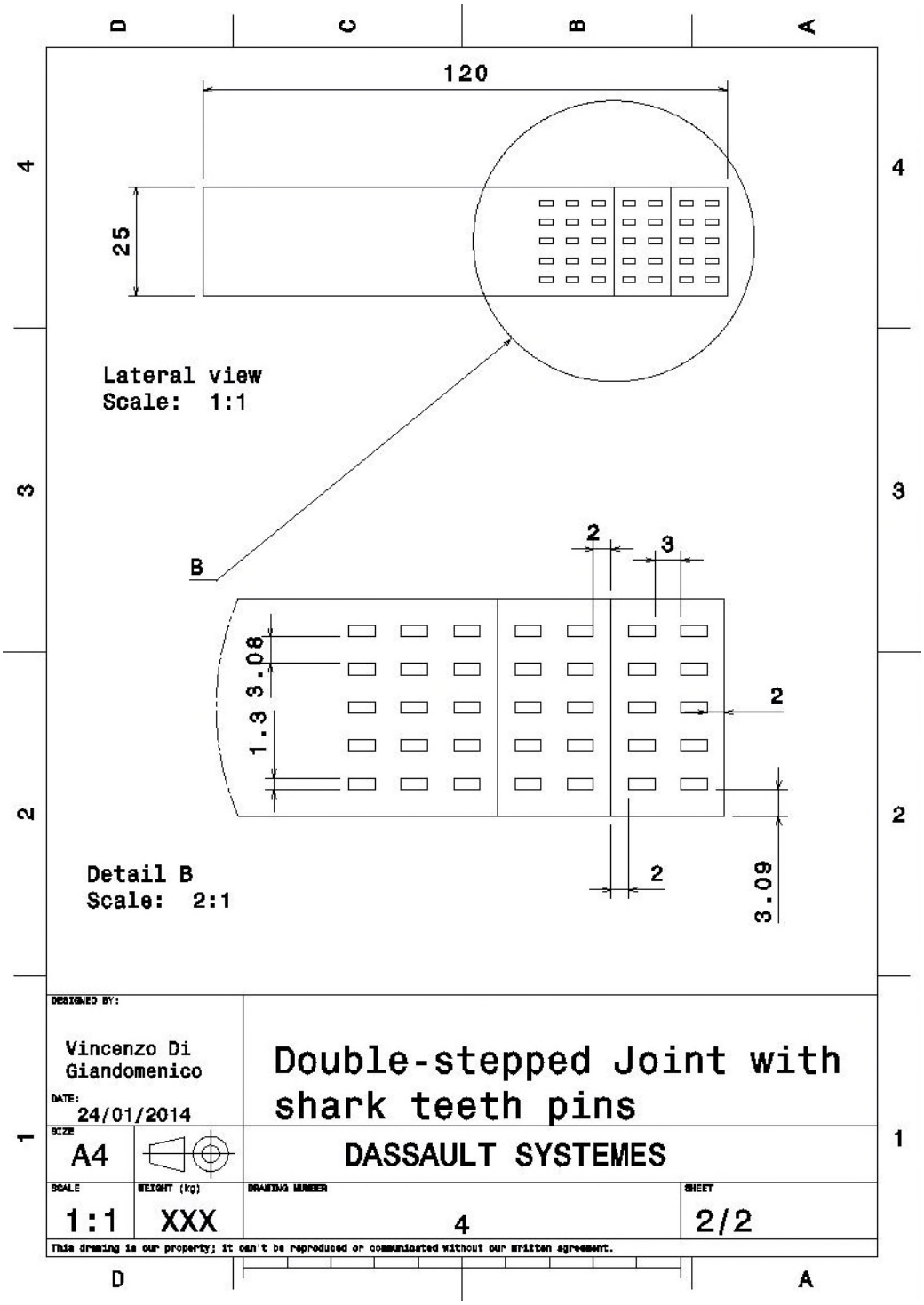

Figure A-5 Double-Stepped joint with shark teeth pins:part 2/2

A.2 Double-Scarf lap joint

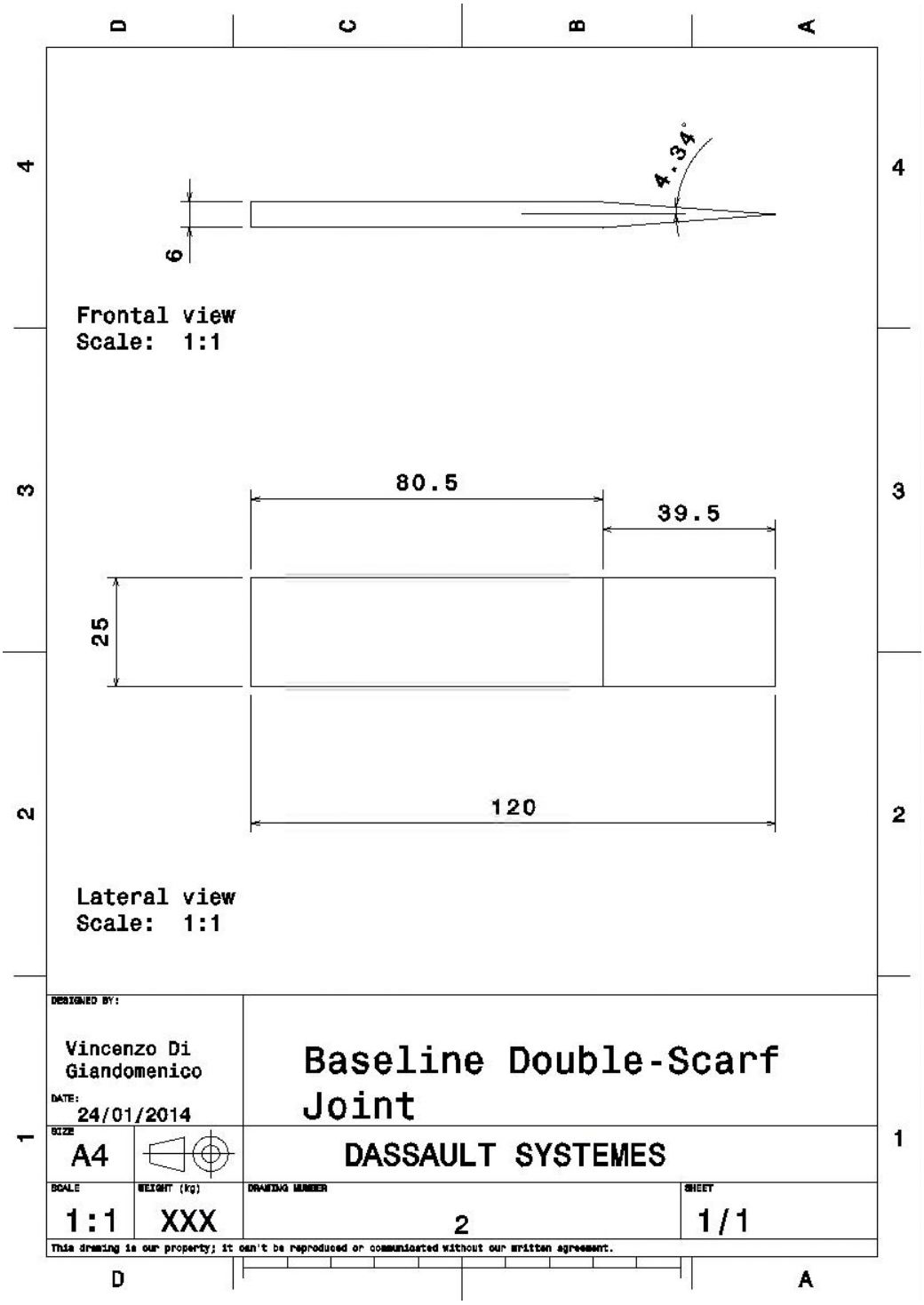

Figure A-6 Baseline Double-Scarf joint

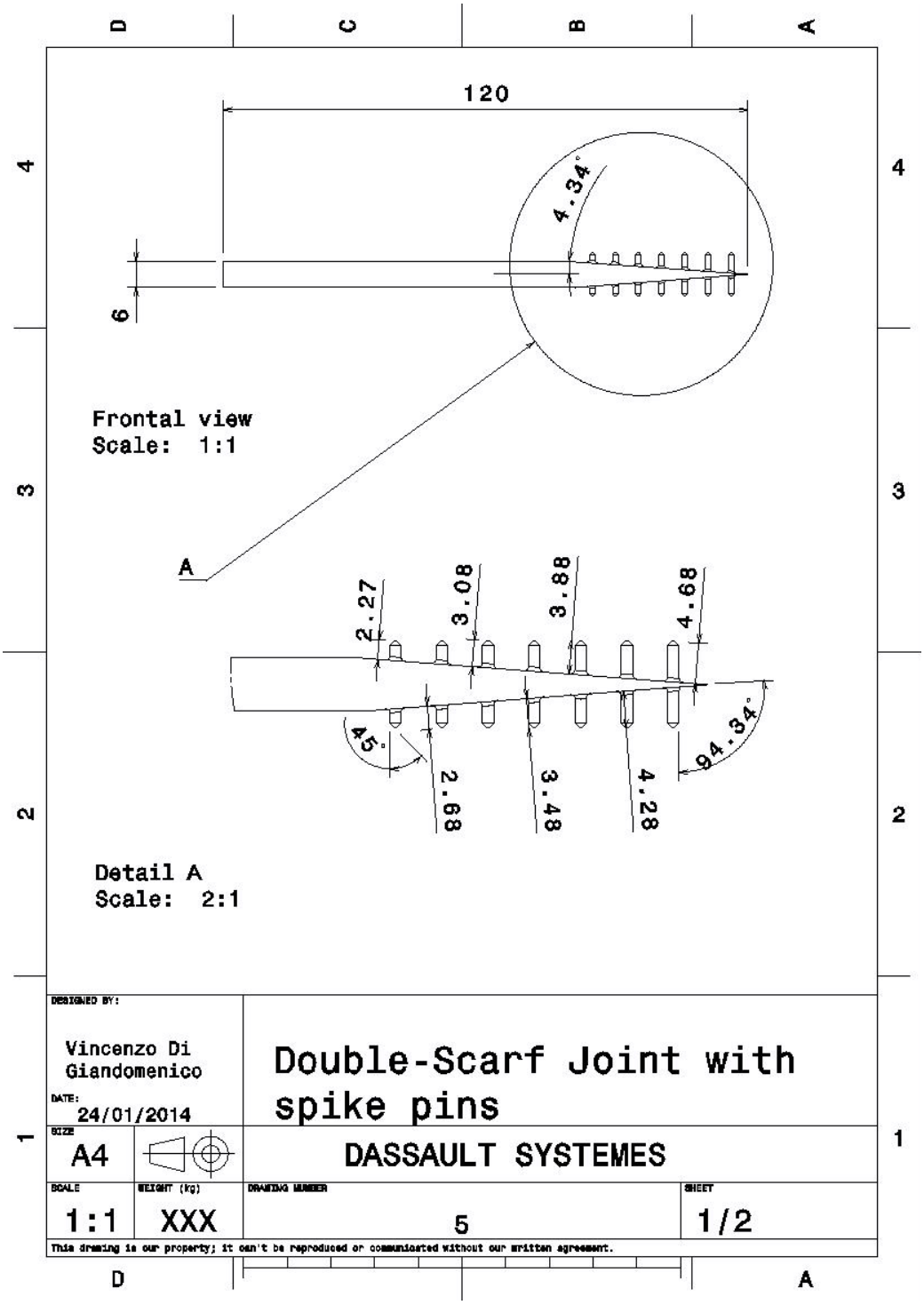

Figure A-7 Double-Scarf joint with spike pins:part 1/2

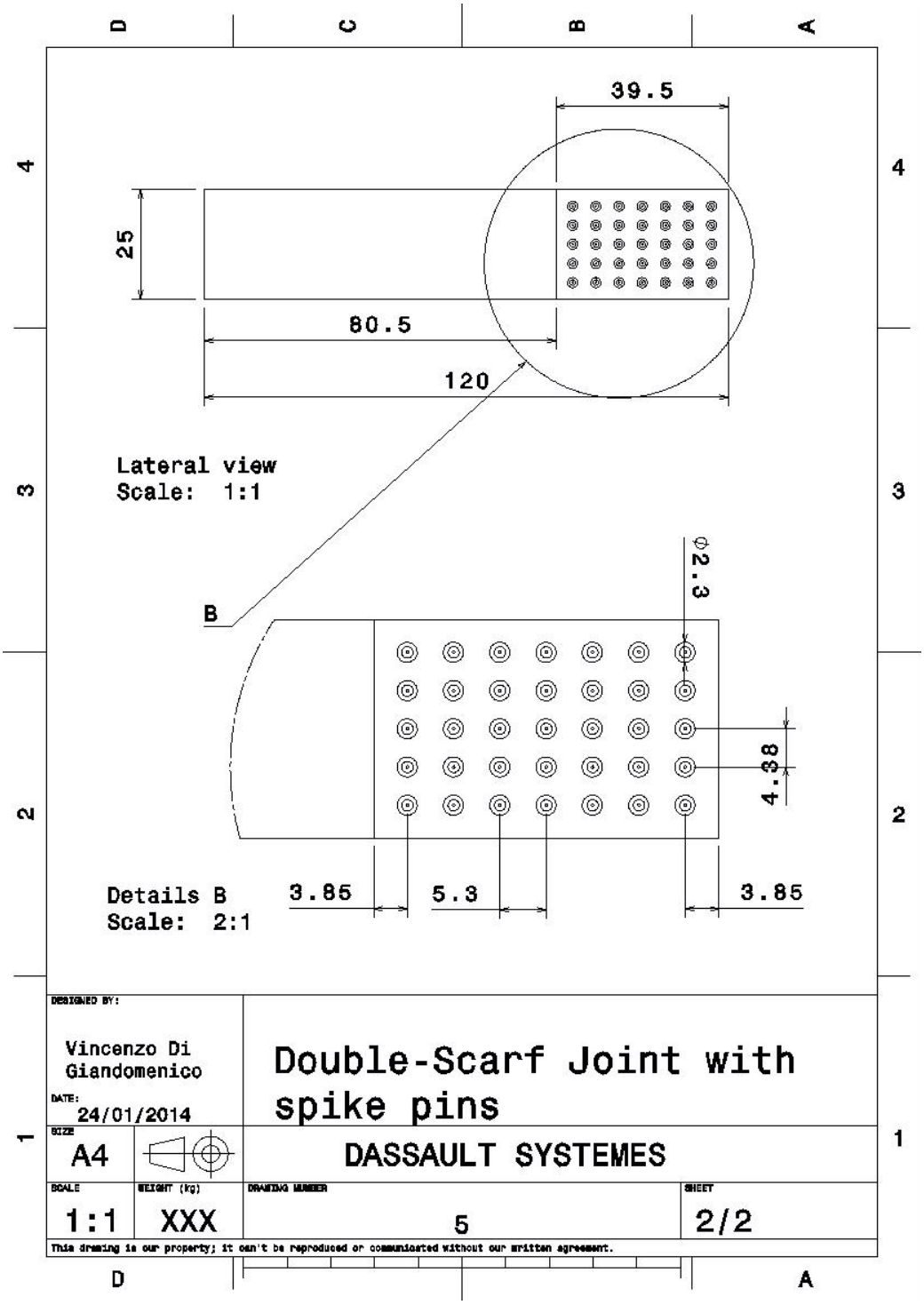

Figure A-8 Double-Scarf joint with spike pins: part 2/2

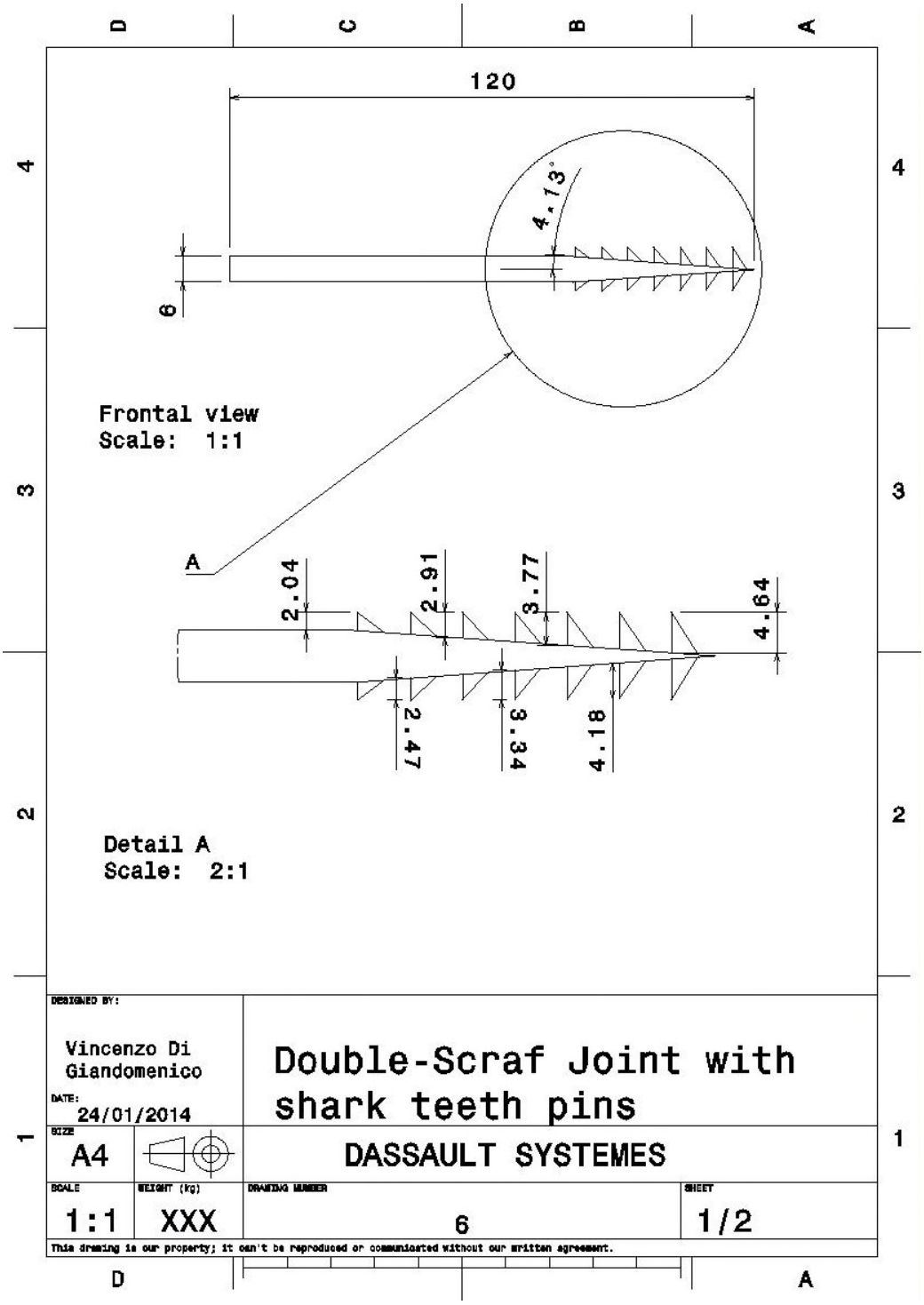

Figure A-9 Double-Scarf joint with shark teeth pins: part 1/2

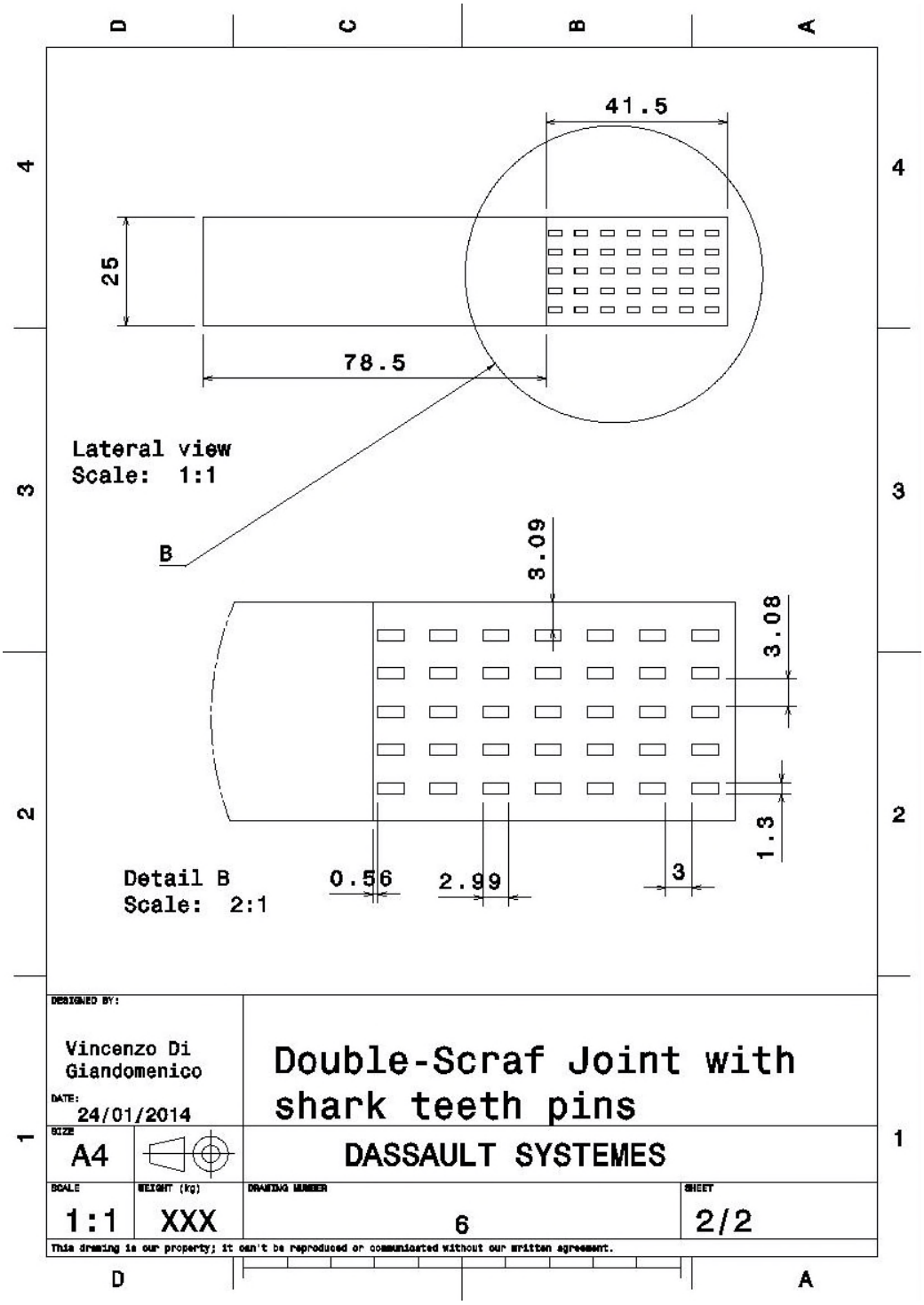

Figure A-10 Double-Scarf joint with shark teeth pins: part 2/2

Appendix B Digital Image Correlation

B.1 Digital Image Correlation concept

Digital Image Correlation (DIC) is a technique that uses digital camera images to measure shape and displacement; it was used since 1980s when applied in solid mechanics [64, 65]. The DIC concepts were the logical development of earlier and related photogrammetry techniques used for microscopy, robotic and aerial imagery. With the development of digital cameras, the next step was to apply them in an experiment by using coherent light for holography and digital speckle pattern interferometry, later using an applied painted speckle pattern [66].

The DIC analysis is obtained by several steps: obtain a calibration image, calibrate the stereo-rig (3D), get speckle images and run analysis [67]: the greater labour is setting up the stereo-rig, optimizing the light and calibrating the system.

The stereo-rig is defined as two cameras calibrated as a unit to take 3D-DIC measurements: the calibration represents the process by which the DIC software scales and orients the camera pictures to the physical world. This procedure depends on intrinsic and extrinsic camera parameters. The extrinsic parameters orient the cameras in the space while the intrinsic parameters such as sensor central point, camera skew, distortions and focal length of lens relate the single camera images to the world.

DIC software divides the images into a numbers of facets for analysis. These square facets, defined in the reference image, are sought in all the subsequent images of both cameras. The original facets will change shape as consequence of sample deformation (figure B-1). A mathematical shape function is defined to accommodate this shape change and motion. For most applications the subset has to be able to move for rigid body translation and warped sufficiently to match the deformed shape or the projection of the subset from a camera to the other. The affine shape function is the commonly used shape function.

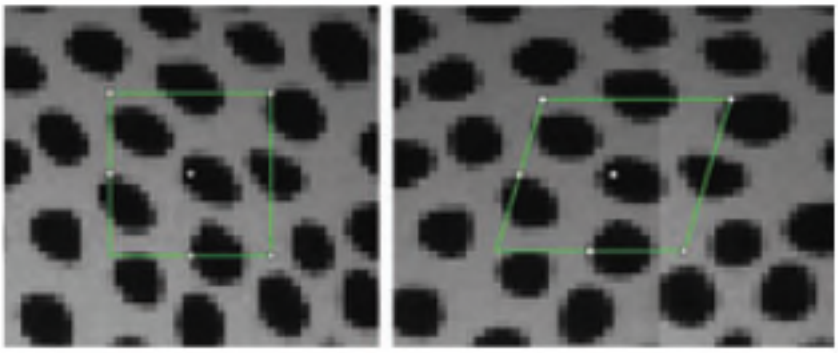

Figure B-1DIC shape function to rapresent strain [68]

The DIC is able to supply results that are subpixel. This ability to resolve displacements of $1/100^{th}$ of pixel enables high-resolution displacement measurements of relatively large field-of-view. The selection of the right interpolation method is essential to ensure interpolation quality and reduce computation time.

The displacement of any subset is defined matching a deformed image with the reference image or matching between the right and left cameras. This includes subpixel information from the interpolation, as well as displacement and deformation from the shape function. The matching is obtained minimizing a function that includes information on pixel intensity information from both the reference and deformed images [69].

The use of two cameras is due to the necessity to define unambiguously the correspondence between the pixel image and the real world. With one camera only it is not possible to define the distance of the object from the camera. This triangulation process, using two cameras, tries to intersect the lines projected from the centres of the related subset to a unique 3D point in the space [70].

Because those lines do not intersect, the optimum triangulation point is found making the assumption that the calibration is correct while the deficiency in intersection is the result of subset mismatch generated by noise in the images (figure B-2). A minimization process is used to find the optimum triangulated 3D point.

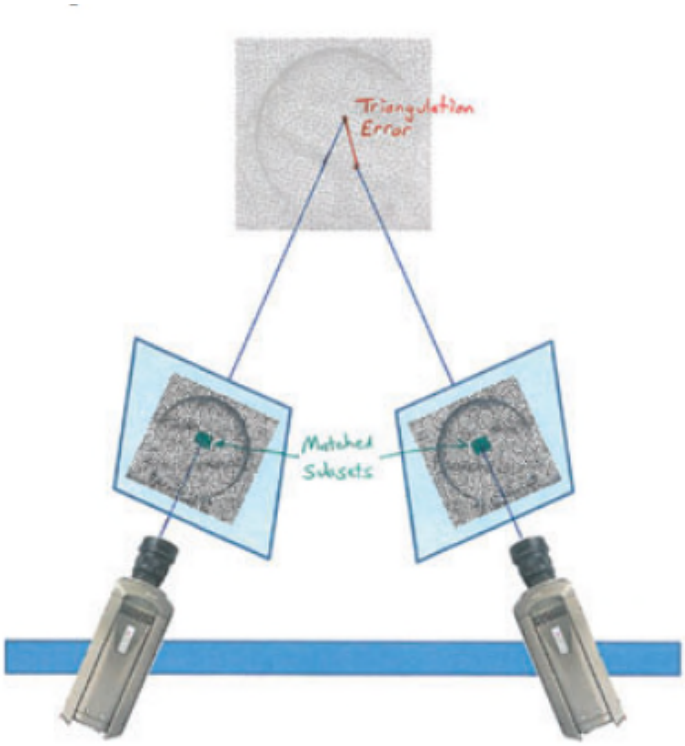

Figure B-2Matching the subset to be triangulated [70]

The DIC results are 3D points, with the displacement being found by subtracting two 3D point clouds. The displacement data are affected by noise. To minimize the noise, more points are used to smooth the results.

Last step of post-processing is done by commercial codes that, according with the definition of strain, use the slope of calculated displacement to define the strain.

Appendix C Stainless steel double-lap joint

C.1 Stainless steel double lap joint with surface features

As a part of embedded joint project a previous study on double lap stainless steel joints with different pin patterns were developed in the past. According to this study the use of pins improve the mechanical properties of co-cured joints.

In order to compare the results obtained for titanium joint the same approach was planned for these joints, investigating the mechanical properties of the pins only. A PTFE film was attached on the surface of both joint configurations before cure (figure C-1) to release the plate. In this way only the pins were locked into the composite and the load of the tensile test was supported only by the pins without any adhesive strength.

Details about lay-up and materials selections are available on .

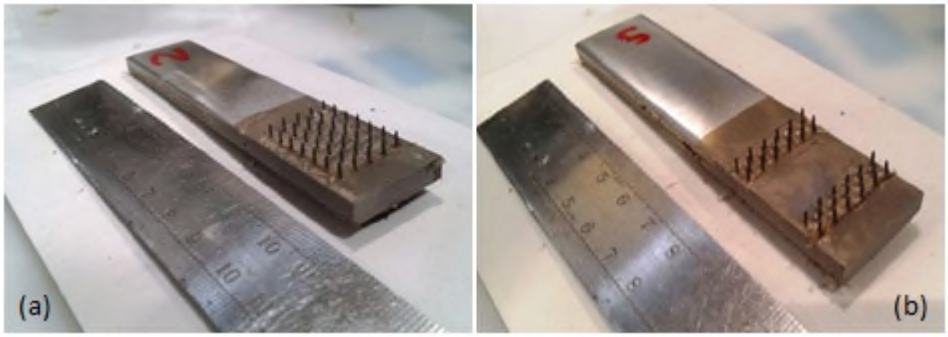

Figure C-1 Stainless steel double lap plate: (a) squared pattern, (b) special pattern

C.1.1 Tensile test, DIC results and microscope analysis

Figure C-2 shows the results of tensile tests carried out according to the procedure described in section 3.3.1. Both configurations show the same mechanical properties and behaviour.

The load history is divided in three main areas: a first part where the load increases linearly until a first threshold value, the second part where the load increases with a nonlinear trend reducing gradually its gradient and finally a third part where the load increases linearly reaching the ultimate tensile load.

The results of tensile test of both configurations are summarised in table C-1.

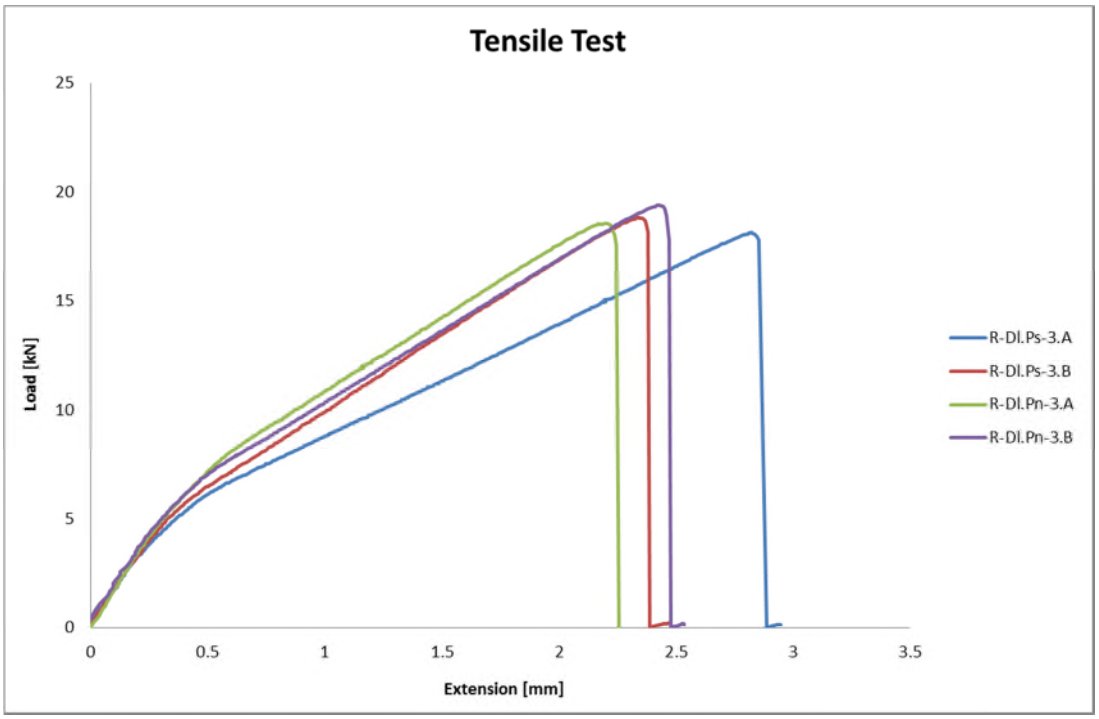

Figure C-2 Tensile test results released pins

The first consideration is obtained analysing the average of ultimate load and the relative ultimate tensile strength which are respectively 18.74 kN and 535 MPa (table C-2). This high ultimate shear strength value, calculated with the total cross section area of pins (the metal plate surface is realised), describes an important aspect of the pin failure. The pins fail in tension and not in shear as was supposed at beginning. This assumption is also confirmed by the mechanical properties of stainless steel shown in table C-3. In fact it is possible to see how the value calculated matches the data sheet value of ultimate tensile strength.

Moreover the microscopy analysis on both configurations confirms this deduction: figure C-4 and figure C-5 describe the failure of pins. Both configurations show that the pins did not fail at interface with the metal plate. The photographs, C-4 &C-5, show a bent area near the base and then the failure occurs in tension after a reduction of the pin cross section area.

Joint	Ultimate tensile load [kN]	Ultimate shear strength of pins [MPa]
R-Dl.Ps-1	18.14	515.71
R-Dl.Ps-2	18.86	536.01
R-Dl.Pn-1	18.55	527.31
R-Dl.Pn-2	19.40	551.52

Table C-1 Released double-lap results

	Ultimate tensile load [kN]	Ultimate shear strength [MPa]
Average	18.74 ± 0.53	535 ± 15

Table C-2Summary of released double-lap mechanical properties

The second consideration that describes the behaviour of pins is obtained with the magnification of the nonlinear area of the loading curve (figure C-3). The nonlinear behaviour is due on the pins bending: because the strength of composite is higher than pins, as soon as the load reaches the value corresponding on the yield of stainless steel, the pins start to bend. This is confirmed by the values calculated at this load: they match the value of yield tensile strength of the material. It is even confirmed by microscopy analysis: from figure C-4 and figure C-5 is possible to see the bent area on the base of the surface features.

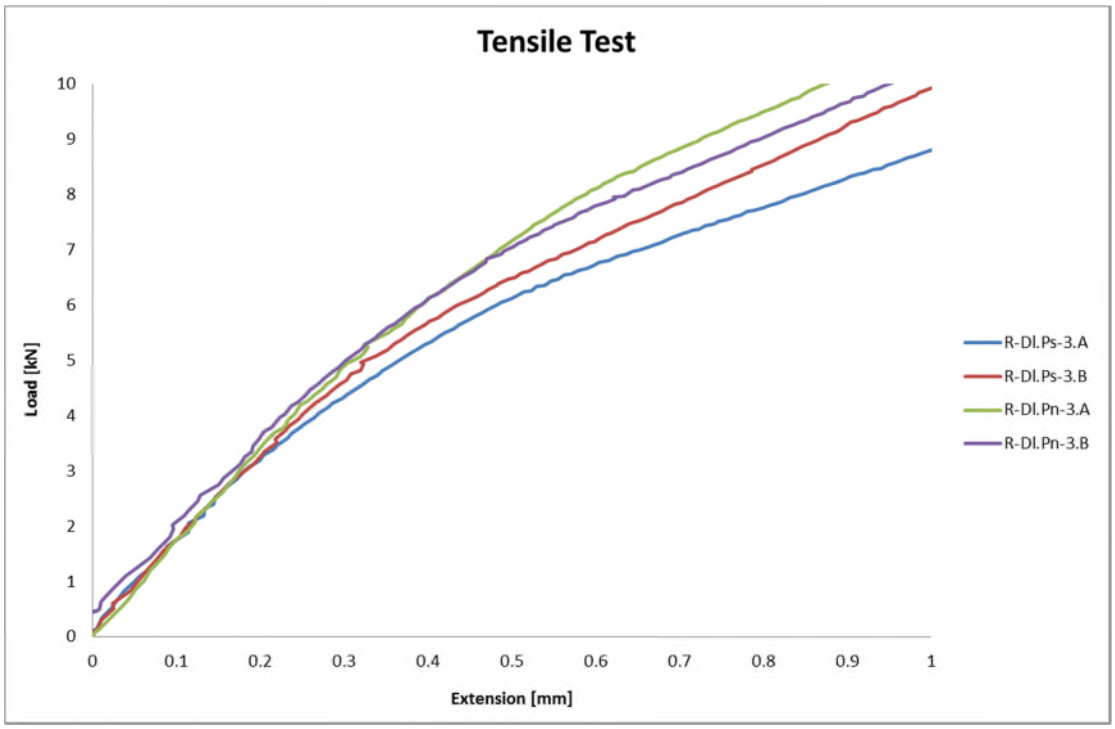

Figure C-3Test result magnification: pins bending

Density	**8.00 g/cc**
Tensile Strength, Ultimate	586 MPa
Tensile Strength, Yield	210 MPa (strain 0.200%)
Elongation at Break	70%
Modulus of Elasticity	193-200 GPa
Poisson Ratio	0.29
Shear Modulus	86.0 GPa

Table C-3 Stainless steel mechanical properties

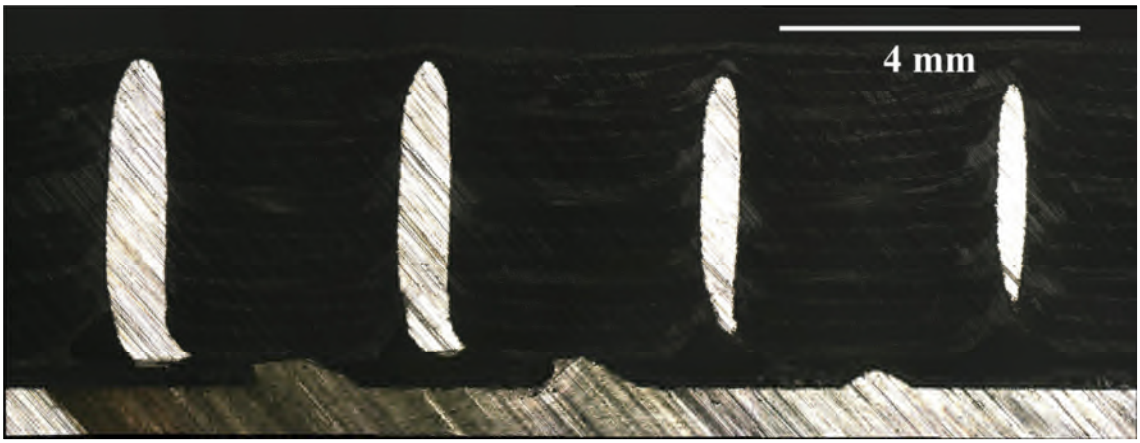

Figure C-4 Pin bending and tensile failure

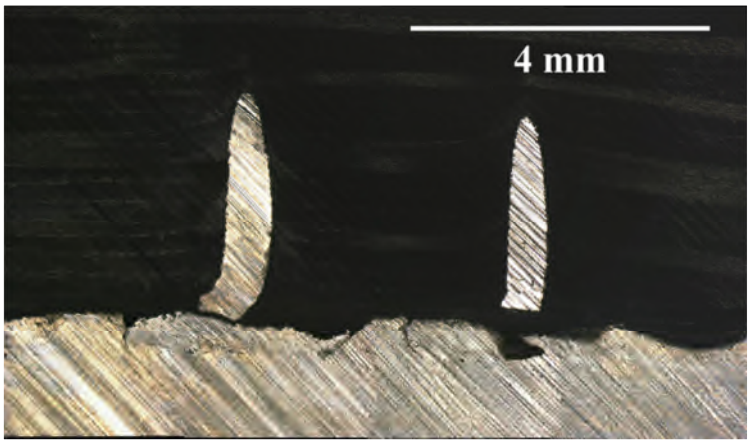

Figure C-5 Pin bending and tensile failure special pattern